





**UNIVERSITY OF PATRAS**



**MECHANICAL ENGINEERING AND AERONAUTICS DEPARTMENT  
SECTION OF APPLIED MECHANICS**

**PhD THESIS**

**EVANGELOS A. PASIPOULARIDIS**

**RESIDUAL STRENGTH  
& LIFE PREDICTION IN  
COMPOSITE MATERIALS  
AFTER FATIGUE**

**PATRAS 2009**

The PhD was elaborated under the supervision of  
Associate Professor Dr Theodore P. Philippidis

*Examining Comete*

Dr Theodore Philippidis - Associate Professor (Supervisor)  
Dr Georgios Papanikolaou - Professor  
Dr Dimitrios Saravanos - Professor  
Dr Vasilios Kostopoulos - Professor  
Dr Spiridon Pantelakis - Professor  
Dr Nikolaos Anifantis - Professor  
(Mechanical Engineering & Aeronautics Dept, University of Patras)

Dr Nikolaos Tsouvalis - Associate Professor  
(Naval Architecture and Marine Engineering Dept, National Technical University  
of Athens)

Defended in public on the 10<sup>th</sup> of July 2008 at the University of Patras

## ΠΡΑΚΤΙΚΟ ΣΥΝΕΔΡΙΑΣΗΣ

Επταμελούς εξεταστικής επιτροπής για την κρίση της διδακτορικής διατριβής του  
κ. Ευάγγελου Πασιπουλαρίδη

Η τριμελής συμβουλευτική επιτροπή, αποτελούμενη από τους κ.κ. Θ. Π. Φιλιππίδη, Αναπληρωτή Καθηγητή (επιβλέπων), Γ. Παπανικολάου, Καθηγητή, Δ. Σαραβάνο, Καθηγητή, άπαντες του Τμήματος Μηχανολόγων & Αεροναυπηγών Μηχανικών του Πανεπιστημίου Πατρών, συμπληρώθηκε σε επταμελή εξεταστική επιτροπή με τους κ.κ. Ν. Ανυφαντή, Β. Κωστόπουλο, Σ. Παντελάκη, άπαντες Καθηγητές του Τμήματος Μηχανολόγων & Αεροναυπηγών Μηχανικών του Πανεπιστημίου Πατρών και Ν. Τσούβαλη, Αναπληρωτή Καθηγητή Σχολής Ναυπηγών Μηχανικών Ε.Μ.Π, σύμφωνα με την υπ' αριθμό 1/25-9-2007 απόφαση της Γενικής Συνέλευσης με την Ειδική Σύμβαση του Τμήματος Μηχανολόγων & Αεροναυπηγών Μηχανικών του Πανεπιστημίου Πατρών.

Η εξεταστική επιτροπή συνήλθε σήμερα, την 10<sup>η</sup> Ιουλίου 2008 ημέρα Πέμπτη και ώρα 17:00, σε συνεδρίαση κατά την οποία η διατριβή με τίτλο: «Εναπομένουσα Αντοχή & Πρόβλεψη Ζωής σε Σύνθετα Υλικά Μετά από Κόπωση», υποστηρίχθηκε από τον υποψήφιο Διδάκτορα κ. Ευάγγελο Πασιπουλαρίδη. Στη συνέχεια υπεβλήθησαν ερωτήσεις στον υποψήφιο και επερατώθη η εξέταση.

Μετά την αποχώρηση του υποψηφίου και των ακροατών, η επιτροπή συζήτησε επί της γενομένης εξετάσεως και αποφάσισε ομόφωνα να κάνει δεκτή τη διατριβή, επειδή αυτή είναι πρωτότυπη και αποτελεί ουσιαστική συμβολή στην επιστήμη, ο δε υποψήφιος την υπερασπίστηκε με άκρως ικανοποιητικό τρόπο και την βαθμολόγησαν με βαθμό άριστα.

### Η Επταμελής Εξεταστική Επιτροπή:

Αναπλ. Καθηγητής Θεόδωρος Π. Φιλιππίδης

Καθηγητής Γεώργιος Παπανικολάου

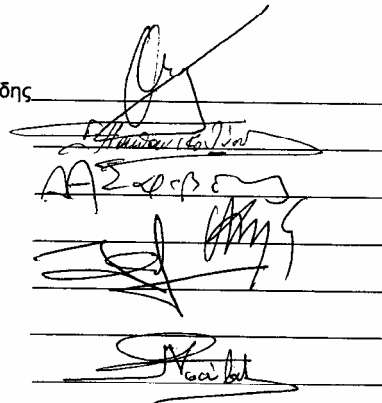
Καθηγητής Δημήτριος Σαραβάνος

Καθηγητής Νικόλαος Ανυφαντής

Καθηγητής Βασίλειος Κωστόπουλος

Καθηγητής Σπυρίδων Παντελάκης

Αναπλ. Καθηγητής Νικόλαος Τσούβαλης





## ACKNOWLEDGEMENTS

The thesis in your hands is the fruit of an effort starting in 2001 and finishing seven years later, thus completing the circle of my PhD studies in the frame of the Applied Mechanics Laboratory at the Mechanical Engineering and Aeronautics Department of the University of Patras. However hard this long task might have appeared in several instances, looking back at these past years leaves only pleasant recollections and a feeling of satisfaction for the experience gained along the path rather than for the prize itself.

This is the reason why I feel a deep need for thanking all those who supported me along the way, starting of course with my beloved wife Dimitra and my family as well as a long list of dear friends who shared with me nice and relaxing times not only during this period but in my life so far. The whole journey of course would have been impossible without the inspired guidance and academic support of my supervisor professor Dr Theodore Philippidis. Following the long line, I should thank my most dear colleagues and friends Alexandros Antoniou and Theoni Asimakopoulou for sharing endless times in the laboratory waiting for specimens to fail. Also special thanks must be given, to all the researchers working at WMC, VUB, RAL-CCLRC, RISOE, CRES, NTUA, and others, who contributed their experience, innovative ideas and of course experimental data necessary for the accomplishment of this work. Finally, I would like to thank the members of my advisory cometeet for their interest in my work as well as all the professors and colleagues who inspired me during my studies.

Last but not least I should acknowledge the major contribution of the European taxpayer who, through the European Comission and Greek General Secretariat of Research and Technology, funded the projects in the frame of which this joint research effort and fruitfull interaction between such a large number of different institutes and laboratories has been made possible.





## TABLE OF CONTENTS

<b>1</b>	<b>SUMMARY</b>	<b>1</b>
<b>2</b>	<b>FORWARD</b>	<b>5</b>
<b>3</b>	<b>MODELING RESIDUAL STRENGTH</b>	<b>9</b>
3.1	INTRODUCTION	9
3.2	RESIDUAL STRENGTH MODELS	13
3.2.1	Broutman & Sahu	14
3.2.2	Hahn & Kim	15
3.2.3	Yang et al.	18
3.2.4	Chou & Croman	24
3.2.5	Harris et al.	26
3.2.6	Schaff & Davidson	27
3.2.7	Sendeckyj	28
3.3	MODIFIED MODELS	33
3.3.1	Introduction	33
3.3.2	Statistical S-N formulation	34
3.3.3	Modified Broutman & Sahu	35
3.3.4	Modified Hahn & Kim model	36
3.3.5	Modified Interaction model	36
3.3.6	Non Linear model	37
3.4	EXPERIMENTS	40
3.4.1	Published Data Sets	40
3.4.2	OPTIMAT BLADES	43
3.4.2.1	Experimental program	43
3.4.2.2	Test Procedure	46
3.4.2.3	Coupon Geometry	47
3.4.2.4	Test Results	51
3.4.2.4.1	Static Strength	51
3.4.2.4.2	Fatigue Life	55
3.4.2.4.3	Residual Strength	58
3.5	VALIDATION OF MODELS	64
3.5.1	Implementation to Experimental Data	64

3.5.2	Residual Tensile Strength	66
3.5.2.1	Degradation Curves	66
3.5.2.2	Statistical Predictions	78
3.5.3	Residual Compressive Strength	88
3.5.4	Models Assessment	90
<b>4</b>	<b>LIFE PREDICTION UNDER SPECTRUM LOADING</b>	<b>93</b>
4.1	INTRODUCTION	93
4.2	IMPLEMENTED SPECTRA	96
4.3	LIFE PREDICTION METHODOLOGY	103
4.3.1	Cycle Counting Method	103
4.3.2	Constant Life Diagram	105
4.3.3	Damage Accumulation	111
4.4	PREDICTIONS UNDER SPECTRAL LOADING	116
4.4.1	Algorithm	116
4.4.2	Experimental Data	117
4.4.3	Results and Discussion	120
4.4.3.1	Residual Strength vs Palmgren-Miner Rule	120
4.4.3.2	Investigation of Different CLD Methods	125
4.4.3.3	Investigation of Different Counting Methods	131
4.4.4	Choosing a Methodology	133
<b>5</b>	<b>FATIGUE SIMULATION OF LAMINATES</b>	<b>137</b>
5.1	INTRODUCTION	137
5.2	FADAS OVERVIEW	139
5.3	MODULES OF FADAS	142
5.3.1	Pre-Processing of Fatigue Loads	142
5.3.2	Failure Criterion	142
5.3.3	Sudden Stiffness Degradation	145
5.3.4	Residual Strength Degradation	147
5.3.5	Gradual Stiffness Degradation	148
5.3.6	CLD Formulation	150
5.3.7	Final Failure	151
5.4	FATIGUE SIMULATION OF MD LAMINATES	152

5.4.1	Experimental data _____	152
5.4.2	FADAS Results and Discussion _____	155
<b>6</b>	<b>CONCLUSIONS _____</b>	<b>161</b>
6.1	RESIDUAL STRENGTH MODEL _____	163
6.2	LIFE PREDICTION MODULES _____	165
6.3	FATIGUE SIMULATION OF MD LAMINATES _____	167
<b>7</b>	<b>FUTURE RESEARCH _____</b>	<b>168</b>
<b>8</b>	<b>REFERENCES _____</b>	<b>171</b>
<b>9</b>	<b>APPENDIX _____</b>	<b>177</b>



## LIST OF FIGURES

Fig. 1	Variations of residual strength degradation trends for different values of parameter $c$ .	16
Fig. 2	Visual comparison of the equivalent static strength distributions (based on the parameters of Yang and the ones derived in the present work) and the experimentally obtained distribution.	21
Fig. 3	Transition of residual strength models from gradual wear out to sudden death.	26
Fig. 4	Schematic representation of the residual strength characterization test matrix	45
Fig. 5	Unified coupon geometry for all types of test (e.g. fatigue, static and residual strength in tension and compression)	49
Fig. 6	Geometry of the ISO 14129 standard coupons used for determination of shear properties of the material.	49
Fig. 7	Pictures of failed OB UD coupons cut at $90^\circ$ and tested in tension (top) and compression (bottom)	52
Fig. 8	Pictures of failed OB UD coupons cut at $0^\circ$ and tested in compression (top) and tension (bottom)	53
Fig. 9	Pictures of failed ISO $[\pm 45]_s$ coupons tested tension for the determination of the shear properties.	53
Fig. 10	Distributions of static tensile and compressive strength of the principle directions of the reference material along with Weibull curves used to fit the data.	54
Fig. 11	Typically buckled (top) and valid (bottom) failure modes of the UD on-axis coupon, under $R=10$ fatigue.	55
Fig. 12	Fatigue life data and S-N curves for the reference material at $0^\circ$ .	57
Fig. 13	Fatigue life data and S-N curves for the reference material at $90^\circ$ .	57
Fig. 14	Fatigue life data and S-N curves for the reference material under shear.	58
Fig. 15	Percentage of premature failures at different laboratories and test cases.	59
Fig. 16	Residual strength data for on-axis UD tested at $R=0.1$ .	59
Fig. 17	Residual strength data for on-axis UD tested at $R=-1$ .	60
Fig. 18	Residual strength data for transverse UD tested at $R=0.1$ .	61
Fig. 19	Residual strength data for transverse UD tested at $R=-1$ .	61
Fig. 20	Residual strength data for transverse UD tested at $R=10$ .	62
Fig. 21	Shear residual strength data at $R=0.1$ .	63
Fig. 22	Comparison of theoretical predictions and experimental data from Glass/Polyester $[\text{CSM}/\text{fabric}/(\text{CSM}/\text{UD})_2]_S$ [26].	67
Fig. 23	Comparison of theoretical predictions and experimental data from the on-axis OPTIMAT UD tested at $R=0.1$ at the stress level of 1000 cycles.	68

Fig. 24	Comparison of theoretical predictions and experimental data from the on-axis OPTIMAT UD tested at R=0.1 at the stress level of 5·10 <sup>4</sup> cycles.	68
Fig. 25	Comparison of theoretical predictions and experimental data from the on-axis OPTIMAT UD tested at R=0.1 at stress level of 106 cycles.	69
Fig. 26	Comparison of theoretical predictions and experimental data from the on-axis OPTIMAT UD tested at R=0.1 at the stress level of 107 cycles.	69
Fig. 27	Comparison of theoretical predictions and experimental data from the on-axis OPTIMAT UD tested at R=-1 at the stress level of 5000 cycles.	70
Fig. 28	Comparison of theoretical predictions and experimental data from the on-axis OPTIMAT UD tested at R=-1 at the stress level of 5·10 <sup>4</sup> cycles.	70
Fig. 29	Comparison of theoretical predictions and experimental data from the on-axis OPTIMAT UD tested at R=-1 at the stress level of 106 cycles.	71
Fig. 30	Comparison of theoretical predictions and experimental data from the transverse direction of the OPTIMAT UD tested at R=0.1 at the stress level of 5000 cycles.	73
Fig. 31	Comparison of theoretical predictions and experimental data from the transverse direction of the OPTIMAT UD tested at R=0.1 at the stress level of 5·10 <sup>4</sup> cycles.	73
Fig. 32	Comparison of theoretical predictions and experimental data from the transverse direction of the OPTIMAT UD tested at R=0.1 at the stress level of 106 cycles.	74
Fig. 33	Comparison of theoretical predictions and experimental data from the transverse direction of the OPTIMAT UD tested at R=-1 at the stress level of 1000 cycles.	74
Fig. 34	Comparison of theoretical predictions and experimental data from the transverse direction of the OPTIMAT UD tested at R=-1 at the stress level of 5000 cycles.	75
Fig. 35	Comparison of theoretical predictions and experimental data from the transverse direction of the OPTIMAT UD tested at R=-1 at the stress level of 5·10 <sup>4</sup> cycles.	75
Fig. 36	Comparison of theoretical predictions and experimental data from the transverse direction of the OPTIMAT UD tested at R=-1 at the stress level of 106 cycles.	76
Fig. 27	Sudden death (SD) model predictions and experimental data for the residual tensile strength on the transverse direction of the OPTIMAT UD tested at R=10 at three stress levels.	78
Fig. 38	Probability distributions of residual strength according to the various models for the data set of Ryder and Walker, at 344.74 MPa, 31400 cycles	79
Fig. 39	Probability distributions of residual strength according to the various models for the data set of Ryder and Walker, at 289.58 MPa, 364000 cycles	80
Fig. 40	Probability distributions of residual strength according to the various models for the data set of Yang et al., at 389.76 MPa, 56000 cycles	80

Fig. 41	Probability distributions of residual strength according to the various models for the data set of OPTIMAT [ $\pm 45$ ]S laminate at 55.62.76 MPa, 110000 cycles	81
Fig. 42	Degradation curves of 10% (right curves) and 90% (left curves) reliability, predicted by different models for the data set of Anderson at the stress level of 284.2 MPa.	83
Fig. 43	Degradation curves of 10% (right curves) and 90% (left curves) reliability, predicted by different models for the 1.29 kN/mm stress level at R=-1.	83
Fig. 44	Degradation curves of 10% (right curves) and 90% (left curves) reliability, predicted by different models for the 0.97 kN/mm stress level at R=-1.	84
Fig. 45	Degradation curves of 10% (right curves) and 90% (left curves) reliability, predicted by different models for the 0.67 kN/mm stress level at R=-1.	84
Fig. 46	Degradation curves of 10% (right curves) and 90% (left curves) reliability, predicted by different models for the 2.14 kN/mm stress level at R=0.1.	85
Fig. 47	Degradation curves of 10% (right curves) and 90% (left curves) reliability, predicted by different models for the 1.43 kN/mm stress level at R=0.1.	85
Fig. 48	Degradation curves of 10% (right curves) and 90% (left curves) reliability, predicted by different models for the 1.05 kN/mm stress level at R=0.1.	86
Fig. 49	Residual strength degradation curves of 90% and 10% reliability for the data set of OPTIMAT [ $\pm 45$ ]S at the stress level of 78.3 MPa.	86
Fig. 50	Residual strength degradation curves of 90% and 10% reliability for the data set of OPTIMAT [ $\pm 45$ ]S at the stress level of 63.6 MPa.	87
Fig. 51	Residual strength degradation curves of 90% and 10% reliability for the data set of OPTIMAT [ $\pm 45$ ]S at the stress level of 48.5 MPa.	87
Fig. 52	Sudden death (SD) model predictions and experimental data for the residual compressive strength on the transverse direction of the OPTIMAT UD tested at R=10 at three stress levels.	89
Fig. 53	Sudden death (SD) model predictions and experimental data for the residual compressive strength on the on-axis direction of the OPTIMAT UD tested at R=0.1 at three stress levels.	89
Fig. 54	WISPER spectrum	96
Fig. 55	Visual Comparison between Wind Turbines used in the composition of WISPER (left) and NEW WISPER (right) loading spectrum (picture taken from [80]).	97
Fig. 56	NEW WISPER spectrum	98
Fig. 57	MWIND spectrum	98
Fig. 58	Comparison of the cumulative composition of the three spectra in terms of stress ranges of their cycles.	99
Fig. 59	Comparison of the three spectra in terms of amplitude (upper) and mean (lower) stress of their segments	100

Fig. 60	Location of the cycles of the three spectra in the mean stress - stress amplitude space.	101
Fig. 61	Details of MWIND (left), WISPER (center) and NEW WISPER (right) spectra.	102
Fig. 62	Load time history and corresponding qualitative stress-strain graph, showing the hysteresis loops (BC, EF and DG) counted by Rainflow algorithm.	104
Fig. 63	Flowchart of the one pass Rainflow algorithm (Algorithm II) proposed by Downing & Soccie.	105
Fig. 64	Goodman Lines constructed for four different fatigue lives	106
Fig. 65	Constant Life Diagram (CLD) constructed based on three S-N curves at R=0.1, R=-1 and R=10.	107
Fig. 66	Regression lines of the f, u and v parameters of BELL CLD, fitted on OPTIMAT UD at 0°.	109
Fig. 67	BELL CLD constructed based on three S-N curves at R=0.1, R=-1 and R=10.	110
Fig. 68	CLD lines constructed based on the assumption that all cycles are described by a single S-N line (R=0.1 in this case) independently of their stress ratio.	111
Fig. 69	Graphical demonstration of residuals strength prediction under two constant amplitude fatigue bocks.	113
Fig. 70	Flow chart of the life prediction algorithm under variable amplitude fatigue.	116
Fig. 71	Life predictions for the [0]4 laminate produced by various models for the WISPER spectrum.	121
Fig. 72	Life predictions for the [0]4 laminate produced by various models for the NEW WISPER spectrum.	121
Fig. 73	Life predictions for the [0]4 laminate produced by various models for the MW spectrum.	122
Fig. 74	Life predictions for the [±45]s laminate under the NW_mod spectrum.	123
Fig. 75	Residual strength degradation of the [±45]S laminate, after application of the NWmod spectrum at a maximum stress level of Smax=102 MPa (upper) and Smax=96 MPa (lower).	125
Fig. 76	Plot of the three CLD formulations implemented: LCLD in continuous, BELL in dashed and R01 in dotted lines, from tests on [0]4 laminate.	126
Fig. 77	Comparison of various models using different CLD assumptions on the [0]4 laminate, under WISPER spectrum.	127
Fig. 78	Comparison of various models using different CLD assumptions on the [0]4 laminate, under NEW WISPER spectrum.	127
Fig. 79	Comparison of various models using different CLD assumptions on the [0]4 laminate, under MWIND spectrum.	128
Fig. 80	Comparison of various models on the [±45]S laminate under NW_mod spectrum.	128
Fig. 81	Comparison of model predictions implementing alternative forms of the R01 formulation with experimental data of W spectrum on the [0]4 laminate.	130



Fig. 82	Predictions of various models using range-mean and rainflow algorithm on Wisper spectrum for the [0]4 laminate.	131
Fig. 83	Predictions of various models using range-mean and rainflow algorithm on New Wisper spectrum for the [0]4 laminate.	132
Fig. 84	Predictions of various models using range-mean and rainflow algorithm on MW spectrum for the [0]4 laminate.	132
Fig. 85	Flowchart of the FADAS algorithm.	139
Fig. 86	Failure locus in the ( $\sigma_2$ , $\sigma_6$ ) stress plane, predicted with Puck failure criterion.	144
Fig. 87	Change of the degradation factor n versus the failure effort.	146
Fig. 88	Normalized residual shear modulus data after fatigue fitted by Eq.(96).	149
Fig. 89	Constant Life Diagrams of the reference UD ply: Parallel to the fibre (left), transversely to the fibre (centre) and in-plane shear (right).	150
Fig. 90	S-N data and model predictions for the MD laminate at R=0.1.	156
Fig. 91	S-N data and model predictions for the MD laminate at R=-1.	157
Fig. 92	S-N data and model predictions for the 10° off-axis MD laminate at R=-1.	157
Fig. 93	S-N data and model predictions for the 60° off-axis MD laminate at R=-1.	158
Fig. 94	Residual strength and maximum cyclic stresses predicted through FADAS for each in-plane property of each ply of the MD coupon at 60° off-axis, cycled at $\sigma_{max}=50$ MPa, R=-1.	159
Fig. 95	MD coupons at 60° off-axis tested at R=-1.	159



## LIST OF TABLES

Table 1: Residual strength degradation theories. $S_0$ , $D$ , $C$ , $G$ are constant model parameters	29
Table 2 Static strength data from Anderson et al. [26].	41
Table 3 Fatigue life data from Anderson et al. [26], under $R=0.1$ stress ratio.	42
Table 4 Verification residual strength data set from Anderson et al. [26] ( $R=0.1$ ).	42
Table 5 Residual strength data set from Anderson et al. [26], used for parameter estimation ( $R=0.1$ ).	43
Table 6 Indicative test frequencies, for various types of fatigue tests, referring to a fatigue life of 50,000 cycles.	47
Table 7 Comparison of UD properties derived from ISO and OB coupon testing.	50
Table 8 Weibull parameters of the in-plane static strength properties of the UD laminate.	54
Table 9 S-N curve parameters at all stress ratios tested for all in-plane properties.	57
Table 10 Parameters of models implemented to the three published data sets.	64
Table 11 Parameters of models implemented to the OPTIMAT data.	65
Table 12 Spectrum fatigue test results from UD coupons.	118
Table 13 Spectrum fatigue and residual strength test results from UD and $[\pm 45]_s$ coupons.	119
Table 14 Puck criterion parameters assumed in [107]	144
Table 27 Elastic properties of the reference UD used in the failure criterion of Puck.	145
Table 16 Degradation of Elastic Properties according to Failure Mode	146
Table 17 Stiffness degradation parameters for the principal directions and shear of the UD ply	149
Table 18 Equivalent number of layers, assuming equal area weight	152
Table 19 Fatigue life test results on MD laminate under $R=0.1$ (GEV207_R0400_XXX)	153
Table 20 Fatigue life test results on MD laminate under $R=-1$ (GEV207_R0400_XXX)	154
Table 21 Fatigue life test results on $10^\circ$ and $60^\circ$ off-axis MD coupons under $R=-1$ .	155



## NOMENCLATURE

X	Static strength.
$X_i$	Tensorial representation of static strength.
$X_T$	Tensile static strength of unidirectional lamina in the fibre direction.
$X_C$	Compressive static strength of unidirectional lamina in the fibre direction.
$Y_T$	Tensile static strength of unidirectional lamina in the transverse direction .
$Y_C$	Compressive static strength of unidirectional lamina in the transverse direction.
S	Shear static strength of unidirectional lamina .
$X_r$	Residual static strength.
$X_{Tr}$	Residual tensile static strength of unidirectional lamina in the fibre direction .
$X_{Cr}$	Residual compressive static strength of unidirectional lamina in the fibre direction .
$Y_{Tr}$	Residual tensile static strength of unidirectional lamina in the transverse direction.
$Y_{Cr}$	Residual compressive static strength of unidirectional lamina in the transverse direction.
$S_r$	Residual shear static strength of unidirectional lamina.
$\sigma_{max}$	Maximum cyclic stress .
$\sigma_{min}$	Minimum cyclic stress.
R	Stress ratio, $R = \frac{\sigma_{min}}{\sigma_{max}}$
n	Number of applied load cycles.
N	Life under constant amplitude fatigue.
$E_1$	Modulus of elasticity in the fibre direction of unidirectional lamina.
$E_{f1}$	Modulus of elasticity of the fibres of unidirectional lamina.
$\nu_{12}$	Poisson ratio of unidirectional lamina.
$\nu_{f12}$	Poisson ratio of the fibres of unidirectional lamina.

- $G_{12}$  Shear modulus of unidirectional lamina.
- $G_{120}$  Initial shear modulus of unidirectional lamina.
- $\kappa, \lambda$  Parameters of gradual stiffness degradation.
- $X_1$  Statistical variable of static strength  $X$ .
- $X_2$  Statistical variable of fatigue life  $N$
- $X_3$  Statistical variable of Residual strength  $X_r$
- $P_X$  Cumulative density function (CDF) of static strength.
- $P_N$  Cumulative density function (CDF) of fatigue life.
- $P_{X_r}$  Cumulative density function (CDF) of residual strength.
- $P_{X, \sigma_{\max}}$  Conditional probability of static strength being smaller than  $X_1$  given it is greater than  $\sigma_{\max}$ .
- $P_{\text{REL}}$  Reliability of static strength or else probability of being greater than  $X_1$ .
- $\beta, \alpha$  Scale and shape Weibull parameters of static strength.
- $\tilde{N}, \alpha_f$  Scale and shape Weibull parameters of fatigue life
- $\tilde{N}_i, \alpha_{fi}$  Scale and shape Weibull parameters of fatigue life at stress level  $i$ .
- $K, b$  Parameters of exponential S-N curve in the form:  $K\sigma_{\max}^b \tilde{N} = 1$
- $S_0, b$  Parameters of exponential S-N curve in the form:  $\sigma_{\max} = S_0 N^{-\frac{1}{b}}$
- $\sigma_0, b$  Parameters of exponential S-N curve in the form:  $\sigma_a = \sigma_0 N^{-\frac{1}{b}}$
- $\sigma_r$  Stress range of load cycle,  $\sigma_r = \sigma_{\max} - \sigma_{\min}$
- $\sigma_m$  Mean stress of load cycle:  $\sigma_m = (\sigma_{\max} + \sigma_{\min})/2$
- $\sigma_a$  Amplitude of stress cycle,  $\sigma_a = (\sigma_{\max} - \sigma_{\min})/2$
- $f_r$  Test frequency during constant amplitude fatigue.
- $f_{\text{ref}}$  Reference test frequency during constant amplitude fatigue.
- $\dot{\sigma}$  Average stress rate during spectral fatigue.
- $\Omega$  Normalised fatigue life (Whitney model).

$\Omega^*$	Statistical variable of normalized fatigue life (Whitney model).
$\Omega_0$	Scale parameter of normalized fatigue life (Whitney model).
D	Damage parameter of Miner rule.
$n_{eq}$	Equivalent number of cycles.
$\sigma_{eq}$	Equivalent stress.
$P_{REL, \sigma_{max}}$	Conditional reliability of static strength or else probability of being greater than $X_1$ given it is greater than $\sigma_{max}$ .
$\sigma_{x_{max}}, \sigma_{y_{max}}, \sigma_{s_{max}}$	Maximum cyclic stress components in plane fatigue, in the $(x, y)$ coordinate system.
$R_x, R_y, R_s$	Stress ratios of plane fatigue components in the $(x, y)$ coordinate system.
$N_1, N_2, N_6$	Life of unidirectional lamina under constant amplitude fatigue in the fibre direction, transversely to the fibre and in shear.
$\sigma_1, \sigma_2, \sigma_6$	Stress components in the principal coordinate system of unidirectional lamina.
$\sigma_{1max}, \sigma_{2max}, \sigma_{6max}$	Maximum cyclic stress components in plane fatigue, in the principal coordinate system of unidirectional lamina.
$\sigma_{1min}, \sigma_{2min}, \sigma_{6min}$	Minimum cyclic stress components in plane fatigue, in the principal coordinate system of unidirectional lamina.





To Sofia and Antigoni



# 1 SUMMARY

Subject of this dissertation is the investigation of the static strength degradation phenomenon caused by fatigue in FRP composite materials and its integration to structural design procedures. Special focus is put on a specific type of Glass/Epoxy composite produced with vacuum assisted resin infusion, used in the Wind Turbine industry for Rotor Blade manufacturing. Said material, referred to as “reference material”, is experimentally characterized, in basic ply level, in terms of all its basic strength and fatigue properties i.e. static strength in tension and compression, fatigue life under typical stress ratios and residual strength, both tensile and compressive, under various cyclic loads and after different fractions of the composite’s fatigue life. These properties, along with the elastic response of the material, are defined for the two symmetry and shear directions of the reference unidirectional ply, i.e. on-axis, transversely to the fiber and in-plane shear, using a common test geometry for all kinds of tests, developed especially for this purpose. All tests have been performed in the frame of the EU project ‘OPTIMAT BLADES’ [1]. It is the first time such a vast experimental program on in-plane residual strength characterization of a laminate is performed by partners that include leading institutes, universities and research centers (RISOE, ECN, DLR, TU Delft, University of Patras, VUB) while supported by the European wind turbine industry (LM, VESTAS, GAMESA) and major certification organizations (GL, DNV).

In the first part of the study, several phenomenological residual strength models from literature, some of them modified to enhance their performance, along with a newly proposed methodology for reliability based residual strength prediction, are implemented to both the experimental data produced as well as to published data referring to a wider range of materials and lay-ups. The implementation procedures proposed are oriented towards simplicity and

minimization of the required experimental effort. Models predictions, regarding both deterministic strength degradation behavior and statistical characteristics of residual strength, are assessed in order to clarify the predictive ability of each method and propose specific engineering solutions for the prediction of residual strength after fatigue. Some of the innovative points in this first part of the PhD thesis, apart from the experimental characterization of the reference material performed, is the implementation of most up-to-date proposed residual strength models and the assessment of their predictions through implementation to experimental data, the introduction of a new degradation formulation and the development of a methodology for producing statistical residual strength predictions.

Once concluded on a number of efficient engineering models, in the second part of this work, residual strength is integrated in life and residual strength prediction methodologies. As a first step, fatigue life prediction of macroscopically studied composite laminates under variable amplitude (VA) loading is attempted. The effect of each module of the state-of-the-art life prediction schemes, i.e. the counting method and constant life diagram (CLD) is investigated along with the possible benefits from incorporating residual strength as damage accumulation metric instead of the commonly used Palmgren-Miner rule. Predictions are evaluated through tests performed on  $[0_4]_T$  and  $[\pm 45]_S$  laminates of the reference material, under three different loading spectra extracted either from processing strain measurements on operating Wind Turbine Rotor Blades (WISPER and NEW WISPER) or from aero-elastic simulations (MWIND). The outline of this chapter concerns the development and experimental verification of a methodology for life prediction under VA cyclic loading, the critical assessment of the three basic modules of state-of-the-art life prediction methodologies and the introduction of the linear strength degradation model as a viable alternative of the Palmgren-Miner rule, for implementation in structural-design-oriented life prediction methodologies for composites. Additionally, the linear residual strength model is proposed as an attractive alternative of the Palmgren-Miner rule, especially for engineering applications.

As a final step, the FADAS (FAtigue DAmage Simulator) life prediction methodology is developed and implemented in MATLAB computer code. The algorithm, takes into account the plane stress conditions developing into each

## 1. Summary

ply during fatigue by means of classical lamination theory, models the ply-by-ply degradation of strength and stiffness and implements progressive damage principles, based on Puck failure criterion, to predict failure of a composite plate of arbitrary stacking sequence under any cyclic loading. Predictions of the FADAS algorithm, once its parameters are tuned accordingly for the reference UD material, are compared with constant amplitude (CA) fatigue tests performed on three types of specimens: The first consist of a multidirectional (MD) laminate of  $[(\pm 45/0)_4, \pm 45]_T$  lay-up under  $R=0.1$  and  $R=-1$  cyclic loads and the other two are  $10^\circ$  and  $60^\circ$  off-axis coupons cut from the same laminate, cycled under  $R=-1$ , in an effort to validate the algorithm under various combinations of imposed stresses and induced damage modes. It is one of the few cases where a complete plane-stress life prediction methodology for multidirectional laminates is developed and implemented to experimental data, being based on the basic properties of the laminate's constitutive ply. Similar reasoning has been used in the work of M.M. Shokrieh et al. [2,3] as well as by Tserpes et al. [4], deferring nevertheless considerably in terms of the basic modules implemented and the experimental validation of the algorithm.



## 2 FORWARD

Fatigue is defined as the degradation of the integrity of a material as a result of external conditions that vary with time. These external conditions are usually in the form of a fluctuating mechanical load and stress, but can also be in other forms, such as a thermally induced cyclic stress or cyclic exposure to moisture. An alternative definition of fatigue is contained in ASTM E 1150 standard [5]. It is defined as: *'The process of progressive localized permanent structural change occurring in a material subjected to conditions that produce fluctuating stresses and strains at some point or points and that may culminate in cracks or complete fracture after a sufficient number of fluctuations'*

Whereas in metallic materials the main process causing fatigue degradation is the growth of a single crack, which initiates from specific imperfections in the material's structure and propagates under specific loading conditions, the structural change caused by fluctuating stresses in composite materials is a much more complicated phenomenon due to their heterogeneous nature. In composite materials, four main fatigue damage mechanisms are observed: Matrix cracking, fibre breakage, delamination, and fibre-matrix interfacial debonding. Depending on the load characteristics, material properties and fibre orientation of each ply (stacking sequence) different combinations of the above mechanisms can propagate simultaneously at different locations of the composite laminate.

The complexity of fatigue damage evolution in composites has driven many researchers to develop a variety of models in an effort to predict the damage state in the micro or meso scale and relate it to the mechanical performance of composites under fatigue. Despite the effort spent on this task up to date, such models are not sufficiently mature, partly due to the complexity of the

phenomenon and the diversity of material combinations and partly due to the lack of extensive experimental databases for this kind of materials. To overcome this obstacle, various researchers have investigated the alternative of quantifying fatigue damage through its direct consequences, i.e. the change of the material's macroscopically observed mechanical properties. One such property, affected by the propagation of fatigue damage inside the composite, is its static strength, called in this case residual strength after fatigue. Its main asset is the bypass of the tedious task of modelling the actual fatigue damage mechanisms through use of macroscopic modelling of the fatigue response of composites being based on a fundamental, easily understandable mechanical property. Such phenomenological approaches constitute the only viable solution for use in structural design reality, until the deeper understanding of fatigue damage mechanisms supports the development of more efficient and - most important- applicable design tools.

The present work investigates different aspects of the static strength degradation phenomenon in composite materials under fluctuating stresses. The study focuses on a specific category of composite materials, Fiber Reinforced Plastics and more precisely Glass/Epoxy laminates. While such materials are widely used in advanced structures due to their good strength to weight ratio, high stiffness and excellent fatigue response, special focus is put on a specific application: Design and manufacturing of Wind Turbine Rotor Blades.

The design of such large scale structures from composite laminates comes up with major difficulties, considering the necessity for low weight and high stiffness as well as strength requirements under extreme and normal operating loads throughout an operational life extending over 20 years, usually under hostile conditions including extreme temperatures, humidity and corrosive environments. One of the issues arising is that in most cases fatigue design is based on the simplistic assumption of uniaxial loading while the fatigue response of the material is determined through uniaxial tests on typical lay-ups, neglecting the variety of stacking sequences and stress conditions developing into different parts of the structure. Another issue concerns the actual ultimate strength of the material after fatigue: Design strength used for dimensioning is provided by statically testing the virgin material, despite the fact that during its operating life, the structure will have to bear probably many times not only a



## *2. Forword*

number of extreme loads, but also a much greater number of smaller amplitude loading cycles which damage its internal structure affecting its residual static strength.

Even though issues like the ones mentioned above are accounted for by safety factors, some blades do fail and many more may be over-designed in order not to. In both cases, the accurate knowledge of the fatigue response and residual strength throughout the material's operational life is necessary in order either to predict more accurately a possible failure or reconsider some of the severe safety factors currently imposed during design.

In this study a number of issues related directly to static strength degradation are investigated: Does a composite laminate, part of a large composite structure, initially designed for specific extreme load cases, continue to satisfy initial design requirements after a fraction of its operational life? How could its life be predicted by designers for any stacking sequence undergoing complex cyclic stresses once basic ply properties are defined? Could this be achieved with reasonable effort and cost? In depth study of the strength degradation phenomenon and its integration into life prediction schemes under uniaxial and in-plane cyclic loads is performed in an attempt to shed some more light into the fatigue response of composite materials.



## 3 MODELING RESIDUAL STRENGTH

### 3.1 INTRODUCTION

Consider the general case of a composite material specimen, which has for example initial static tensile strength  $X$  on one axis and is subjected to a dynamic load history on the same axis. After a number of load fluctuations has been applied on the material, one will observe that when the specimen is statically tested, its static strength  $X_r$  will have eventually decreased. This phenomenon, correlated with fatigue damage is known as static strength degradation or residual strength after fatigue, denoted herein as  $X_r$ .

Residual strength, for a specific material, is in general a complicated function of the loading history. Assuming constant amplitude (CA) cyclic loading, residual strength can be assumed to be a function of maximum cyclic stress,  $\sigma_{\max}$ , fatigue stress ratio  $R$ , loading frequency  $\nu$ , number of applied cycles  $n$ , and of course of the initial static strength  $X$ :

$$X_r = f(\sigma_{\max}, R, n, \nu, X) \quad (1)$$

For the case of an anisotropic material system, e.g. an orthotropic FRP layer, strength is expressed rather by a tensor than a scalar quantity, i.e.  $X_i$  instead of  $X$ .

Generalizing Eq.(1) for the case of static strength degradation on one axis due to fatigue on another axis, or even due to a full plane fatigue loading, i.e.

$\{\sigma_x, \sigma_y, \sigma_s\}$ , yields:

$$X_{f_i} = f_i(\sigma_{x_{max}}, \sigma_{y_{max}}, \sigma_{s_{max}}, R_x, R_y, R_s, n, X_1, X_2, \dots) \quad (2)$$

where  $X_{f_i}$  denotes the  $i$ -th component of the residual strength tensor, expressed as a function,  $f_i$ , of in-plane fatigue parameters. For example, index  $i$  takes values 1, 2,... 5 for plane stress conditions. In this contracted tensor notation,  $X_1$  stands e.g. for the tensile strength along axis-1 of the material symmetry system,  $X_2$  for the tensile strength in direction-2,  $X_3$  for the compressive strength in direction-1 etc.

Therefore, the engineering model required for residual strength of an anisotropic laminate is of the general form of Eq.(2), assuming of course plane stress conditions and proportional loading, i.e. same number of cycles and at the same frequency for stress components  $\sigma_x$ ,  $\sigma_y$ ,  $\sigma_s$ . The problem is to conclude on the form of functions  $f_i$ , based on a properly designed experimental program.

In the following sections, attempts to approach this target are presented. As shown, only one-dimensional models are considered, i.e. models that consider residual strength degradation in a material axis due to fatigue loading along this same direction. Even though this simplification of the problem is not always accurate (for instance a unidirectional laminate cycled transversely to its fibres is sure to experience degradation of its compressive static strength in the fibre direction), taking into account such interactions would lead to highly complicated models while requiring huge experimental effort for material characterization. The models studied in this work are also phenomenological i.e. they do not correlate the actual state of damage inside the composite material to the macroscopically observed degradation of its static strength, the latter being assumed to depend only on the initial strength and stress characteristics. Further on, some of the models presented neglect the -usually large- scatter of residual strength and propose a deterministic formulation of the phenomenon, while others incorporate simple techniques in order to predict its probability distribution. Assuming deterministic description of residual strength as inapplicable in design and a rather oversimplifying approach, in the subsequent section a methodology is proposed, using simple assumptions and

### *3. Modeling Residual Strength*

state of the art models, for predicting residual strength at specific reliability levels. Various experimental data sets both from literature as well as produced in the course of this work, are used for assessing the models under consideration.



## 3.2 RESIDUAL STRENGTH MODELS

Both deterministic and statistical residual strength engineering models are based on a degradation equation which relates static strength to fatigue loading parameters such as stress level, stress ratio and number of cycles. The complexity of this equation varies from linear to multi parametric non-linear functions, while the parameters are estimated through application of different procedures. Three basic assumptions or conventions common to most models are made.

First, the initial static strength of the composite is assumed to be represented by a two parameter Weibull distribution of the form:

$$P_x = P(X \leq x_1) = 1 - \exp\left(-\left(\frac{x_1}{\beta}\right)^\alpha\right) \quad (3)$$

where  $\beta$  and  $\alpha$  are its scale and shape parameters respectively and  $x_1$  denotes the statistical variable of static strength.

For the study of the residual strength phenomenon it is convenient to derive the static strength probability distribution that excludes the part of the population that has static strength smaller than the maximum cyclic stress and therefore is expected to fail during the first loading cycle. This is achieved through the conditional probability given by the following expression:

$$P_{B/A} = \frac{P_{A \cap B}}{P_A} \quad (4)$$

Considering the reliability of static strength and the probability of static strength being greater than  $\sigma_{\max}$  to be given respectively by the following equations:

$$P_{\text{REL}} = P(X > x_1) = \exp\left(-\left(\frac{x_1}{\beta}\right)^\alpha\right) \quad (5)$$

$$P(X > \sigma_{\max}) = \exp\left(-\left(\frac{\sigma_{\max}}{\beta}\right)^\alpha\right) \quad (6)$$

the conditional reliability is derived through substitution of eqs (5 and 6) into Eq.(4):

$$P_{REL,\sigma_{max}} = P(X > x_1 / X > \sigma_{max}) = \exp\left(-\left(\frac{x_1}{\beta}\right)^\alpha + \left(\frac{\sigma_{max}}{\beta}\right)^\alpha\right) \quad (7)$$

Finally, the respective conditional probability is given by the following expression:

$$P_{X,\sigma_{max}} = P(X \leq x_1 / X > \sigma_{max}) = 1 - \exp\left(-\left(\frac{x_1}{\beta}\right)^\alpha + \left(\frac{\sigma_{max}}{\beta}\right)^\alpha\right) \quad (8)$$

The second convention is that the  $S-N$  curve of the material,  $\sigma_{max}$  being the maximum cyclic stress at a specified stress ratio  $R$ , is expressed by:

$$K\sigma_{max}^b N = 1 \quad (9)$$

with  $K$  and  $b$  the experimentally derived  $S-N$  parameters.

The third assumption is referred to as *the fracture condition*, implying that fatigue failure occurs when the residual strength reduces to the maximum applied cyclic stress:

$$X_r = \sigma_{max} \quad \text{when} \quad n = N \quad (10)$$

Some of the most typical residual strength models proposed in literature, since the phenomenon first started to be investigated for composite materials in the late 1960s, are presented in the following paragraphs.

### 3.2.1 Broutman & Sahu

Broutman and Sahu [6] have presented one of the first attempts for modeling static strength degradation of GFRP composites. In 1972, in an effort to develop a modified Palmgren-Miner rule which would account for load sequence effects, they assumed a simple model to predict residual strength, based on linear



strength degradation. Their experiments were performed on a Glass/Epoxy cross-ply laminate. Keeping the same symbols as before ( $N$  denoting the characteristic life of the specimen at strength level  $\sigma_{\max}$ ) their equation can be written as:

$$X_r = X - (X - \sigma_{\max}) \left( \frac{n}{N} \right) \quad (11)$$

As Broutman and Sahu point out themselves, the assumption of linear strength degradation does not agree well with the experimental results, especially in low fatigue stress levels, but it has been the best alternative in their study, given the few residual strength tests available.

### 3.2.2 Hahn & Kim

In their study [7] on fatigue life and proof testing of composites, Hahn and Kim introduce the concept of rate of change of residual strength. They assume the time rate of decrease of residual strength to be inversely proportional to the residual strength to a certain power. They also introduce an important assumption on the relation between static strength and fatigue life, stating that specimens with higher initial static strength have also longer fatigue lives. In their own words: «A specimen of a certain rank in the fatigue life distribution is assumed to be equivalent in strength to the specimens of the same rank in the static strength distribution». Chou and Croman named this later on “strength-life equal rank assumption” [8] or SLERA and investigated its validity through proof tests performed in [7], [9], [10].

In order to derive their residual strength relationship Hahn & Kim use the following assumptions:

a. The relation they propose for residual strength is the following rate type equation:

$$\frac{dX_r}{dt} = -AX_r^{-(c-1)} \quad (12)$$

b. The positive parameter  $A(\sigma)$  depends on the applied dynamic load  $\sigma(t)$  and the exponent  $c$  is a material constant. The behavior of the above equation is shown in Fig. 1. Depending on whether parameter  $c$  is above or below unity, the above equation represents a slow strength degradation followed by a rapid one, or vice versa. Fatigue failure occurs when the residual strength reduces to the maximum applied stress.

c. The above-mentioned SLERA.

d. Static strength is described by a two parameter Weibull Distribution (Eq.(8)) while the same formulation is used for the description of fatigue life:

$$P_N = P(N > x_2) = 1 - \exp \left[ - \left( \frac{x_2}{\tilde{N}} \right)^{\alpha_f} \right] \quad (13)$$

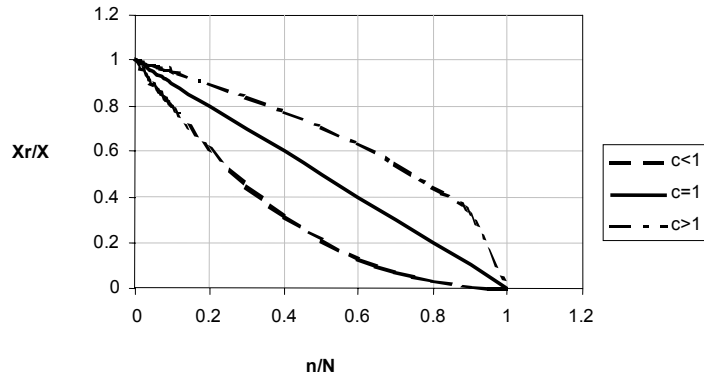


Fig. 1: Variations of residual strength degradation trends for different values of parameter  $c$ .

Integrating Eq.(12) between the initial time  $t_0$  and  $t$ , considering the case of CA fatigue, yields:

$$X_r^c = X^c - cD(t - t_0) \quad (14)$$

Hahn & Kim point out that parameter  $D$ , which is the integral of  $A(\sigma)$  from  $t_0$  to  $t$ , in general depends on the characteristics of fatigue loading. In constant amplitude fatigue, appropriate parameters are the stress amplitude, stress ratio and frequency. In their case [7], all the above are kept constant, so  $D$  is also a

### 3. Modeling Residual Strength

constant. Variables  $t$  and  $t_0$  can be replaced by load cycles  $n$  and  $n_0$  respectively, while by including the SLERA into Eq.(14) for  $t_0 = n_0 = 0$  one obtains the functional form of strength-life equal rank assumption:

$$N = \frac{(X^c - \sigma_{\max}^c)}{cD} \quad (15)$$

Solving Eq.(15) for  $cD$  and substituting in Eq.(14), from  $n_0 = 0$  to  $n$ , we obtain the residual strength degradation equation as a function of fatigue load parameters.

$$X_r^c = X^c - (X^c - \sigma_{\max}^c) \frac{n}{N} \quad (16)$$

The probability distribution of residual strength is derived by substituting Eq.(16) into Eq.(8) resulting in the following relationship where  $x_3$  is the statistical variable of residual strength:

$$P_{X_r} = P(X_r \leq x_3 / X > \sigma_{\max}) = 1 - \exp \left[ - \left( \frac{x_3^c - cDn}{\beta^c} \right)^{\frac{\alpha}{c}} + \left( \frac{\sigma_{\max}}{\beta} \right)^{\alpha} \right] \quad (17)$$

To derive the fatigue life distribution Hahn & Kim use the following reasoning: Those specimens that survive  $n$  cycles must at that point have strength greater than the applied stress  $\sigma_{\max}$ . Therefore at the particular stress level, the probability of fatigue life being greater than  $x_2$  is equal to the probability of the residual strength being greater than  $\sigma_{\max}$  when  $n = x_2$  :

$$P_N = P(N \leq x_2) = 1 - \exp \left[ - \left( \frac{\sigma_{\max}^c - cDx_2}{\beta^c} \right)^{\frac{\alpha}{c}} + \left( \frac{\sigma_{\max}}{\beta} \right)^{\alpha} \right] \quad (18)$$

Fatigue life tests performed on Glass/Epoxy are used to evaluate model optimum parameter values for  $c$  and  $D$ , using least squares fit.

This model, combined with a stiffness degradation theory, has been used lately by Whitworth [11] to predict residual strength. Experiments on [ $\pm 35$ ]<sub>2S</sub>

T300/5280 Graphite/Epoxy laminates show that it produces acceptable predictions of the residual strength probability distribution.

Hahn and Kim's model for  $c=1$  reduces to the linear degradation equation of Broutman and Sahu.

### 3.2.3 Yang et al.

Yang et al have, since 1975, published various works on residual strength [12]-[15] and in later works on stiffness degradation of composites due to fatigue [16], [17].

Their first attempt to model residual strength degradation is based on the assumption that residual strength is a monotonically decreasing function of load cycling, in a concept similar to that proposed by Hahn and Kim [7]. Their formulation is based on the following assumptions:

a. The rate equation describing residual strength is of the form:

$$\frac{dX_r(n)}{dn} = \frac{-f(\sigma_{\max}, f_r, R)}{cX_r^{c-1}} \quad (19)$$

in which  $f(\sigma_{\max}, f_r, R)$  is a function of the maximum cyclic stress, frequency and stress ratio, while  $c$  is a constant.

b. Static strength follows a 2-parameter Weibull distribution (see Eq.(3)):

c. The fracture condition (Eq.(10))

Integration of Eq.(19) from 0 to  $n$  results in:

$$X_r^c = X^c - f(\sigma_{\max}, f_r, R)n \quad (20)$$

Using assumptions (b) and (c) along with the proposed degradation function, Eq.(20), the following expression is obtained for the fatigue life  $N$ :

### 3. Modeling Residual Strength

$$N = \frac{X^c - \sigma_{\max}^c}{f(\sigma_{\max}, f_r, R)} \quad (21)$$

Combining eqs (21) and (3) yields the probability distribution of fatigue life:

$$P_N = P(N \leq x_2) = 1 - \exp \left[ - \left( \frac{x_2 + \frac{\sigma_{\max}^c}{f(\sigma_{\max}, f_r, R)}}{\frac{\beta^c}{f(\sigma_{\max}, f_r, R)}} \right)^{\frac{\alpha}{c}} \right] \quad (22)$$

Equating the scale parameter of this distribution with the characteristic life obtained from an S-N curve of the form:

$$K \sigma_{\max}^b \tilde{N} = 1 \quad (23)$$

One obtains the following expression for  $f(\sigma_{\max}, v, R)$ . [14]-[12],[18]-[20]:

$$f(\sigma_{\max}, f_r, R) = \beta^c K \sigma_{\max}^b \quad (24)$$

In the above equation,  $\sigma_{\max}$  is the maximum cyclic stress and  $\beta$  is the Weibull scale parameter of the static strength distribution. It must be noted that Yang proposes in his model the expression of the S-N curve, Eq.(23), in terms of the stress range  $\sigma_r$  rather than the maximum cyclic stress which is adopted in the present work. This choice does not actually affect the results as long as the fatigue and residual strength data used to fit the model refer to a single stress ratio  $R$ . If this is not the case, the stress ratio is included in the calculations as well, through the relationship  $\sigma_r = (1-R) \sigma_{\max}$ .

$K$ ,  $b$ , and  $c$  in Eq.24 are constants. The calculation of these three constant parameters, once the static strength distribution of the material is known, is performed with relatively limited experimental effort (30-40 fatigue and residual strength tests), implementing what is referred to as Equivalent Static Strength (ESS) concept, described below.

The final form of the residual strength degradation equation is:

$$X_r^c(n) = X^c - \beta^c K S^b n \quad (25)$$

The ESS concept assumes that each tested specimen (fatigue or residual strength) is attributed a fictitious static strength value (equivalent static strength) which can be calculated using Eq.(25) solved for  $X$ , through substitution of each specimen's data (i.e. maximum cyclic stress  $\sigma_{max}$ , number of fatigue cycles  $n$  and residual strength  $X_r$  measured). In the case of fatigue test data the residual strength is considered equal to the maximum applied cyclic stress according to the fracture condition while theoretically even static strength data can be implemented considering  $n=1$  and  $X_r=X$ . Consequently, a fictitious strength distribution in parametric form (depending on  $c$ ,  $b$  and  $K$ ) emerges. The parameters are subsequently determined through application of an adequate optimization procedure that aims to match the above parametric distribution to the experimentally obtained static strength distribution by means of minimizing the difference of their first moments. The objective function to be minimized can be expressed as:

$$f_{obj}(c,b,K) = \xi_1 (M_1 - m_1) + \xi_2 (M_2 - m_2) + \xi_3 (M_3 - m_3) \quad (26)$$

where  $M_i$  and  $m_i$  are the first three moments of the equivalent and experimental static strength distributions ( $m_1$  the mean,  $m_2$  the variance and  $m_3$  the skewness of the experimental static strength distribution), while  $\xi_i$  are weight factors expressing the relative importance of matching the means, variances or skewnesses of the two distributions.

Although the concept is straight forward, its application results in numerical problems since Eq.(26) comes with infinite local minima and is highly sensitive to the choice of the initial values, more so when the skewness is taken into account through a non-zero value of  $\xi_3$ . To overcome this implication,  $\xi_3$  is assumed zero with a negligible error since the static strength distribution is very close to symmetrical. Furthermore, the initial values for parameters  $b$  and  $K$  are taken the S-N curve parameters of the material at the specific stress ratio (which actually is their physical interpretation), assisting the routine to converge easily to a unique set of parameters which is far less dependent on the initial

### 3. Modeling Residual Strength

value of  $c$ , while the derived  $b$  and  $K$  remain very close to their initial values thus keeping their physical sense in Eq.(25).

The quality of the results can be easily assessed by plotting the CDF of the experimental data along with the data points of the ESS distribution, as for example in the following figure where an experimental data set of Yang is used [21]. Along with the experimental distribution, the equivalent static strength data obtained using the parameters proposed by Yang and the ones derived using the above procedure are shown.

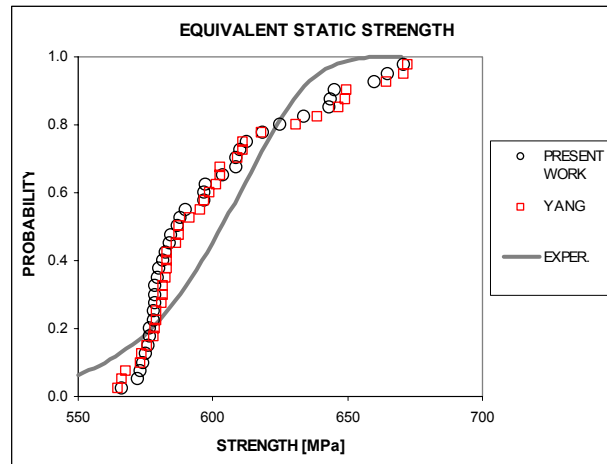


Fig. 2: Visual comparison of the equivalent static strength distributions (based on the parameters of Yang and the ones derived in the present work) and the experimentally obtained distribution.

The probability distribution of the residual strength after  $n$  cycles under a given stress level  $\sigma_{\max}$  is derived by combining eqs (25) and (3):

$$P_{X_r} = P(X_r \leq x_3) = 1 - \exp \left[ - \left( \frac{x_3^c + \beta^c K \sigma_{\max}^b n}{\beta^c} \right)^{\frac{\alpha}{c}} \right] \quad (27)$$

This first model of Yang is validated experimentally on a Graphite/Epoxy laminate under various fatigue loading conditions: Tension-tension fatigue,  $R=0.1$ , for  $\sigma_{\max}$  varying from 62% to 85% of the ultimate tensile strength [14], tension-compression fatigue,  $R$  from 0 to -0.3, and various  $\sigma_{\max}$  [12] (based on

data by Ryder and Walker from [22]), and shear loading, by testing axially  $[\pm 45]_{2s}$  coupons [20], [23]. The model has been also implemented in the investigation of load sequence effects using normal straight edge coupons [23] and bolted joints in composites [19]. Additionally, other researchers have used it for modeling residual strength e.g.[24].

In subsequent publications by Yang et al. [15], [25], the aforementioned methodology is generalized to include different kinds of composite materials, e.g. Glass/Epoxy, having a stronger residual strength degradation rate compared to the previously studied Graphite/Epoxy laminates.

The main new assumption on the theoretical derivation of the new model is the application of the SLERA. This statistically implies that X and N are completely correlated so they are functionally related. This functional relationship is derived from the equation of the corresponding distribution functions of  $P_X$  and  $P_N$ .

Equating the two distributions, eqs (8) and (13), one obtains:

$$N = \tilde{N} \left\{ \left( \frac{X}{\beta} \right)^{\frac{\alpha}{\alpha_f}} - \left( \frac{\sigma_{\max}}{\beta} \right)^{\frac{\alpha}{\alpha_f}} \right\} \quad (28)$$

Eq.(21) and Eq.(28) yield:

$$f(\sigma_{\max}, f_r, R) = \frac{1}{\tilde{N}} \cdot \frac{\left( \frac{X}{\beta} \right)^c - \left( \frac{\sigma_{\max}}{\beta} \right)^c}{\left( \frac{X}{\beta} \right)^{\frac{\alpha}{\alpha_f}} - \left( \frac{\sigma_{\max}}{\beta} \right)^{\frac{\alpha}{\alpha_f}}} \quad (29)$$

In this way, the resulting model includes also the statistical characteristics of the fatigue life. The final equation is:

$$X_r^c(n) = X^c - \frac{X^c - \sigma_{\max}^c}{X^{\omega} - \sigma_{\max}^{\omega}} \beta^{\omega} K \sigma_{\max}^b n \quad (30)$$



### 3. Modeling Residual Strength

In the above equation  $\omega = \frac{\alpha}{\alpha_f}$ , while  $\alpha$  and  $\alpha_f$  are the Weibull shape

parameters of static strength and fatigue life respectively.

This form constitutes a more generalized form of the residual strength model, since it includes the previous model of Yang for  $c=\omega$ , the model of Hahn and Kim for  $\omega=0$ , and the linear model of Broutman and Sahu for  $\omega=0$  and  $c=1$ .

The six model parameters are determined experimentally:  $\alpha$  and  $\beta$  from static strength tests,  $b$ ,  $\omega$  and  $K$  from fatigue life data and  $c$  from residual strength tests implementing the ESS concept described above. Experimental verification of this model is performed through testing Glass/Epoxy coupons (under dual stress level [25]) as well as Graphite/Epoxy ones (proof loading studies) with satisfactory results. Andersons et al. also adopt this model while investigating high cycle fatigue of GRP composites [26].

The probability distribution of residual strength is derived by replacing Eq.(30) into the static strength distribution, Eq.(3). The distribution derived this way is not in closed form since Eq.(30) cannot be solved for  $X$ . Nevertheless, it can be obtained indirectly by associating different levels of probability to the corresponding values of static strength using Eq.(3) and subsequently to the respective value of residual strength using Eq.(30).

In order to obtain the strength degradation equation at a specific reliability level  $1-P$  one has to follow the inverse procedure, i.e. solve the static strength distribution, Eq.(3), for the static strength and substitute it into Eq.(30). The expression derived this way is:

$$X_r^c = \beta^c \left[ -\ln(1-P) \right]^{\frac{c}{\alpha}} - \frac{\beta^c \left[ -\ln(1-P) \right]^{\frac{c}{\alpha}} - \sigma_{\max}^c}{\beta^\omega \left[ -\ln(1-P) \right]^{\frac{\omega}{\alpha}} - \sigma_{\max}^\omega} \beta^\omega K \sigma_{\max}^b n \quad (31)$$

The most general form of Yang model can be found in [13], [27], [28]. One more parameter  $\gamma$  is introduced to the degradation rate equation of residual strength, reflecting the non linear dependence of residual strength degradation rate on the number of fatigue cycles [13]:

$$\frac{d\left(\frac{X_r(n)}{\beta}\right)}{dn} = \frac{-\gamma n^\gamma f(\sigma_{\max}, X)}{c\left(\frac{X_r}{\beta}\right)^{c-1}} \quad (32)$$

Integration leads to:

$$X_r^c(n) = X^c - \frac{X^c - \sigma_{\max}^c}{(X^\omega - \sigma_{\max}^\omega)^\gamma} \beta^{\omega\gamma} (K\sigma_{\max}^b n)^\gamma \quad (33)$$

In Eq.(32), the expression of  $f(\sigma_{\max}, X)$  is derived by applying the fracture condition, Eq.(10), into the integral of Eq.(32), and replacing for the fatigue life the expression from Eq.(28).

Model parameters are determined as above, while  $\gamma$  is defined, similar to  $\omega$ , from residual strength test data by applying the ESS concept.

### 3.2.4 Chou & Croman

In the presentation of their theory on residual strength [8], [29], Chou and Croman consider the restrictions imposed by the assumptions of the models proposed by Hahn [7] and Yang's early model [14]. In particular, they point out that these models contain only two parameters, (e.g.  $f(\sigma_{\max}, f_r, R)$  and  $c$ ) which are determined completely by the fatigue life distribution data. Thus, for a given material under a specific cyclic load, once the static strength and fatigue life distributions are known, the residual strength throughout its fatigue life is completely defined. In other words, according to these models, two materials having the same static strength and fatigue life distribution must also have the same residual strength distribution.

In order to overcome this restriction, they propose, on one hand a different wear-out model, including an additional free parameter [8], and on the other hand they introduce the sudden-death model [29], as a limiting case in the residual strength study. This latter is the case for which the residual static strength remains constant, i.e. independent of load cycles, until immediately prior to failure and then drops suddenly.

Their degradation equation is based on the following assumptions:

### 3. Modeling Residual Strength

a. Static strength and fatigue life are two-parameter Weibull distributed (see Eqs.(3, 13)):

b. The SLERA, already introduced by Hahn and Kim, in the following form:

$$P_{REL,\sigma_{max}}(x_\gamma) = 1 - P_N(n_\gamma) \quad (34)$$

In this equation  $P_{REL,\sigma_{max}}(x_\gamma)$  is the conditional probability of a specimen having initial static strength greater than  $X_\gamma$ , where  $X_\gamma$  is the minimum required initial static strength for the specimen to withstand at least  $n_\gamma$  fatigue cycles, which is the number of cycles at which residual strength is measured.

c. The fracture condition, Eq.(10).

Assumptions (a) and (b) yield:

$$n_\gamma^{\alpha_f} = X_\gamma^\alpha - \sigma_{max}^\alpha \quad (35)$$

In the above equation, static strength and life are normalized by their Weibull scale parameters  $\beta$  and  $\tilde{N}$  respectively, while  $\alpha$  and  $\alpha_f$  are their respective shape parameters. The form of the degradation equation they adopt is the following:

$$X_r^\alpha = X_\gamma^\alpha - n_\gamma^{\alpha_f} \left( \frac{n}{n_\gamma} \right)^{i\alpha_f} \quad (36)$$

In other words  $X_\gamma$  and  $n_\gamma$  are the static strength and fatigue life respectively, that give a value of  $(1-\gamma)$  in the cumulative distribution function (CDF). By assuming different values for parameter  $i$ , a family of degradation curves is obtained, ranging from gradual wear-out to sudden death behavior, as seen in Fig. 3.

The probability distribution of residual strength derived by Chou and Croman [8] can be computed only numerically.

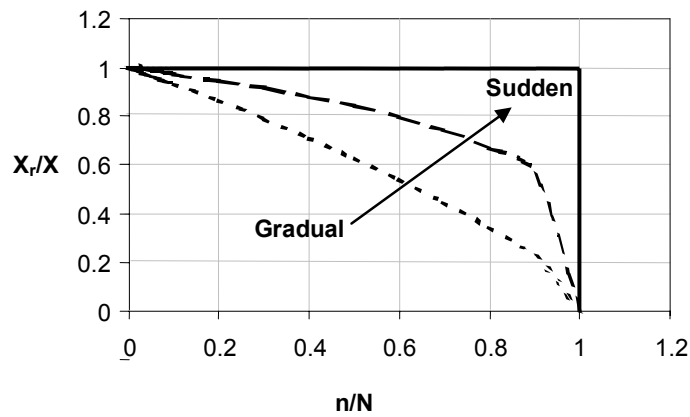


Fig. 3: Transition of residual strength models from gradual wear out to sudden death.

### 3.2.5 Harris et al.

Bryan Harris and his research group have published a number of papers on the fatigue behavior of various types of composite materials [30]-[33]. Their work includes life prediction of Carbon T800 [34] as well as GRP, CFRP and KFRP exposed to various environmental conditions [30]. They have also investigated the fatigue behavior of hybrid Carbon/E Glass/Kevlar composites [31]. In reference [30] they query the validity of the wear out model of Broutman and Sahu, stating that it oversimplifies to some extent the sequence of events immediately preceding failure. In their first approach, they use the resemblance of residual strength test on GRP with the decay curve in viscoelasticity or relaxation, to introduce the following rate equation for residual strength, which they call the *decay model*.

$$\frac{dX_r}{dn} = -BX_r \quad (37)$$

In the above equation B is a positive constant, depending linearly on  $\sigma_{max}$ :

$$\log B = \log D + C\sigma_{max} \quad (38)$$

Integration of Eq.(37) yields:

$$X_r = X \exp\{D \exp(C \sigma_{\max})\} \quad (39)$$

The above formulation was quickly abandoned by the authors. A second approach, called *interaction model*, is motivated by the apparent similarity of the residual strength curves at various stress levels, and the possible event of some appropriate normalized formulation. Towards this direction, they introduce the residual strength ratio as:

$$r = \frac{X_r - \sigma_{\max}}{X - \sigma_{\max}} \quad (40)$$

As well as the cycle (or log-time) ratio:

$$t = \frac{\log n - \log 0.5}{\log N - \log 0.5} \quad (41)$$

These two normalized quantities are combined under the appropriate boundary conditions, i.e. points (1,0) and (0,1), through the following expression:

$$t^x + r^y = 1 \quad (42)$$

x and y are determined through fitting on residual strength data, using one of the different procedures proposed in [30].

### 3.2.6 Schaff & Davidson

Schaff and Davidson [43] have adopted in their study on life prediction the following assumptions:

a. The degradation equation of residual strength is of the following form.

$$X_r(n) = X - f(X, \sigma_{\max}, R)n^v \quad (43)$$

b. Both fatigue life and static strength are described by two parameter Weibull distributions in the form of Eqs.(3),(13).

c. The fracture condition, Eq.(10).

In Eq.(43)  $v$  is called *strength degradation parameter*. By imposing the failure condition, the above equation takes its final form:

$$X_{r(n)} = X - (X - \sigma_{\max}) \left( \frac{n}{N} \right)^v \quad (44)$$

Eq.(44) is identical to the one used by Reifsnider e.g. [35] for modeling static strength degradation of his *Critical Element Model*.

An innovative point in their paper is the formulation of the residual strength Weibull probability distribution with a shape parameter that is not constant but depends linearly on the number of load cycles. This is to take into account the increased scatter of residual strength, observed at higher life fractions. The shape parameter of the Weibull distribution of residual strength is arbitrarily assumed to vary linearly between that of the static strength distribution,  $\alpha$ , and that of the fatigue life,  $\alpha_t$ . The form of the predicted CDF is:

$$P_{X_r} = P(X_r \leq x_3) = 1 - \exp \left[ - \left( \frac{x_3}{X - (X - \sigma_{\max}) \left( \frac{n}{N} \right)^v} \right)^{\alpha - (\alpha - \alpha_t) \left( \frac{n}{N} \right)} \right] \quad (45)$$

The parameter  $v$  is determined using optimization schemes that try to match the above parametric CDF with an experimental one.

### 3.2.7 Sendeckyj

In a review work on life prediction of composite materials [36], Sendeckyj is referring extensively on residual strength theories as a means of predicting life under constant and variable amplitude fatigue, as well as their statistical formulations. He resumes a number of previously released residual strength theories into 6 models, based on the following assumptions:

### 3. Modeling Residual Strength

- a. The static strength is two-parameter-Weibull distributed (Eq.(3)).
- b. The residual static strength  $X_r$  after  $n$  cycles of constant amplitude loading is related to the initial static  $X$ , by a deterministic equation of the form:

$$\frac{dX_r}{dn} = -\left(\frac{1}{Y}\right) f \sigma_{\max}^{\varphi} X_r^{(1-\varphi)} \quad (46)$$

In which  $f$  and  $\varphi$  are two dimensionless functions, independent of stress.

- c. The fracture condition, Eq.(10).

Integration of Eq.(46), assuming the residual strength equal to the initial static strength for failure during the first cycle, yields the following expression, in which  $\varphi$  has been replaced by  $1/S$ :

$$X = \sigma_{\max} \left[ \left( \frac{X_r}{\sigma_{\max}} \right)^{\frac{1}{S}} + (n-1)f \right]^S \quad (47)$$

Eq.(47) can produce a variety of residual strength degradation models for different expressions of the parameters  $S$  and  $f$  (see Table1).

Table 1: Residual strength degradation theories.  $S_0$ ,  $D$ ,  $C$ ,  $G$  are constant model parameters

	$S$	$f$
W1	$S_0$	1
W2	$S_0$	$C$
W3	$S_0$	$C(1-R)^G$
W3A	$S_0(1-R)^G$	$C(1-R)^G$
W4	$S_0 + D(1-R)^G$	$C(1-R)^G$
W4A	$S_0(1-R)^D$	$C(1-R)^G$

According to Sendecyk's own words: "Fatigue model W1 is the classical power law fatigue criterion giving a straight line representation of the S-N curve on a

log-log plot. It is the simplest model that one can use. Fatigue model W2 is the wearout model in the form used by Sendeckyj [37]. Since it assumes that S and f are constant, it can only be used to correlate fatigue data at a specified stress ratio. Fatigue model W3 is a three parameter fatigue model that is similar to those used by Yang (discussed above) or Whitney [38],[39]. It is the simplest fatigue model that can take into account the stress ratio dependence. It gives the same asymptotic slope for the S-N curve at different stress ratios, thus it does not model the dependence of the slope of the S-N curve on R. Models W4 and W4A are four parameters models that attempt to account for the R-dependence of the slope of the S-N curve. As it was shown, these fatigue models do not yield unique estimates of the model parameters. Finally, fatigue model W3A is a special case of fatigue model W4A. It is a three-parameter fatigue model that takes into account the R-dependence of the slope of the S-N curves. Moreover it corresponds to one of the optimum selections of parameters in model W4A.”

Applying assumption (c) upon the general expression of the residual strength model, Eq.(47), we obtain the shape of the S-N curve associated with the assumed residual strength degradation model:

$$X = \sigma_{\max} \left[ 1 + (N - 1)f \right]^{-S} \quad (48)$$

The probability distribution of fatigue life is derived from assumption (a) and Eq.(48), considering conditional probabilities to account for the fact that the initial static strength should be greater than the maximum applied stress:

$$P(N < x_2 / X \geq \sigma_{\max}) = \exp \left\{ \left( \frac{\sigma_{\max}}{\beta} \right)^\alpha - \frac{x_2 - \left( \frac{1-f}{f} \right)}{\left( \frac{\beta}{\sigma_{\max}} \right)^{\frac{1}{S}} f} \right\}^{S\alpha} \quad (49)$$



### 3. Modeling Residual Strength

The probability distribution of residual strength is derived from assumption (a) and Eq.(47), considering also conditional probabilities to account for the fact that the residual strength should be greater than the maximum applied stress:

$$P(X_r < x_3 / X \geq \sigma_n) = \exp \left\{ \left( \frac{\sigma_n}{\beta} \right)^\alpha - \left[ \left( \frac{x_3}{\beta} \right)^{\frac{1}{S}} + \left( \frac{\sigma_{\max}}{\beta} \right)^{\frac{1}{S}} f(n-1) \right]^{S\alpha} \right\} \quad (50)$$

where

$$\sigma_n = \sigma_{\max} [1 + (n-1)f]^S \quad (51)$$



## 3.3 MODIFIED MODELS

### 3.3.1 Introduction

Some of the models presented in the above section, like the models of Yang or Sendekyj, result in equations describing the probability distribution of residual strength, while others treat the phenomenon in terms of averaging values putting aside its statistical characteristics. While both approaches have been shown to be based on a deterministic degradation equation typical of each model, probabilistic models combine it with simple statistical assumptions to obtain a formulation of the strength's Cumulative Density Function (CDF). Nevertheless, CDF formulations in these works do not require a priori the knowledge of the statistical behavior of fatigue life, and for good reason, since residual strength is often used as a means for ultimately predicting this very statistical behavior of fatigue life. This approach usually leads to predicting more or less truncated fatigue lives, thus inducing in the applications considered herein an error which could be easily avoided, since the fatigue behavior of the material is one of the few properties whose accurate knowledge is a prerequisite for certification of structural designs. Consequently, the methodology proposed in this section considers that fatigue life and its statistical characteristics are known, while the focus is put on the prediction of residual strength at a specific level of reliability through use of simple statistical assumptions and residual strength degradation formulations.

Three basic assumptions are made. First, the initial static strength of the composite is assumed as previously to be described by a two parameter Weibull distribution of the form of Eq.(3)

The second assumption is the 'Strength Life Equal Rank Assumption' already cited above. In fact the SLERA is extended herein since it is assumed that a specimen has the same rank on all three probability distributions of static strength, fatigue life and residual strength. This assumption, when referring to a specific coupon, is expressed by the following equation:

$$P_x = P_{x_r} = P_N = P \quad (52)$$

The third assumption is the fracture condition, expressed by Eq.(10).

### 3.3.2 Statistical S-N formulation

In order to describe fatigue life at a certain probability level, the model of Whitney [42], relating fatigue stress and life at a specific reliability level, is implemented. This methodology is adopted, since it is based on the solid ground of direct processing of experimental data bypassing the need for using any assumption apart from considering the Weibull distribution adequate for fitting the fatigue life data. Furthermore, its implementation requires no more testing than the typical 15 to 20 fatigue life experiments necessary for any trustworthy S-N curve derivation.

The method of Whitney is based on Weibull statistics assumption for fatigue life tests. Tests are performed at  $m$  stress levels each containing  $n_i$  ( $i=1, \dots, m$ ) fatigue data points. The data set at each stress level is fitted to a Weibull distribution:

$$P(N_i \geq x_{3i}) = \exp\left(-\left(\frac{x_{3i}}{\tilde{N}_i}\right)^{\alpha_{fi}}\right) \quad i=1, \dots, m \quad (53)$$

$\tilde{N}_i$  and  $\alpha_{fi}$  are parameters of the distributions which are calculated using Maximum Likelihood Estimators. Subsequently, the experimental fatigue lives at each stress level are normalized by the respective characteristic life  $\tilde{N}_i$ . The resulting population is also assumed to follow a Weibull distribution:

$$P(\Omega \geq \Omega^*) = \exp\left(-\left(\frac{\Omega^*}{\Omega_0}\right)^{\alpha_f}\right) \quad (54)$$

in which  $\Omega$  is the *normalized life* quantity and  $\Omega^*$  its variable. The parameters of this 'global' Weibull distribution are  $\Omega_0$  and  $\alpha_f$  which are derived using as above

Maximum Likelihood Estimators. The scale parameter  $\Omega_0$  is expected to be very close to unity, otherwise the Weibull scale parameter of life at each stress level  $\tilde{N}_i$  is corrected by multiplication  $\Omega_0$  times. After this procedure has converged, the fatigue life  $N$  can be related to the stress level  $\sigma_{\max}$  at a specific reliability level  $1-P_N$ , using the following relationship:

$$N = \frac{[-\text{Ln}(1-P_N)]^{\frac{1}{\alpha_f}}}{K\sigma_{\max}^b} \quad (55)$$

Parameters  $K$  and  $b$  are derived through fitting of the following S-N formulation to the  $(\sigma_{\max i}, \tilde{N}_i)$  data points:

$$K\sigma_{\max}^b \tilde{N} = 1 \quad (56)$$

Once the terms of Eq.(55) are determined, the procedure described in the following paragraphs is followed to derive the reliability based residual strength formulations, for different degradation models:

### 3.3.3 Modified Broutman & Sahu

A prediction of the cumulative probability function (CDF) of residual strength is derived solving Eq.(11) for the initial static strength  $X$ , and substituting it into the static strength distribution. Since the residual strength distribution is based on the specimens having strength greater than  $\sigma_{\max}$ , the truncated static strength distribution, Eq.(8), is used leading to:

$$P_{X_r} = P(X_r < x_3 / X \geq \sigma_{\max}) = 1 - \exp \left[ - \left( \frac{x_3 - \sigma_{\max} \left( \frac{n}{N} \right)}{\beta \left( 1 - \frac{n}{N} \right)} \right)^\alpha + \left( \frac{\sigma_{\max}}{\beta} \right)^\alpha \right] \quad (57)$$

When N is replaced by Eq.(55) into Eq.(57) and taking into account Eq.(52), the equation used for calculation of the residual strength at stress level  $\sigma_{\max}$ , after n load cycles and at a specific reliability level 1-P, becomes:

$$X_r = \beta \left( 1 - \frac{nK\sigma_{\max}^b}{[-\ln(1-P)]^{\frac{1}{\alpha_r}}} \right) \cdot \left( \left( \frac{\sigma_{\max}}{\beta} \right)^\alpha - \ln(1-P) \right)^{\frac{1}{\alpha}} + \frac{nK\sigma_{\max}^{b+1}}{[-\ln(1-P)]^{\frac{1}{\alpha_r}}} \quad (58)$$

Eqs.(11) & (58) will be referred to as the linear model and will be denoted by BR.

### 3.3.4 Modified Hahn & Kim model

In order to generalize the model for various stress levels, the stress dependent parameter D must be expressed as a function of loading characteristics. Such a dependency is expressed already in Eq.(16)

Solving Eq.(16) for X and substituting into Eq.(8) gives an expression to predict the probability distribution of the residual strength:

$$P_{X_r} = P(X_r < x_3 / X \geq \sigma_{\max}) = 1 - \exp \left( - \left( \frac{x_3^c - \sigma_{\max}^c \frac{n}{N}}{\beta^c \left( 1 - \frac{n}{N} \right)} \right)^{\frac{\alpha}{c}} + \left( \frac{\sigma_{\max}}{\beta} \right)^\alpha \right) \quad (59)$$

The engineering model defined by Eqs.(16), (59) will be denoted as H.

### 3.3.5 Modified Interaction model

The deterministic interaction model by Harris et al. is also enhanced with statistical features. The CDF of residual strength can be derived as above using the degradation equation and the static strength distribution: Eqs.(40, 41) are substituted into Eq.(42), which is solved for the static strength X and substituted

into Eq.(8). The resulting probability distribution according to the, henceforth denoted, INT model is given by:

$$P_{X_r} = P(X_r < x_3 / X \geq \sigma_{\max}) = 1 - \exp\left(-\left(\frac{x_3 - \sigma_{\max}(1-p)}{\beta p}\right)^\alpha + \left(\frac{\sigma_{\max}}{\beta}\right)^\alpha\right) \quad (61)$$

where

$$p = (1 - t^x)^{\frac{1}{y}}$$

Solving for the residual strength one obtains the degradation equation according to the, henceforth denoted INT-P model, at a given reliability level 1-P:

$$X_r = \left(\left(\frac{\sigma_{\max}}{\beta}\right)^\alpha - \text{Ln}(1-P)\right)^{\frac{1}{\alpha}} \beta q + \sigma_{\max}(1-q)$$

where

$$q = \left(1 - \frac{\left(\left(\frac{\log n - \log 0.5}{\log\left(\frac{[-\text{Ln}(1-P)]^{\frac{1}{\alpha_r}}}{K\sigma_{\max}^b} - \log 0.5}\right)\right)^x\right)^{\frac{1}{y}}}{\log\left(\frac{[-\text{Ln}(1-P)]^{\frac{1}{\alpha_r}}}{K\sigma_{\max}^b} - \log 0.5}\right)}\right)^{\frac{1}{y}} \quad (61)$$

### 3.3.6 Non Linear model

The linear strength degradation model presented above can be modified to account for material non linear degradation behavior, introducing an additional parameter as shown in the following equation:

$$X_r = X - (X - \sigma_{\max})\left(\frac{n}{N}\right)^k \quad (62)$$

Eq.(62), which has been also used by other researchers, e.g. Schaff [43], Reifsneider [35], includes one parameter,  $k$ , and can predict apart from the linear case (for  $k=1$ ), a steep initial fall in strength slowing down up to fracture ( $k<1$ ) or an initially constant static strength followed by a steep drop of strength during the last part of the specimen's life ( $k>1$ ), that latter being close to a *sudden death* behavior for  $k>>1$ .

Exponent  $k$  can also be considered to be a function, e.g. of fatigue loading parameters. Experimental results from tensile ( $R=0.1$ ) cyclic tests on  $[\pm 45]_s$  G/Ep coupons suggest that  $k$  in Eq.(62) can be modeled as a function of the fatigue life fraction. A suitable expression for function  $k$  is given by [44]:

$$k = k_1 \exp\left(k_2 \frac{n}{N}\right) \quad (63)$$

The CDF of residual strength is obtained through substitution of Eq.(62) into the static strength distribution, Eq.(8):

$$P_{X_r} = P(X_r < x_3 / X \geq \sigma_{\max}) = 1 - \exp\left[-\frac{\left(x_3 - \sigma_{\max} \left(\frac{n}{N}\right)^k\right)^\alpha}{\beta \left(1 - \left(\frac{n}{N}\right)^k\right)} + \left(\frac{\sigma_{\max}}{\beta}\right)^\alpha\right] \quad (64)$$

The reliability based degradation equation is derived as above and is given by the following expression:

$$X_r = \left(\left(\frac{\sigma_{\max}}{\beta}\right)^\alpha - \ln(1-P)\right)^{\frac{1}{\alpha}} \beta \left(1 - \left(\frac{nK\sigma_{\max}^b}{[-\ln(1-P)]^{\frac{1}{\alpha_f}}}\right)^k\right) + \sigma_{\max} \left(\frac{nK\sigma_{\max}^b}{[-\ln(1-P)]^{\frac{1}{\alpha_f}}}\right)^k \quad (65)$$



### *3. Modeling Residual Strength*

The approach of constant  $k$  will be referred to as the REI model, while when Eq.(63), in which  $N$  is taken from the reliability based form described by Eq.(55), takes the place of parameter  $k$  in Eq.(62), the model will be referred to as OM.

## 3.4 EXPERIMENTS

### 3.4.1 Published Data Sets

Although several researchers have performed and shared with the scientific community residual strength experiments on a variety of materials and lay-ups, limited are the cases when such data sets are wide enough or include all the information necessary for obtaining a clear, global picture of the residual strength degradation phenomenon in composite materials. Usually residual strength tests are performed at a specific cyclic stress and fraction of life, e.g. the tests performed on cross-ply specimens by Broutman & Sahu [6], on MD Graphite/Epoxy coupons of Yang and Liu [14] or tests by Ryder and Walker presented in [22]. Almost in all cases cyclic loads in the tension-tension quadrant is considered, while possible degradation of the compressive static strength is altogether overlooked. Few are also the cases where residual strength is investigated at various stress levels and throughout a material's entire fatigue life, as for instance in the studies of Anderson et al. [26]. Even fewer data sets aim to exploring the fully in-plane strength degradation behavior of a unidirectional or multidirectional laminate, one of the few exceptions being the tests on Graphite/Epoxy performed by Shokrieh & Lessard [45] who show results at  $R=0.1$  and  $R=10$  for each in-plane principal direction and at  $R=0.1$  in shear.

The reason for such a limited variety of comprehensive residual strength experimental data sets is simple: The creation of such data bases is extremely expensive in terms of both testing time and actual financial cost. This becomes evident by considering that a single fatigue test can last for weeks or even months and that in-detail residual strength characterization at a single stress ratio might require several times the effort necessary for the determination of a single S-N curve.

In the present study three published data sets are used for validation of the various features of the residual strength formulations that have been presented in the previous section. The first one is a data set produced by Ryder and Walker [22] on 934/T300 Graphite/Epoxy laminates with  $[0/45/90/-45_2/90/45/0]_2$  layup. The stress ratio is  $R=0$ , i.e. purely tensile with the minimum load equal to zero, and loading frequency of fatigue tests is 10 Hz. The second one is a data set produced by Yang et al. [21]. The Graphite/Epoxy material used in that case is the Rigidite 5020-Thornel 300 system and the layup used is a  $[90/45/-45/0]_2$ . As before, testing frequency is kept constant at 10 Hz while the stress ratio is again in the T-T domain equal to  $R=1/36$ . Both data sets are

### 3. Modeling Residual Strength

used for validating the CDF predictions of the various models since they mainly include satisfactorily populated residual strength samples (about 20 data points) at specific stress levels and number of cycles.

The third data set is the one reported by Anderson et al. [26]. It is one of the few existing comprehensive data sets and provides residual strength information at a number of different life fractions of a single stress level. This makes it convenient first of all for the assessment of the degradation trend predicted by various models and secondly for the validation of reliability based predictions, since a satisfactory number of coupons are tested at each life fraction. Moreover, the material investigated is of interest in the frame of this work, since it is a Glass/Polyester composite in a stacking sequence typical of the spar region of wind turbine rotor blades. The lay-up is [CSM/fabric/(CSM/UD)<sub>2</sub>]<sub>s</sub>, where CSM stands for chopped strand mat and fabric is assumed to be a woven or non-crimp layer of unknown type (possibly a [0/90]).

Since the experimental results are not directly available, the values are interpreted by the graphs shown in [26]. The static strength and fatigue life data are presented in Table 2 and Table 3. Residual strength data are randomly divided in two groups. The first one, shown in Table 4, is used for implementation of the various models and derivation of their parameters while the second one, shown in Table 5, is used for validating models predictions.

Table 2 Static strength data from Anderson et al. [26].

Static Strength (Mpa)	
678.00	650.50
697.00	663.70
672.00	659.30
687.00	665.80
630.00	663.80
688.00	712.00
656.00	687.00

Table 3 Fatigue life data from Anderson et al. [26], under R=0.1 stress ratio.

Stress Level $\sigma_{max}$ [Mpa]	Cycles to failure	Stress Level $\sigma_{max}$ [Mpa]	Cycles to failure	Stress Level $\sigma_{max}$ [Mpa]	Cycles to failure
235.2	925000	284.2	75000	323.4	23000
264.6	216000	284.2	85000	323.4	23000
264.6	281000	284.2	114000	323.4	25000
264.6	315000	284.2	133000	323.4	25000
264.6	319000	284.2	163000	323.4	27000
264.6	346000	284.2	213000	323.4	33500
264.6	398000	284.2	227000	323.4	34000
264.6	413000	284.2	261000	323.4	35000
264.6	630000	294.0	43500	303.8	74000

Table 4 Verification residual strength data set from Anderson et al. [26] (R=0.1).

Residual Strength [MPa]	Number of Cycles	Fatigue Stress Level $\sigma_{max}$ [Mpa]	Residual Strength [MPa]	Number of Cycles	Fatigue Stress Level $\sigma_{max}$ [Mpa]
575.30	25000	284.20	531.60	100000	284.20
586.80	25000	284.20	470.70	100000	284.20
594.50	25000	284.20	559.00	100000	284.20
630.80	25000	284.20	548.00	100000	284.20
644.80	25000	284.20	534.00	100000	284.20
546.30	50000	284.20	528.90	124000	284.20
559.80	50000	284.20	500.00	124000	284.20
498.80	50000	284.20	585.90	124000	284.20
567.50	50000	284.20	517.00	124000	284.20
575.70	50000	284.20	542.40	124000	284.20
539.10	50000	284.20	369.00	124000	284.20
613.50	50000	284.20			

### 3. Modeling Residual Strength

Table 5 Residual strength data set from Anderson et al. [26], used for parameter estimation (R=0.1).

Residual Strength [MPa]	Number of Cycles	Fatigue Stress Level $\sigma_{max}$ [Mpa]	Residual Strength [MPa]	Number of Cycles	Fatigue Stress Level $\sigma_{max}$ [Mpa]
579.6	25000	284.2	624.9	200000	235.2
614.0	25000	284.2	549.9	400000	235.2
513.4	50000	284.2	602.0	400000	235.2
579.7	50000	284.2	597.2	400000	220.5
410.3	100000	284.2	606.3	400000	220.5
493.1	100000	284.2	621.2	400000	220.5
362.8	124000	284.2	640.7	400000	220.5
536.0	124000	284.2	673.8	400000	220.5
600.1	200000	235.2			

## 3.4.2 OPTIMAT BLADES

Probably the most extensive and detailed experimental program investigating residual strength degradation in Glass/Epoxy composites up to date has been undertaken in the frame of the EU project OPTIMAT BLADES [1]. Its major outcomes are presented in this paragraph.

The project's overall aim has been the proposal of accurate design recommendations for the optimised use of contemporary Glass/Epoxy composite materials as well as to achieve improved reliability within wind turbine rotor blades. The subjects investigated during the project are load sequence effects and variable amplitude loadings, complex stress states, techniques for repairing damaged composite laminates, the influence of extreme environmental conditions on material properties, residual strength and non destructive techniques for damage monitoring in composites.

All the above would provide a better understanding of the material's behaviour under different types of loads and environmental conditions, as well as optimal use of the material through better understanding of the safety factors already imposed by certification organizations. Considering all these, the major deliverable of the project would be improved design recommendations for the next generation of rotor blades.

### 3.4.2.1 Experimental program

A Glass/Epoxy material consisting of a single type of unidirectional lamina has been chosen as reference material for all experiments. Amongst the large variety of tests

performed, considerable effort and time has been spent for the full in-plane characterization of the basic UD lamina, called henceforth reference material. Its characterization has been performed in direction parallel to the fibres, transversely to them as well as under in-plane shear. In detail, the experimental program includes the definition of the static strength properties of the material in tension, compression and shear, as well as fatigue life characterization at three different R ratios, 0.1, -1 and 10, for each property, in order to define fatigue response under purely tensile, alternating and purely compressive cyclic loads. Fatigue life tests in shear has been performed only for R=0.1, while exceptionally the coupon geometry used is the one proposed by the respective ISO 14129 standard [46].

The residual strength test program is designed as follows: Strength at each material's direction is assumed to be affected only by stresses on the same direction. This is not necessarily true in all cases, for instance the residual compressive strength in the on-axis direction is affected by tension-tension fatigue transversely to the fibres, since the latter one creates longitudinal cracks that intensify fibre instability problems. Nevertheless, investigating such interactions would lead, apart from the obvious issues in designing and performing such tests, to an explosion of the -already vast- test matrix. Consequently each coupon fatigued at a single stress ratio is afterwards tested to fracture under quasi-static loading. The same three stress ratios as for the case fatigue life tests are used for the case of residual strength in the two symmetry directions of the basic UD ply: R=0.1, -1 and 10. Three stress levels are then chosen, corresponding to approximate lifetimes (with some exceptions) of 1,000, 50,000 and 1,000,000 cycles while at each stress level fatigue is interrupted after 20%, 50% and 80% of the nominal life. To each of those life fractions a set of 8 coupons is fatigued and subsequently statically loaded to failure, half of this sample in tension and half in compression. This way the residual tensile (RST) and compressive (RSC) strength at the specific life fraction, stress level, R ratio and material's direction is defined. The setup of the experimental program is given schematically in Fig. 4 (see also [47]).

### 3. Modeling Residual Strength

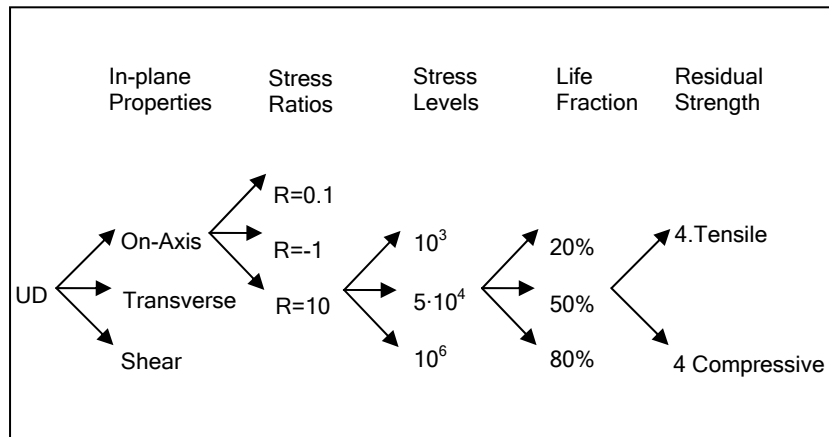


Fig. 4 Schematic representation of the residual strength characterization test matrix

This residual strength test program includes 72 tests per stress ratio and a total of 216 tests per material's principal direction, half of them ultimately tested in tension and half in compression. In the shear direction, due to the geometry used and the reasonable assumption that positive and negative shear would produce the same fatigue damage, only RST tests have been performed after cycling under R=0.1 (72 coupons tested).

In total, the test matrix for the definition of the basic properties of the UD reference lamina ideally includes 105 fatigue tests, 125 static tests and 504 residual strength tests. This substantial amount of experiments has been partitioned between 5 research institutes:

University of Patras (UP-Greece)

Council for the Central Laboratory of the Research Councils (CCLRC-UK)

Center for Renewable Energy Sources (CREG-Greece)

Vrije University Brussel (VUB-Belgium)

WMC knowledge Centre (Delft University/ECN-The Netherlands)

Due to premature failures and test program's rearrangements, the testing performed during the project and discussed in this work, includes 132 static strength tests (all performed by UP), 184 fatigue tests used for the determination of 7 SN curves (performed mostly by UP) and a total of 468 residual strength tests (divided between

the partners listed above), both RST and RSC including 133 premature failures during fatigue.

### **3.4.2.2 Test Procedure**

All tests have been performed at hydraulic test rigs using hydraulic gripping and either displacement (static tests) or force control (fatigue). MTS strain gauges have been attached to the coupons: Coupons used for determination of static tensile strength in the direction parallel to the fibres transversely to them as well as in shear, have been equipped with a 6mm strain gauge rosette on one side and a single 6mm gauge on the other, while compressive strength coupons were equipped with single 6mm back to back strain gauges.

All specimens intended for fatigue testing have been equipped with back to back single gauges (6mm length) to monitor bending, buckling or other suspect behavior. Strain measurements are taken during a small number (usually 5) of very slow cycles applied prior to normal fatigue. The elastic modulus of each coupon is also measured during this step. The frequency of the fatigue test varies according to the stress level, in order to retain the maximum temperature (measured on the surface of the specimen with a thermocouple) below 35°C. This choice is considered satisfactorily safe taking in account that the  $T_G$  of the specific epoxy matrix is at 80°C. For the safe choice of test frequency a thermocouple is applied on the surface of a number of specimens of each S-N curve near the tabs where the temperature rise is expected to be greater. In case the temperature read reaches the limit the test frequency is reduced and the procedure repeated. An -admittedly limited- assistance in the cooling of the specimens is provided by retaining a constant air flow around the coupons during cycling, along with the use of air-conditioning to keep room temperature around 20°C.

The definition of the testing frequency in each case has been optimized with great care, in order to satisfy the temperature criterion while the fatigue proceeds as fast as possible to keep testing times as low as possible. Once a reference frequency is optimized through testing at a specific stress level, frequency at other stress levels can be defined based on the reference one, through the following equation whose derivation is based on the strain energy release rate [48].



$$\frac{f_r}{f_{ref}} = \left( \frac{\sigma_{max_{ref}}}{\sigma_{max}} \right)^2 \quad (66)$$

Testing frequencies at an indicative stress level corresponding to fatigue life of 50,000 cycles, according to the guideline defined during the benchmark tests ([49], [50]), are summarized in Table 6.

Table 6 Indicative test frequencies, for various types of fatigue tests, referring to a fatigue life of 50,000 cycles.

Property	Stress Ratio	Stress Level	Frequency [Hz]
Parallel to Fibres	0.1	1.43 kN/mm	3.15
	-1	0.97 kN/mm	2.17
	10	-	-
Transversely to Fibres	0.1	31.85 MPa	3.03
	-1	23.26 MPa	3.13
	10	126.11 MPa	4.04
±45°	0.1	63.60 MPa	1.99

### 3.4.2.3 Coupon Geometry

The geometry of the test specimens is an issue of major importance during mechanical testing, since specific failure modes must be achieved for each type of test, which in turn requires control of the stress fields developed during loading of the coupons. That is the reason why standardization organizations propose specific test geometries that - at least in metallic materials- cover a wide range of mechanical properties. In composites however, whose study started relatively recently, the definition of certain mechanical properties proves to be quite a demanding task, mostly due to the

extensive damage and visco-elastic effects that play a significant role on their response. As a consequence, the standardized procedures for deriving their mechanical properties are confined to a limited number of cases. Geometries and testing procedures are standardized e.g. for quasi-static tension by ISO standards ISO 527-5 (1997) [51] or ISO 14126 (1999) [52] for the case of compressive static tests, while ASTM D3518M-94 [53], ISO 14129 (1997) [54] and ASTM D5379M-98 [55] provide standards for shear strength determination through testing of UD off-axis or V-notched coupons. Regarding fatigue of composites, from the standardization point of view, things are more obscure, since only ASTM D3479M-96 [56] proposes specific procedures using the ASTM D3039 [57] coupon geometry for fatigue testing in the tension-tension quadrant, while alternating or purely compressive fatigue are not considered by standards due to a variety of issues arising with most significant coupon's Euler buckling.

All of the above mentioned specimens for tensile tests are long and thin, producing clear failure modes during in-plane characterization and ultimately providing high values for the mechanical properties (which is of special importance regarding design) in a reliable and repeatable way. Compressive tests, most often suffering from elastic instability, have a much shorter gauge length in order to fail due to the compressive load and not due to bending caused by buckling.

When the question comes to special types of tests, such as residual strength tests including acoustic emission monitoring during loading, things are much more demanding. The specific example, being a combination of fatigue followed by a static strength test, must be performed on a coupon geometry able to be tested under tensile or compressive cyclic loads while being robust enough to sustain for instance static compression without use of anti-buckling jigs. Moreover it must allow enough space on its gauge length for acoustic emission sensors to be attached.

One of the goals of the experimental program designed in the frame of OPTIMAT BLADES [1] project has been the development of such a unified coupon geometry, suitable for all types of tests included in the test matrix. Incorporating a unified specimen design provides the additional advantage of neutralizing possible effects of the coupons geometry, thus helping in the correlation of results obtained from quite different types of tests (e.g. compressive static strength and residual tensile strength tests). Several UD coupon geometries have been tested during benchmarking, including 6 straight edge coupons of various gauge lengths and thicknesses and 5

### 3. Modeling Residual Strength

waisted (or 'dog-bone') specimens of different geometries [58]. An optimized solution balancing between requirements for robustness, sufficient gauge length (necessary for attaching strain measurement equipment) and thickness (for reasonable cooling of the specimens) has been finally obtained, and is presented in Fig. 5. An important parameter in the optimization process has been the limitation of the on-axis coupon's thickness, imposed by the fact that several of the testing machines available during the project are limited to 100 kN capacity. Different coupon thicknesses are used for testing in the  $0^\circ$  and  $90^\circ$  case.

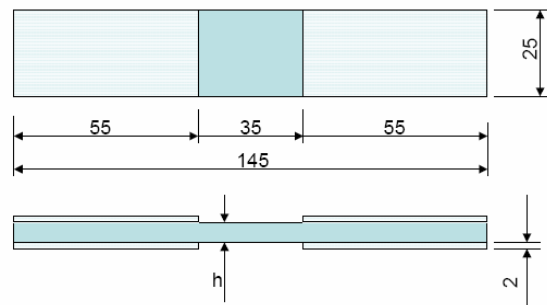


Fig. 5 Unified coupon geometry for all types of test (e.g. fatigue, static and residual strength in tension and compression)

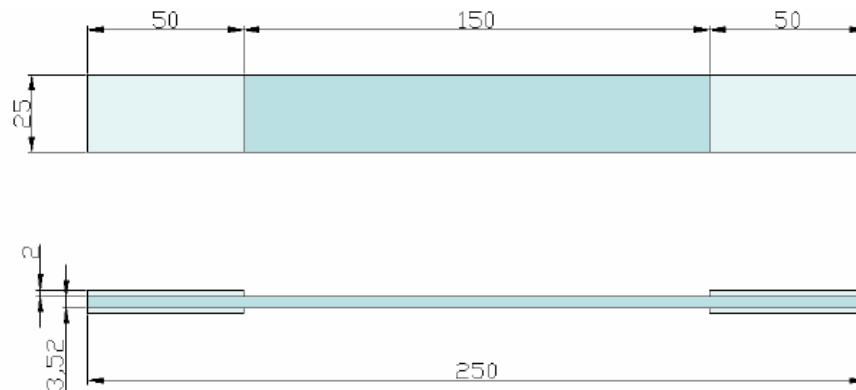


Fig. 6 Geometry of the ISO 14129 standard coupons used for determination of shear properties of the material.

To determine both static and fatigue response of the material in shear, the specimen geometry proposed by ISO 14129 [46] standard (Fig. 6) has been used.

The nomenclature of coupons is chosen accordingly to describe its basic characteristics. All coupons names considered herein start with GE defining the material (Glass/Epoxy) followed by V for the production method (Vacuum Assisted Resin Infusion - VARI). Subsequently the lay-up of the plate each coupon comes from is given using a code number (e.g. 206 for  $[0^\circ]_4$ , 208 for  $[\pm 45^\circ]_5$  or 213 for  $[0^\circ]_7$ ), the coupon geometry (e.g. R03 for the geometry of Fig. 5 or I10 for the geometry of Fig. 6) and then the off-axis angle of each coupon. The last number of the name gives the serial number of the coupon in the database.

From the benchmark tests performed, including different coupon geometries and testing procedures, useful conclusions can be drawn. The most indicative quantity for the comparison of different test methods used for the determination of the same property is the value of the property itself since a higher value assures that the test method brings the material closer to its limits. Next to that is the scatter of the results which is best being small, while an acceptable failure mode, relevant of the respective measured property, is a prerequisite in all cases.

The overall picture of the test results on the OB geometry compared to those on ISO standard specimens is seen in Table 7, presenting the difference between the ISO standard's values and OB coupon's values of typical static strength and elastic properties obtained during the benchmarking phase of the test program. A positive value of the difference indicates a higher property value obtained using the ISO specifications. Except the on-axis compressive test in which there is a considerable difference, the difference is acceptable if one takes into account all the aforementioned advantages of a unified geometry.

Table 7 Comparison of UD properties derived from ISO and OB coupon testing.

	Direction	Property	% Difference
ELASTIC PROPERTIES	On-Axis	Tensile Modulus	-0.0769
		Compressive Modulus	1.1320
	Transverse	Tensile Modulus	7.0812
		Compressive Modulus	-4.5157
STRENGTH	On-Axis	Tensile Strength	3.2704
		Compressive Strength	23.9681
	Transverse	Tensile Strength	2.0487
		Compressive Strength	-2.0433

While results of the OB geometry are encouraging regarding static properties some problems have been spotted during fatigue testing, including mostly tab-failures (which nevertheless did not seem to have a significant impact on the fatigue life obtained).

A more serious implication during fatigue, leading to poor results, has been buckling of several specimens under compression-compression stress ratios ( $R=10$ ). This problem, caused by the combination of material stiffness and coupon geometry, has been intensified by the test's sensitivity to misalignment during gripping or manufacturing imperfections.

#### **3.4.2.4 Test Results**

Experimental results for all in-plane properties of the UD lamina of the reference material are presented in this paragraph. These include static strength, fatigue life and residual strength tests as discussed above.

##### ***3.4.2.4.1 Static Strength***

A total of 132 coupons are used for the definition of the in-plane static strength properties of the reference material in tension (STT), compression (STC) [59] and shear [50].

Test results, including strength and stiffness properties of the UD material in the direction parallel to the fibers, both in tension and in compression are presented in Table A1 in the appendix. It must be pointed out that variations in the measurements of the coupons thicknesses, induced by surface treatment, differences in the fiber ratio etc, have been the cause for problems in calculating the actual UD properties on the fibre direction, these latter depending entirely on the number of UD layers included in the laminate. In view of this, the use of another stress quantity, force through the width of the specimens (in kN/mm), has been proposed and adopted for static as well as fatigue tests in this direction. Nevertheless strength in this table, both tensile and compressive, is calculated based on a nominal (or more precisely average) thickness of 3.74mm.

As already mentioned, the OB geometry suffers buckling problems at high compressive loads. The back to back strain gauges attached, monitoring buckling, indicate excessive buckling only in four cases, which in Table A1 are marked in grey

and are excluded from further treatment. Buckling in the other coupons, quantified by the calculated bending strain [52], even though within the acceptable limits of 10%, has most probably caused the deviation from the ISO geometry shown in Table 7.

Static strength tests in the transverse direction showed in general good results both in terms of failure modes and in comparison to the ISO-testing obtained values. Test data are shown in Table A2 in the appendix.

In Fig. 7 and 8 are shown pictures of typical failures of the OB UD reference material, transversely and parallel to the fibres, in tension and in compression.

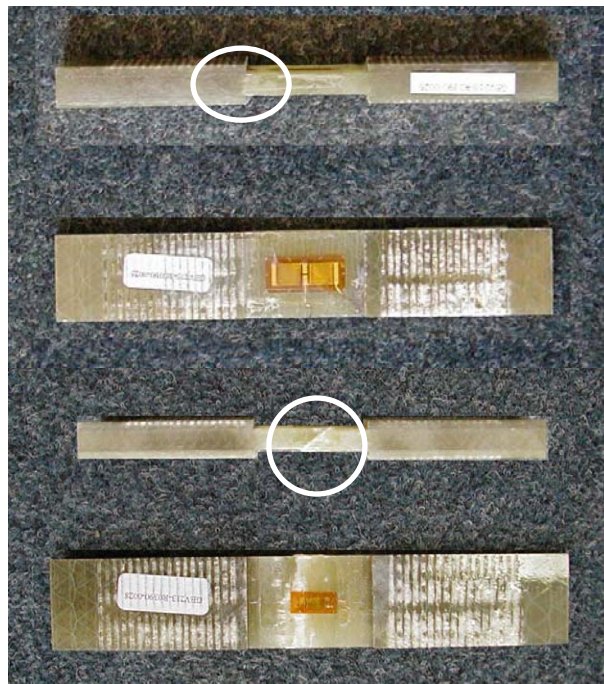


Fig. 7 Pictures of failed OB UD coupons cut at 90° and tested in tension (top) and compression (bottom)

### 3. Modeling Residual Strength

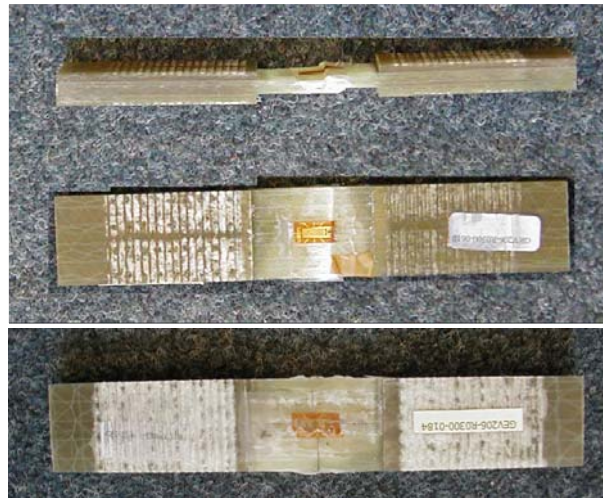


Fig. 8 Pictures of failed OB UD coupons cut at 0° and tested in compression (top) and tension (bottom)

Tests for the determination of the shear properties of the UD laminate, shown in Table A3 in the appendix, are explicitly presented in [50]. A typical failure of the ISO coupon is shown in Fig. 9.

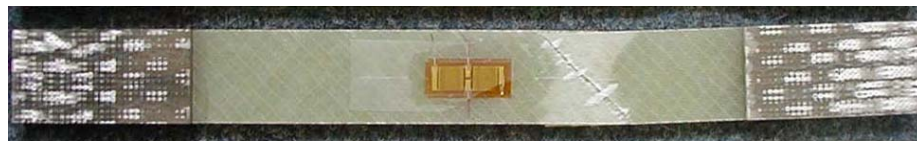


Fig. 9 Pictures of failed ISO  $[\pm 45]_s$  coupons tested tension for the determination of the shear properties.

The data shown in the above tables are fitted to a two parameter Weibull distribution of the form of Eq.(3). In this equation  $\alpha$  and  $\beta$  (shape and scale parameters of the distribution), represent respectively a characteristic value of the described variable and a dimensionless measure of the scatter around this value. The distribution's scale parameter  $\beta$ , corresponding to a value of probability of 63%, shall be used henceforth as a characteristic value for either fatigue life or static strength, while averaging values shall be used for fatigue stresses or elastic properties. Experimental values for the Weibull parameters of static strength are shown in Table 8.

Table 8 Weibull parameters of the in-plane static strength properties of the UD laminate.

	Property	$\beta$ [MPa]	$\beta$ [kN/mm]	$\alpha$
On-axis	Static Tension	793.24	2.967	32.6
	Static Compression	-542.49	-2.029	34.9
Transverse	Static Tension	55.23	-	22.7
	Static Compression	-166.95	-	41.6
Shear	Shear Strength	56.63	-	59.8

It could be mentioned here that the Weibull distribution, used already extensively in the previous sections, is not the only statistical distribution that describes adequately strength or fatigue life since others, e.g. normal or log-normal, do the job equally well. Nevertheless its compact and closed form makes it convenient for implementation in statistical models as the ones discussed in the previous section.

The test results are presented graphically in Fig. 10, normalized by the respective  $\beta$ , along with the fitted Weibull curve. It is clear that the specific distribution describes fairly well the statistical nature of all static strength components of the UD reference material tested.

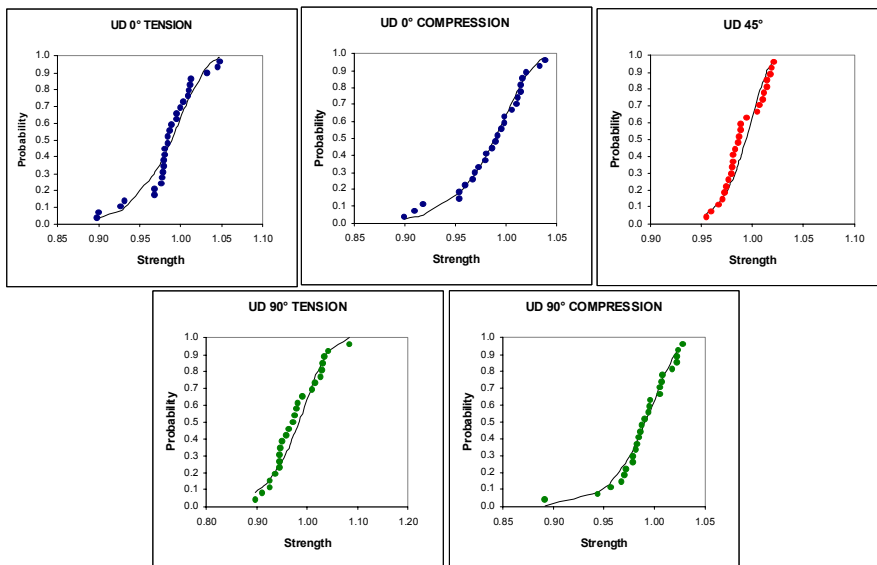


Fig. 10 Distributions of static tensile and compressive strength of the principle directions of the reference material along with Weibull curves used to fit the data.



### 3.4.2.4.2 Fatigue Life

Fatigue life characterization of the UD laminates includes the determination of the S-N behavior at three R ratios, in the tension-tension ( $R=0.1$ ), tension-compression ( $R=-1$ ) and compression-compression ( $R=10$ ) region. Test results are discussed in detail in [60], while a short overview of the data is shown in Table A4 of the appendix. Data marked in grey are not included in the S-N definitions due to the reasons indicated in the footnotes.

While the OB geometry behaves reasonably well in the pure tension and reversed loading fatigue, buckling problems, already mentioned for static testing, are evident in the compression-compression domain. At this point it must be noted that the characterization of 'buckled' or 'not buckled' seen in the above table, judging only from the first few cycles of the coupon's life is not safe. The cyclic loading itself probably causes stiffness degradation of the specimen and consequently, buckling, possibly only marginally avoided during the first cycles, could occur later on. The problem becomes even more complicated when considering the stiffness of the test rig itself or slight misalignments between the grips which cause instabilities to occur during loading. The already problematic definition of the fatigue response under  $R=10$  is made worse by the flat S-N behavior, causing large differences in fatigue life due to small changes in the applied stress. Finally, a compromised solution for determining the S-N curve is adopted, being based on several tests performed at UP and WMC (values shown in Table A4 in the appendix). A typically buckled coupon and a valid coupon can be seen in Fig. 11.



Fig. 11 Typically buckled (top) and valid (bottom) failure modes of the UD on-axis coupon, under  $R=10$  fatigue.

Fatigue testing in the transverse direction does not come up with so many challenges as in the fibre one. This is mainly due to the lower static and fatigue strength of the material, which in combination to the higher thickness of the coupon (a [90]<sub>7</sub> lay-up of the reference material is used in this case) and despite its lower modulus of elasticity keeps buckling loads safely above maximum forces applied during compressive cycles.

As for tensile fatigue, even though the failure modes observed are quite satisfactory, considering the brittle behavior of the material, failure often occurs right next to the tab. Although this can be considered a disadvantage of the OB geometry, in the specific case ultimate strength does not deviate much from the one derived by ISO standard testing as discussed above, thus this effect can be neglected.

Test results are presented in [61] and summarized in Table A5 in the appendix.

Two additional comments are in order. The first concerns sensitivity of the material to mishandling during strain gauge attachment and small overloads during load compensation, especially during slow cycles. Such events have caused in some cases cracking and failure of specimens and might have affected fatigue life of some more. The second comment regards -hopefully limited- plate variations observed during the project, which are made more evident during transverse tests. In fact a whole plate is suspected of having poor transverse properties and is thus excluded from analysis.

Results of tests performed on the [±45]<sub>s</sub> laminate for the determination of the shear fatigue response of the UD material are reported in [50]. Since either tensile or compressive tests would produce identical shear stresses in the laminate, only tensile tests at R=0.1 are performed. Fatigue results are summarized in Table A6 in the appendix.

Fig. 12, Fig. 13 and Fig. 14 present the fatigue life data for each direction. All strength quantities are normalized by their respective Weibull scale parameter. The SN curves used in this case for fitting the data are of the form:

$$\sigma_{\max} = S_o N^{-\frac{1}{b}} \quad (66)$$

S-N curve parameters for all cases are given in Table 9.

### 3. Modeling Residual Strength

Table 9 S-N curve parameters at all stress ratios tested for all in-plane properties.

In-plane property	Stress Ratio	$S_0$		b
Parallel to Fibre	R=0.1	4.35	[kN/mm]	9.74
	R=-1	3.73	[kN/mm]	8.04
	R=10	2.49	[kN/mm]	23.88
Transverse to Fibre	R=0.1	111.58	[MPa]	8.63
	R=-1	87.52	[MPa]	8.43
	R=10	196.77	[MPa]	24.32
[±45] <sub>s</sub>	R=0.1	169.16	[MPa]	11.06
Shear	R=0.1	82.9	[MPa]	11.06

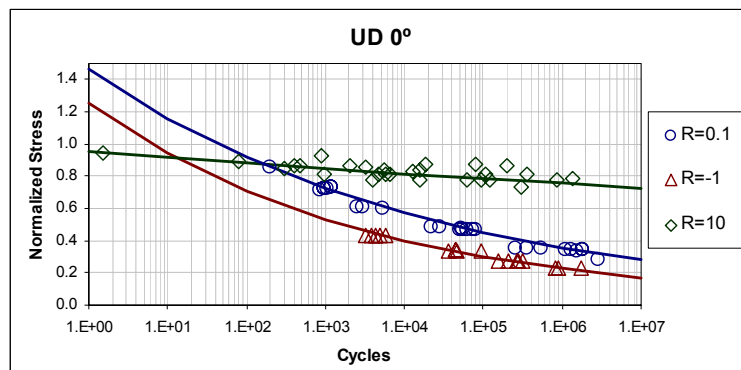


Fig. 12 Fatigue life data and S-N curves for the reference material at 0°.

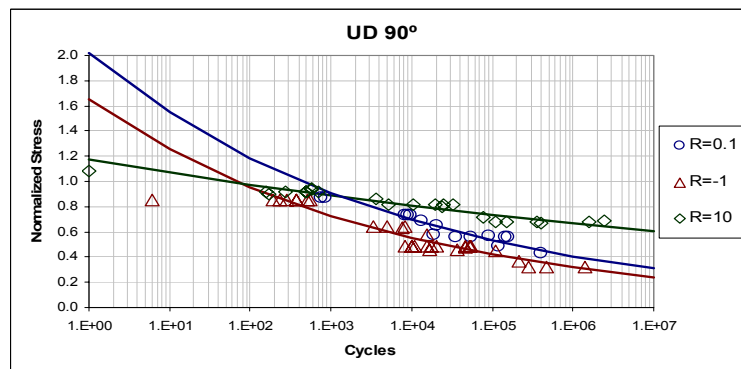


Fig. 13 Fatigue life data and S-N curves for the reference material at 90°.

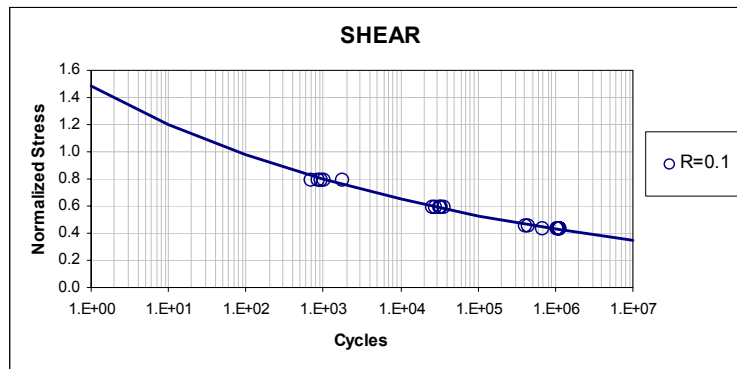


Fig. 14 Fatigue life data and S-N curves for the reference material under shear.

### 3.4.2.4.3 Residual Strength

Experimental results from residual strength characterization of the reference UD material are presented in this section. As discussed above, extensive residual strength testing has taken place during the project, aiming at the thorough investigation of all in-plane strength components degradation occurring due to various cyclic loading, i.e. different stress ratios and stress levels. Results of the full experimental program, which has been divided between several laboratories, can be accessed through [62], since in most cases residual strength test results are not explicitly reported.

A drawback of such a vast experimental program partitioned between so many laboratories proves to be the inevitable induction of variations due to different testing machines, different laboratory conditions, variation of the material -which could not be avoided during the manufacturing of the about 3600 coupons required for the whole project, and other minor parameters that in the end make questionable any statistical conclusions concerning measured properties. An implication of this is, for instance, the highly varying number of failures, taking place during the cycling that precedes residual strength measurement, between different laboratories. An indicative plot of them for the various stress ratios and test cases is shown in Fig. 15 as a percentage on the total tests performed for the corresponding test category at each lab. Premature failures vary significantly between different stress ratios, indicating a possible deficiency of the test geometry in certain types of tests, e.g. at R=10 in the transverse direction. Nevertheless differences between laboratories exists even for test setups that should not be so sensitive to the geometry, e.g. R=0.1 parallel to the fibres, indicating other

### 3. Modeling Residual Strength

causes as well. Of course in Fig. 15 are included all the premature failures which may have been caused by possible material variations.

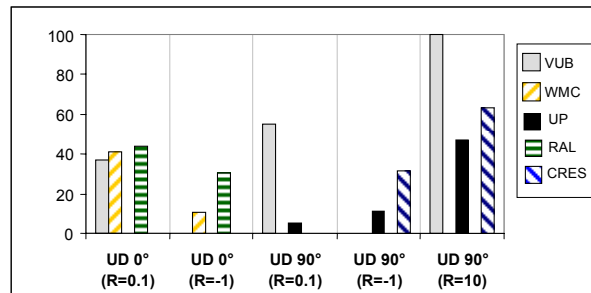


Fig. 15 Percentage of premature failures at different laboratories and test cases.

Regarding Residual strength tests in the fibre direction, initially planned to be performed at the same three stress ratios as in fatigue, are finally confined to R=0.1 and R=-1, due to the buckling problems observed during compressive cycling under R=10. In addition to that, the very flat S-N behavior observed in this case, reveals the great sensitivity of fatigue life on the cyclic stress. Considering that cyclic loads as well as strength of the coupons are subject to errors and variations respectively, one should expect that residual strength tests would show large scatter, many premature failures and high uncertainty regarding the actual fatigue life each test is referring to.

An overview of all RST and RSC tests is given in Tables A7 to A12 in the appendix.

Residual strength tests on the  $[\pm 45]_s$  laminate are explicitly reported in [63] and [64]. Main test outcomes are presented in Table A12 in the appendix.

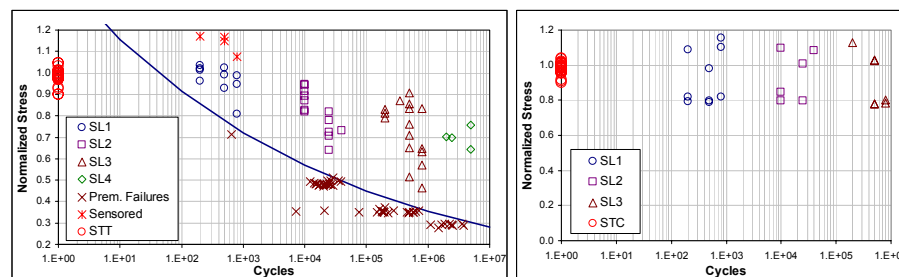


Fig. 16 Residual strength data for on-axis UD tested at R=0.1.

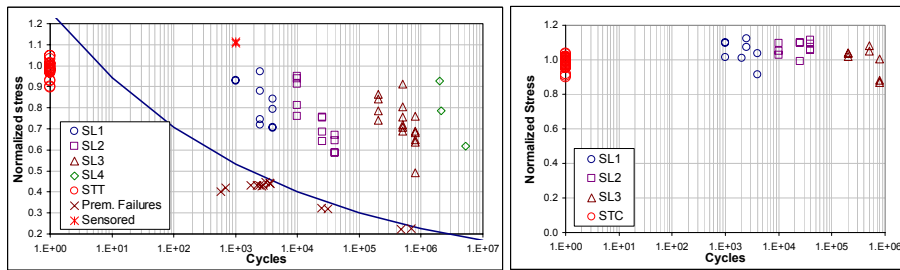


Fig. 17 Residual strength data for on-axis UD tested at R=-1.

Residual tensile strength in the direction parallel to the fibres shows gradual degradation in both stress ratios investigated, as seen in normalized values in Fig. 16 and 17. Premature failures, static strength data and the respective S-N curves are also shown in the figures. Different symbols refer to different cyclic stress levels, while each group of symbols is in most cases divided between three sub-groups, each one located at the life fraction where the residual strength tests have been performed (at 20%, 50% and 80%).

The experimental data indicate that the loss of static strength reaches up to 40% and is more apparent at the lower stress levels, which indicates a change of damage mechanisms when maximum cyclic stress drops below roughly 50% of the UTS. It is also interesting to note that a considerable amount of the total loss of strength - particularly at the lower stress levels, occurs as early as up to 20% of the nominal life, indicating a gradient degradation starting early in the material's life. On the other hand, strength degradation during low-cycle fatigue, especially at the 1000 cycles stress level, follows a different trend, with strength starting to drop during the second half of the coupon's life, while during the first half it remains unchanged or even increased. This latter behavior, although reported in literature e.g. by Reifsneider [35], is in most cases attributed to stress redistribution due to relaxation around notches, even though in some cases it is associated with better alignment of UD fibers after fatigue [45]. In this particular case indications exist that it is mainly due to plate properties variations rather than to an actual increase in strength after fatigue.

The above mentioned difference of the degradation behavior suggests that, the damage modes developing in the high cycle case, including fiber-matrix debonding, localized delaminations etc have a much more serious impact on static strength than

### 3. Modeling Residual Strength

failure modes that develop during high cyclic loads at fiber dominated lay-ups, such as matrix cracking or random fiber failures.

Results of residual strength tests in the transverse direction as graphically shown in Figs. 18, 19 and 20. indicate that in general, the degradation trend can be considered similar to the one in the fibre direction: High stress levels in stress ratios that include tension have a less severe effect to static strength than high cycle fatigue, in which case the strength degrades up to 40% for higher life fractions. Nevertheless, static strength in this material orientation remains unaffected during the first part of cycling, even at lower stress levels which is reasonable considering the simple damage mechanism developing in this orientation of the material, including mostly cracks parallel to the fibres

Regarding the degradation of tensile strength in the transverse direction under R=10 no clear trend can be observed. Looking at the experimental data, limited strength degradation can be assumed even though the actual behavior of the material, given the small sample available, is masked by the large variation of the results.

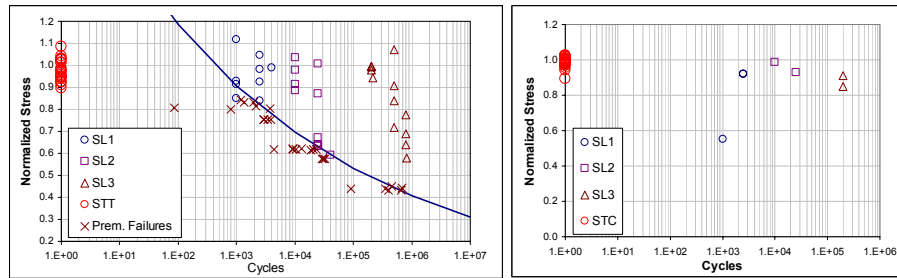


Fig. 18 Residual strength data for transverse UD tested at R=0.1.

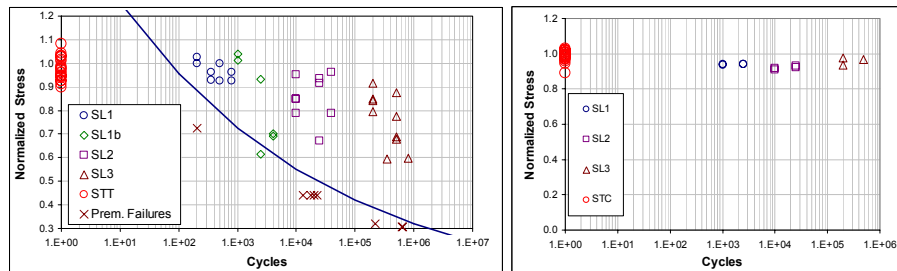


Fig. 19 Residual strength data for transverse UD tested at R=-1.

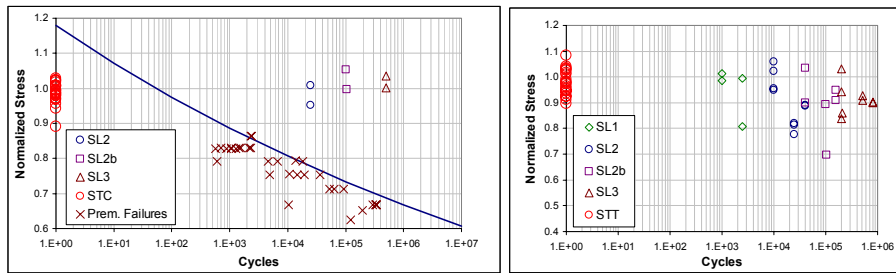


Fig. 20 Residual strength data for transverse UD tested at R=10.

Compressive strength seems in general to be unaffected by fatigue. This experimental observation is very interesting since the damage induced by fatigue especially in the fibre direction at  $R=0.1$  or  $-1$  (Fig. 16 and 17) creates the conditions for degradation of static strength: matrix cracks propagating along the fibre-matrix interface and subsequent local delaminations should make the laminate more vulnerable to micro-buckling and consequently to a loss of strength. Unfortunately such mechanisms remain more or less within the scatter of the static strength data sample. Test results from compression-compression fatigue at  $R=10$  do not provide sufficient information for drawing definite results, even though the damage modes that would cause loss of strength are not expected in this case. A limited degradation of tensile residual strength could be assumed to occur, even though any definite conclusion is hindered by the large scatter of the data.

Results for the case of the shear strength present a considerable advantage in contrast to the ones of the two symmetry directions: All tests are performed at a single laboratory (UP) and no problems or unexpected behavior has been experienced during cycling. This is reflected to the reasonable number of premature failures obtained. In addition to that, since only tensile tests are performed, buckling problems are excluded, while the material itself could be easily and safely handled and tested. This leads to statistically utilizable data samples, more so since the number of tests is double (8 RST tests per stress level and life fraction) compared to the other two material orientations investigated. Test results are presented in Fig. 21. Nonetheless, the main conclusions on the strength degradation behavior drawn above are still valid: Degradation is more severe during high cycle fatigue while even few cycles at higher levels (e.g. 1000 cycles at the 5000 cycles stress level) can cause enough damage to decrease strength by a clear 10%. This is no surprise, since the specific combination of imposed loading and stacking sequence is expected to result in extensive matrix



### 3. Modeling Residual Strength

damage during cycling before final failure occurs. Apart from that, a considerable loss of up to almost 40% of strength is evident at lower stress levels while the scatter of the results is increased at higher life fractions compared to the one of the static strength tests.

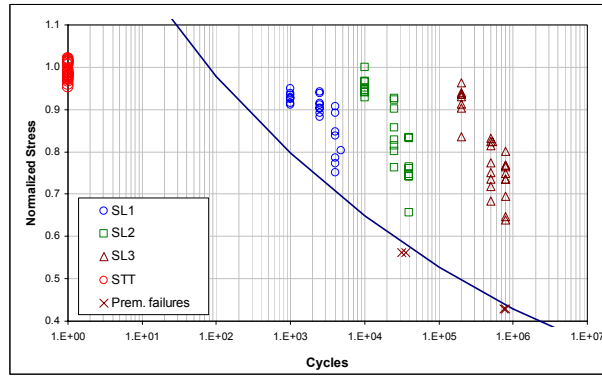


Fig. 21 Shear residual strength data at R=0.1.

### 3.5 VALIDATION OF MODELS

#### 3.5.1 Implementation to Experimental Data

All models, except of course the linear one, require the derivation of one or more parameters to fit their respective degradation equations to the residual strength characteristics of the material under consideration. The procedure proposed in each case is a key element of each methodology, especially when referring to design-oriented phenomenological models such as the ones considered herein, since the kind and amount of tests, necessary for characterizing a material, can limit or enhance the model’s applicability. A reasonable approach one could imagine, i.e. choosing a number of stress ratios, then perform at each one tests at various stress levels and life fractions and finally fit a model for each set using regression analysis, proves to be quite a demanding task in terms of both time and cost. To overcome this restriction, a variety of more efficient procedures have been proposed up to date, making use of fatigue life data (e.g. Hahn and Kim), normalization of residual strength data (e.g. Harris) or based on the probability distribution of static strength (e.g. Yang, Sendekyj).

Table 10 Parameters of models implemented to the three published data sets.

Model	Anderson [26]	Ryder & Walker[22]	Yang & Miller [21]
INT	x= 6.09 y=2.71	x=3.85e-8 y= 52.95	x= 9.49 y= 0.76
SC	v=0.26	NA	NA
H	c=4.58	16.20	-0.94
REI	k=5.30	5.68	0.68
OM	NA	NA	NA
W1	S=0.072	S=0.032	S=0.037
W2	S=0.082 C=0.245	S= 0.037 C=0.163	S=0.045 C=0.160
Y1	c=23.83 K=6.88E-39 b=13.47	c=28.09 K=7.74e-66 b=23.76	c=13.29 K=8.38e-48 b=16.20
Y2	ω= 11.91 K= 8.04E-39 b= 13.40 c= 1.44	ω=27.47 K=1.89e-64 b=23.17 c=2.78	ω=13.34 K=8.43e-048 b=16.15 c=0.105

### 3. Modeling Residual Strength

For the assessment of the models, attempted in the present section, the methodology proposed by each author to the corresponding model is implemented. In the cases when the proposed methodology does not account for the stress level dependency or when no specific procedure is proposed, the equivalent static strength (ESS) concept introduced by Yang (see section 3.2.3), is adopted. In this way, a limited amount of residual strength and/or fatigue life tests are required for deriving a model's parameters, while the procedure is flexible enough to adaptable to various degradation equations of one or more parameters. Nevertheless the method has its limitations since, as already mentioned, the objective function arising is trapped to infinite local minima when the model includes many parameters. An alternative method is proposed by Sendeckyj who uses as optimization criterion the maximization of the Weibull shape parameter of the occurring (parametric) ESS distribution. Even though the two methods usually lead to similar results, the methodology of Yang has the advantage of providing an easy way to check the result of the optimization visually, by plotting together the two static strength distributions.

Table 11 Parameters of models implemented to the OPTIMAT data.

Model	On-Axis Direction		Transverse Direction		±45
	R=0.1	R=-1	R=0.1	R=-1	R=0.1
INT	x= 4.5795 y=3.6406	x=3.82 y= 4.25	x= 7.97 y= 2.57	x= 1.70 y= 7.32	x= 6.73 y= 2.99
SC	v=0.36	v=0.0685	v=0.320	v=1.65	v=1.04
H	c=4.68	c=3.87	c=6.35	c=8.25	c=5.63
REI	k=2.77	k=3.19	k=3.42	k=5.82	k=3.05
OM	k <sub>1</sub> =0.557 k <sub>2</sub> =2.42	k <sub>1</sub> =0.700 k <sub>2</sub> =2.05	k <sub>1</sub> =1.6484 k <sub>2</sub> =1.0152	k <sub>1</sub> =0.4907 k <sub>2</sub> =3.2142	k <sub>1</sub> =0.864 k <sub>2</sub> =1.52
W1	S=0.079	S=0.105	S=0.0407	S=0.056	S=0.055
W2	S=0.108 C=0.0204	S=0.120 C=0.235	S=0.116 C=0.0022	S=0.0056 C=0.132	S=0.0091 C=0.0929
Y1	c=12.64 K=1.024E-6 b=8.58	c=17.24 K=2.25e-5 b=6.85	c=13.88 K=1.39e-18 b=8.65	c=15.36 K=3.17e-17 b=8.36	c=14.28 K=1.89e-25 b=11.11
Y2	ω= 11.97 K= 6.86E-7 b= 9.56 c= 5.88	ω=9.78 K=2.12e-5 b=9.40 c=1.73	ω=10.74 K=2.12e-18 b=8.54 c=9.95	ω=17.13 K=1.64e-17 b=8.52 c=7.80	ω=12.92 K=1.20e-25 b=11.18 c=4.96

Implementation of the various residual strength models to the data sets discussed in previous section is realized in MATLAB commercial code, using library routines when available (see also [65]). Derived parameters for the three published data sets used, are shown in Table 10.

Model parameters for the OPTIMAT project data sets, presented in the previous sections, are given in Table 11.

## **3.5.2 Residual Tensile Strength**

### **3.5.2.1 Degradation Curves**

A first and critical step in validating residual strength models is the ability of their deterministic degradation equations to fit the general degradation trend observed for the material in question, which is assessed through the accurate estimation, in terms of average values, of the residual strength at any stress level and life fraction. In this validation of the degradation behavior, only the published data of Anderson along with the OPTIMAT data sets are applicable. The reason is that only these data sets contain the necessary amount of residual strength data at various life fractions and specific stress levels that enable us to conclude on the predictive ability of each model from the beginning of fatigue life until near failure.

Additionally, validating predictions at different stress levels, corresponding e.g. to low and high cycle fatigue, and furthermore at different stress ratios e.g. in the tension-tension and compression-compression domain, provides useful information on the adaptability of each model to different fatigue conditions as well as on its ability to predict the strength degradation caused by various damage modes. In that direction, the residual strength tests performed in the frame of the OPTIMAT project are especially valuable.

Model predictions for the tensile residual strength of the data set of Anderson, under tension-tension fatigue at  $R=0.1$  are shown in Fig. 22. The maximum cyclic stress, approximately at 40% of the static tensile strength of the material, corresponds to a fatigue life of almost 140.000 cycles. The predictions referring to the fibre direction of the OPTIMAT reference UD laminate are shown in Fig. 23-26 for the stress ratio  $R=0.1$  and in Fig. 27-29 for the stress ratio  $R=-1$ .

### 3. Modeling Residual Strength

Different line styles refer to different strength degradation models. In the figures the experimental points of the corresponding stress ratio and stress level are also shown. These data points are arrayed in groups situated at 20%, 50% and 80% of the nominal fatigue life of said stress level. A limited number of specimens (e.g. in Fig. 25) deviate from the above mentioned life fractions due to premature interruption of cycling.

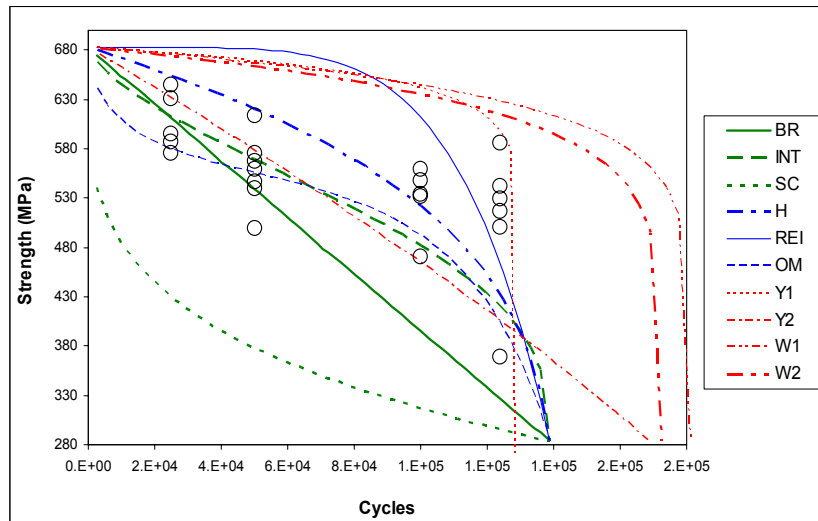


Fig. 22 Comparison of theoretical predictions and experimental data from Glass/Polyester [CSM/fabric/(CSM/UD)<sub>2</sub>]<sub>s</sub> [26].

Results from the various strength degradation models presented in the above graphs suggest that the majority of model predictions are not corroborated satisfactorily by all the experimental data while in many cases over-optimistic estimations of residual strength are provided. Models like those of Broutman (BR) or Hahn (H), predicting linear or linear like behavior, succeed to yield good predictions during the initial part of specimen life, while others, like those of Yang (Y1 & Y2) and the non linear model (REI), follow better the trend of steep degradation towards final fracture. Nevertheless, the degradation behavior observed in the experimental data examined, seems to be more of the kind 'initial drop of strength, then slow degradation and finally steep degradation at the end of life', reminding of the stiffness degradation behavior of composites

proposed by some authors (e.g. [66]). The observation stands for both investigated materials, i.e. the Glass/Polyester laminate of Anderson [26] and the UD laminate of the OPTIMAT reference material, as could be expected for such fibre dominated lay-ups.

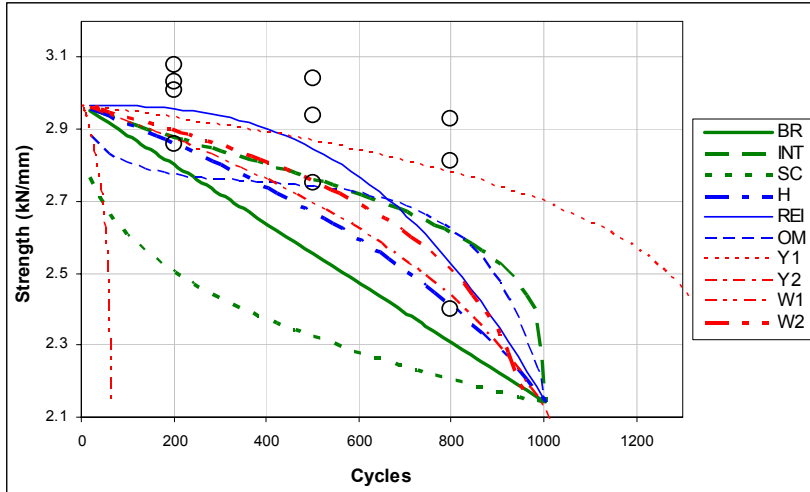


Fig. 23 Comparison of theoretical predictions and experimental data from the on-axis OPTIMAT UD tested at R=0.1 at the stress level of 1000 cycles.

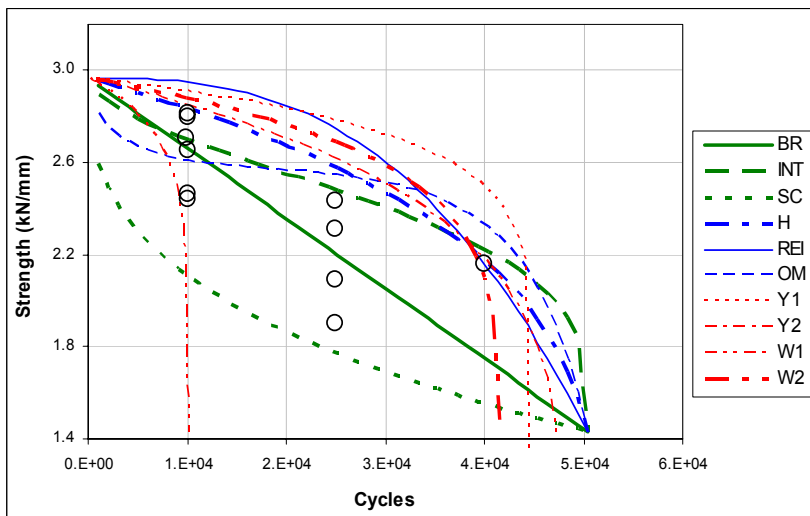


Fig. 24 Comparison of theoretical predictions and experimental data from the on-axis OPTIMAT UD tested at R=0.1 at the stress level of  $5 \cdot 10^4$  cycles.

### 3. Modeling Residual Strength

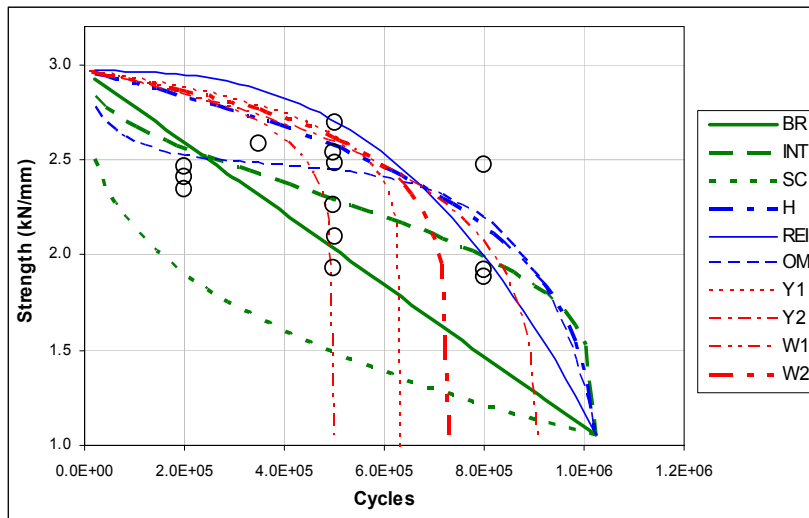


Fig. 25 Comparison of theoretical predictions and experimental data from the on-axis OPTIMAT UD tested at R=0.1 at stress level of  $10^6$  cycles.

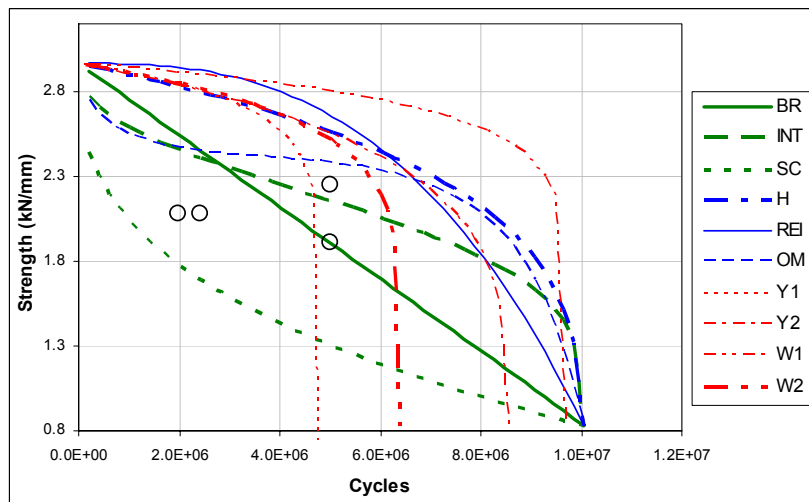


Fig. 26 Comparison of theoretical predictions and experimental data from the on-axis OPTIMAT UD tested at R=0.1 at the stress level of  $10^7$  cycles.

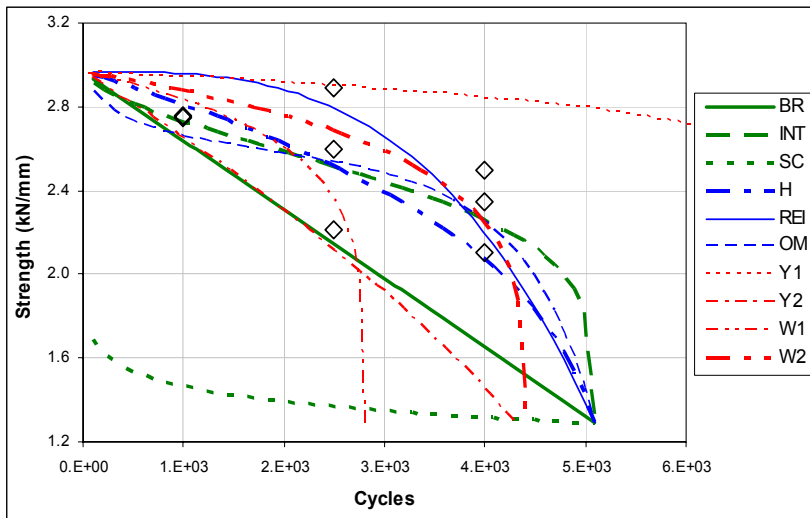


Fig. 27 Comparison of theoretical predictions and experimental data from the on-axis OPTIMAT UD tested at R=-1 at the stress level of 5000 cycles.

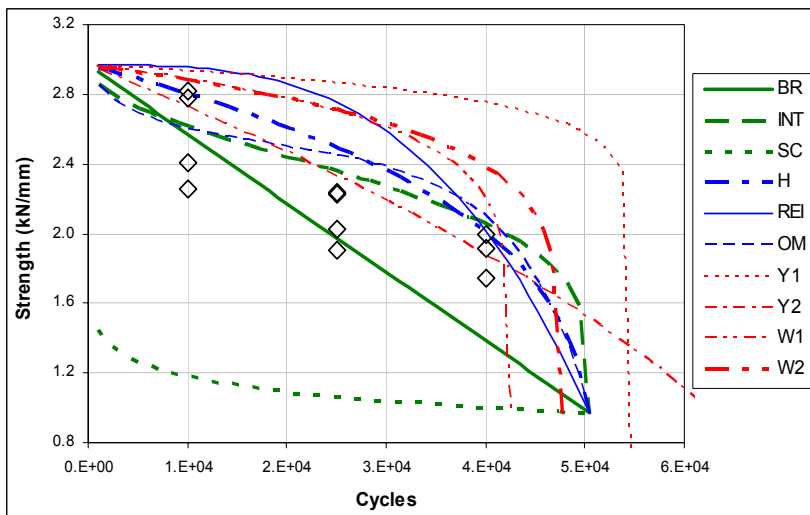


Fig. 28 Comparison of theoretical predictions and experimental data from the on-axis OPTIMAT UD tested at R=-1 at the stress level of  $5 \cdot 10^4$  cycles.



### 3. Modeling Residual Strength

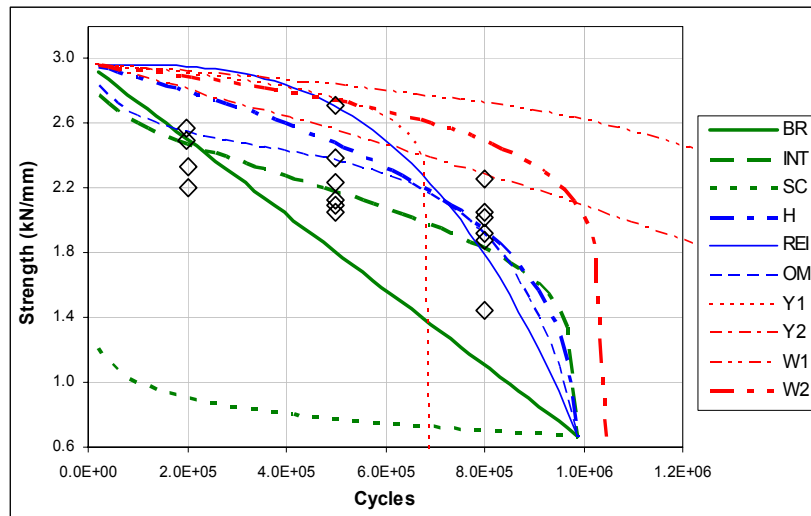


Fig. 29 Comparison of theoretical predictions and experimental data from the on-axis OPTIMAT UD tested at  $R=-1$  at the stress level of  $10^6$  cycles.

The change in the degradation trend observed between higher and lower stress levels during fatigue, which is reflected to the ‘sudden death’-like behavior at SL1 or SL1b, implies that models that predict a monotonically increasing degradation rate up to failure, e.g. REI or Y2, are better suited for low cycle fatigue, since in this case strength does not seem to degrade significantly during the initial part of the specimen life. On the other hand, models like INT or OM, seem to apply better on residual strength description under lower cyclic stresses, e.g. SL2, SL3 and SL4, in which cases there seems to be a clear loss of strength during the first 20% of fatigue life, followed by a plateau and a final steep fall before fracture. This transition between higher and lower cyclic stresses must be attributed to a change of the damage mechanisms that cannot be accounted for by any model from those investigated: Even though stress level dependencies are expressed in the degradation equations, a common degradation trend for all stress levels is implied. The observed behavior should be modeled by more complex degradation equations including additional parameters, whose derivation would in turn require more intense experimentation. In this work and since the models are investigated on the basis of their applicability to structural design, models like the OM or INT can be considered more advantageous and the previously mentioned effect can be

disregarded for two reasons. The first is that said behavior is observed at higher cyclic stresses which few composite structures are likely to suffer, since most of them are designed for lives of several million cycles, while the second one is that even in this case, the assumed decreased strength shall lead to a more conservative and thus safer design when these are used.

Models like Sendeckyj's W1 & W2, whose degradation equation does not inherently satisfy the fracture condition, often yield failure predictions that differ considerably from the ones experimentally observed. This effect is seen also in the predictions of Y1 and Y2, even though in this case the fracture condition is included in their formulation. The reason for this is the inclusion of the S-N curve parameters K and b in the optimization process, which alters their original values. Especially a small difference in the slope of the S-N line (parameter b) can lead to a dramatic truncation of the predicted fatigue life. Finally, the rather irrational predictions of the SC model must be attributed to the questionable procedure for determination of parameter  $\nu$  and additionally, in case of the OPTIMAT data, to the small fatigue data samples available, that could only roughly approximate the probability distribution of fatigue life, which in this case is necessary for estimating the parameter.

Residual tensile strength, for the transverse direction of the reference OPTIMAT UD material, presents a slightly different degradation picture from the on-axis direction, even though considerable experimental scatter is observed due to the reasons discussed during the presentation of the experimental results. The combination of increased scatter and few test data at each life fraction hinder the reliable assessment of the models. Nevertheless, useful conclusions can be drawn on the general applicability and validity of the various models under different fatigue damage conditions. Predicted degradation of tensile residual strength for the stress ratios of  $R=0.1$  and  $R=-1$  are shown in Fig. 30-36.

### 3. Modeling Residual Strength

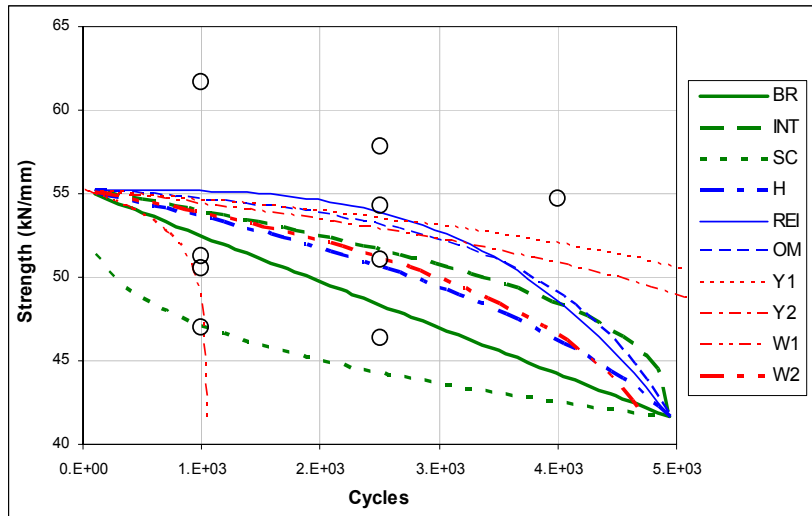


Fig. 30 Comparison of theoretical predictions and experimental data from the transverse direction of the OPTIMAT UD tested at R=0.1 at the stress level of 5000 cycles.

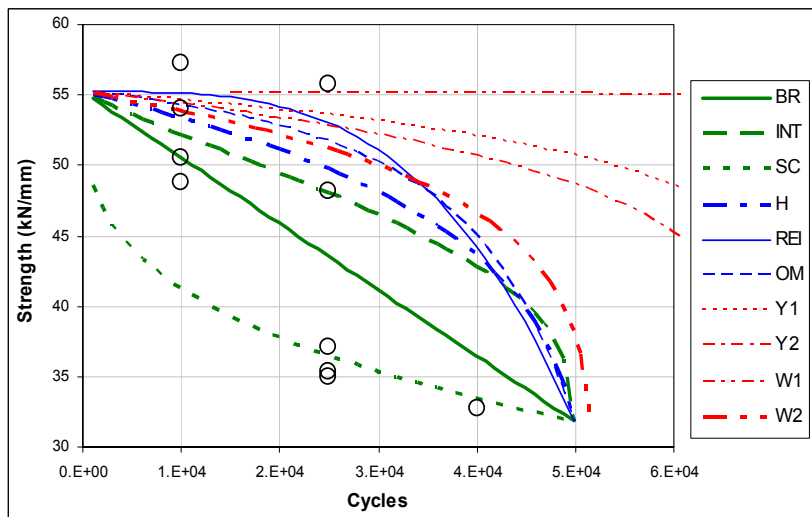


Fig. 31 Comparison of theoretical predictions and experimental data from the transverse direction of the OPTIMAT UD tested at R=0.1 at the stress level of  $5 \cdot 10^4$  cycles.

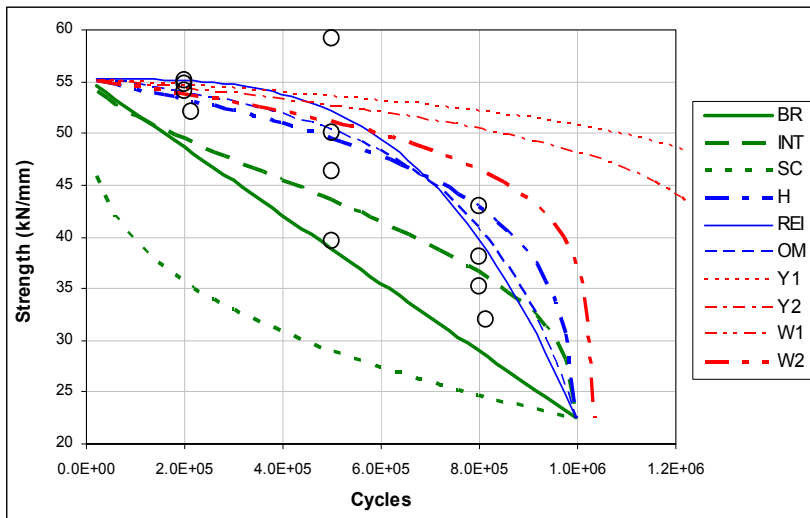


Fig. 32 Comparison of theoretical predictions and experimental data from the transverse direction of the OPTIMAT UD tested at R=0.1 at the stress level of 106 cycles.

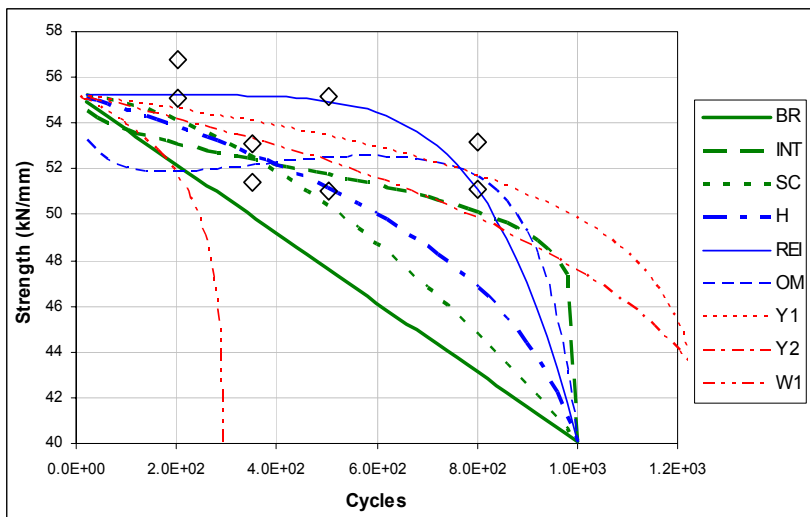


Fig. 33 Comparison of theoretical predictions and experimental data from the transverse direction of the OPTIMAT UD tested at R=-1 at the stress level of 1000 cycles.

### 3. Modeling Residual Strength

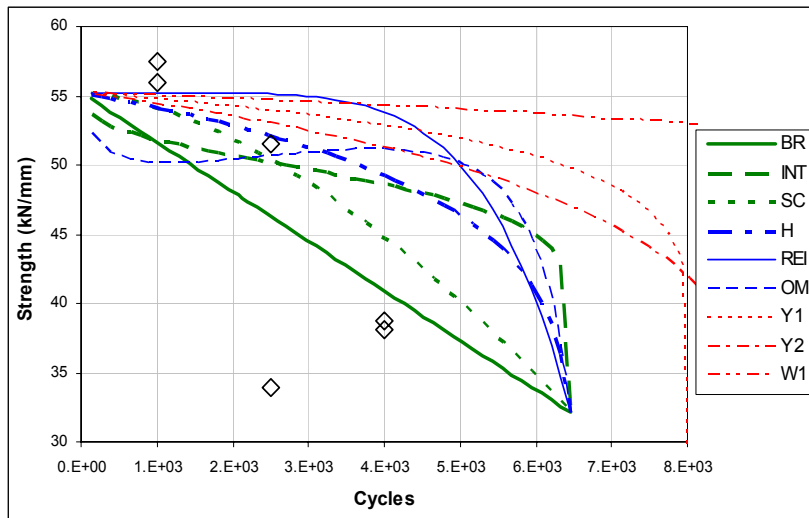


Fig. 34 Comparison of theoretical predictions and experimental data from the transverse direction of the OPTIMAT UD tested at R=-1 at the stress level of 5000 cycles.

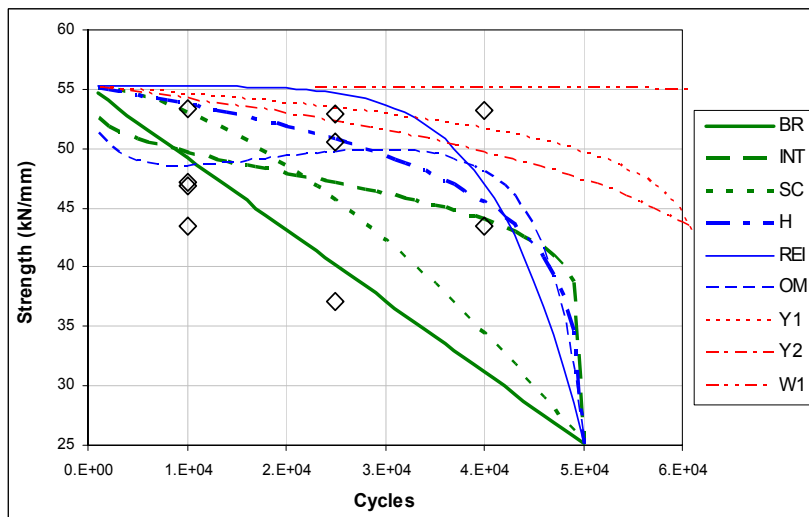


Fig. 35 Comparison of theoretical predictions and experimental data from the transverse direction of the OPTIMAT UD tested at R=-1 at the stress level of  $5 \cdot 10^4$  cycles.

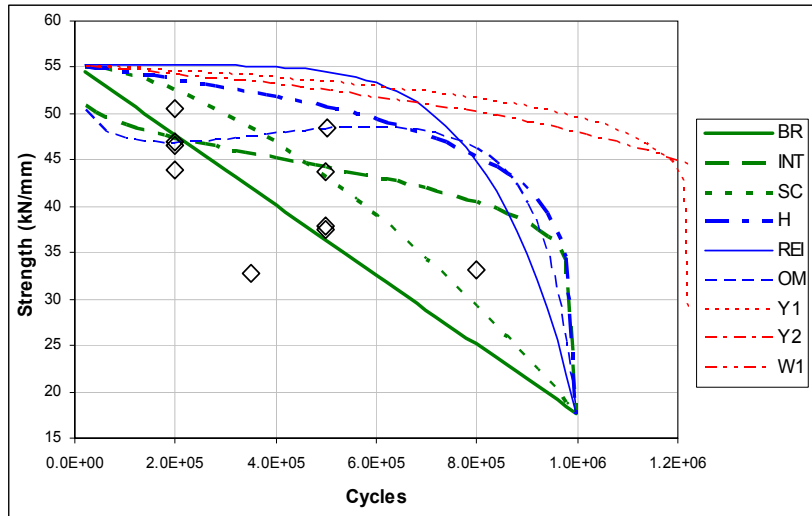


Fig. 36 Comparison of theoretical predictions and experimental data from the transverse direction of the OPTIMAT UD tested at R=-1 at the stress level of  $10^6$  cycles.

For the case of the R=0.1 stress ratio, predictions of several models seem to corroborate satisfactorily with the experimental results. The trend of early drop of static strength during the initial part of the material's life, which is clearly observed in the on-axis case, does not seem to apply in this case. Some specimens tested at high stress levels do present degraded residual strength, but this can be assumed to be caused by variations in the strength properties of the coupons or damage induced during handling. The typical behavior can be assumed to be the one of SL3 in Fig. 32, indicating a gradual wear out of strength intensifying during the second half of fatigue life. Such behavior is modeled acceptably by H, INT or OM mode, while also the linear model gives satisfactory results lying slightly on the safe side.

Regarding the residual strength predictions at R=-1, conclusions still have a degree of uncertainty. Even though fewer premature failures occurred during testing at this stress ratio, suggesting less scatter at least in the fatigue life distribution, statistical variations appear to be increased in this case, which is partly masking (in combination of course with the small samples available) the actual degradation behavior of the material. This is also reflected to models predictions: No definite conclusion on a model's validity can be drawn, apart from the obviously unsatisfactory predictions of the models Y and W which is

### 3. Modeling Residual Strength

caused by a -most of the times- optimistic prediction of the expected fatigue life as well as the weird trend predicted by the OM model which shows strength to increase after an initial drop. This latter is probably an artifact caused by the large scatter, which shows the average residual strength to increase in some cases (e.g. SL2 in Fig. 35) as well as by the inherent flexibility of the specific model to predict a behavior other than the monotonically decreasing one. Again, the linear BR formulation results to slightly conservative predictions, which nonetheless are within the experimental scatter of the residual strength tests, especially at lower stress levels, which are of special interest in fatigue dominated composite structures.

Residual strength tests under compression-compression cyclic loads at  $R=10$ , performed on the transverse direction of the UD material, do not indicate any loss of static tensile strength, since test results remain within the statistical variation of static strength. Nevertheless, assuming the fracture condition still valid, the 'Sudden Death' or SD model, predicting constant strength throughout life and a steep degradation prior to failure, is attributed to the material in this case. The 'sudden death' degradation equation can be represented by Eq.(62) in which the value of parameter  $k$  takes theoretically an infinite value. In this case, the parameter is assumed to take a value of  $k=50$ . Resulting curves for all three stress levels are shown in Fig. 37. Again different symbols refer to different levels of maximum cyclic stress. As can be seen in the figure, it is assumed that residual tensile strength drops to zero after compressive cycling which is in most cases a reasonable assumption given the explosive failure modes observed during failure in compression.

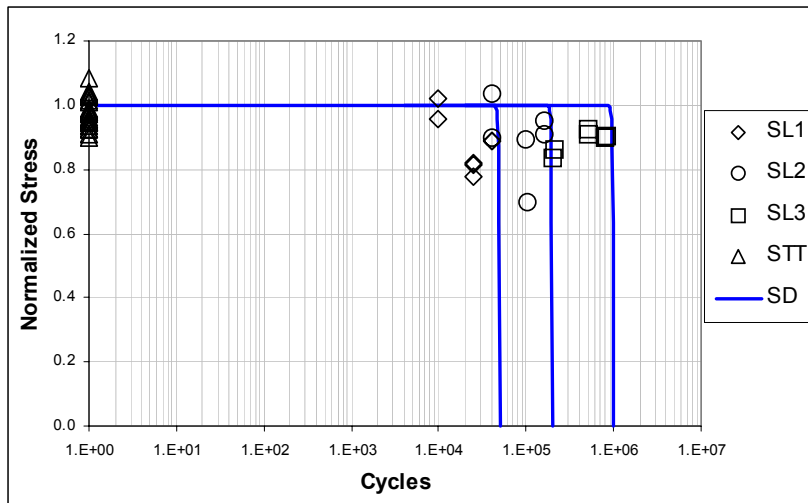


Fig. 37 Sudden death (SD) model predictions and experimental data for the residual tensile strength on the transverse direction of the OPTIMAT UD tested at R=10 at three stress levels.

### 3.5.2.2 Statistical Predictions

In the discussion of residual strength models in the previous sections the statistical behavior of residual strength has been neglected and predictions have been assessed simply by means of average values. Such a treatment of residual strength as a deterministic quantity must be considered as an oversimplification: Test data suggest a strong stochastic behavior of residual strength, tending to become even more intense at higher life fractions. This fact induces uncertainties on the actual load carrying capacity of the material (or the whole structure) after cyclic loading, especially in the cases when this knowledge would be most needed, i.e. at higher life fractions, when safety margins have become small due to degradation of the strength of the laminate. As a consequence, especially when residual strength modeling is to apply on structural design, the application of procedures that predict this statistical behavior is necessary.

In literature, the derivation of the CDF of residual strength based on simple concepts, as shown in the previous sections, is the most common means for accounting for its statistical nature. In the present section, such predictions



### 3. Modeling Residual Strength

produced both by published and by modified models are compared with three different experimental data sets at specific stress levels and life fractions.

Model predictions corresponding to two statistical samples from the tests of Ryder and Walker [22] on a Carbon/Epoxy  $[0/45/90/-45_2/90/45/0]_2$  laminate are shown in the following figures. CDF predictions and residual strength tests in Fig. 38 refer to 31400 cycles under a maximum cyclic stress of 344.77 MPa, corresponding to a life fraction of approximately 77% at the specific stress level, while the ones in Fig. 39 refer to 364000 cycles under a maximum cyclic stress of 289.58 MPa corresponding to a life fraction of almost 16%.

Residual strength data and predictions from the second data set produced by Yang et al. [21] on a Carbon/Epoxy  $[90/45/-45/0]_S$  laminate after 56000 cycles under a maximum cyclic stress of 389.76 MPa, i.e. approximately after 47% of the average life at this stress level, are presented in Fig. 40.

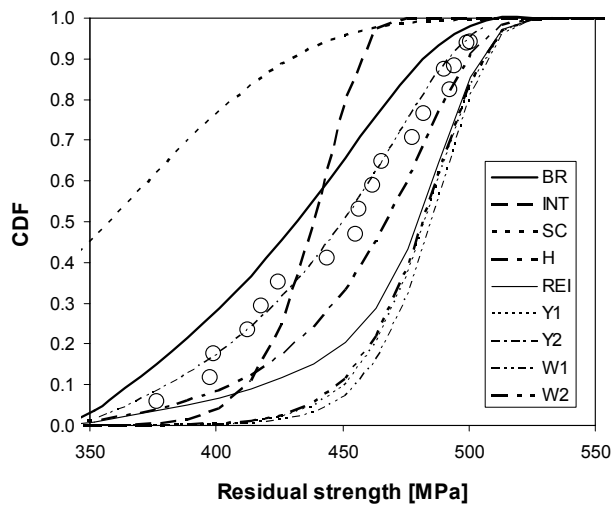


Fig. 38 Probability distributions of residual strength according to the various models for the data set of Ryder and Walker, at 344.74 MPa, 31400 cycles

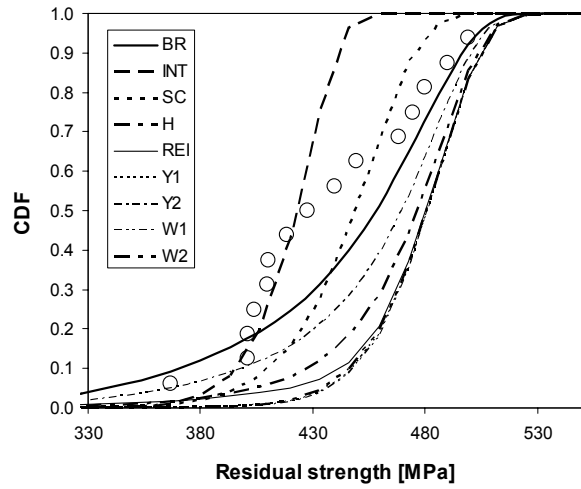


Fig. 39 Probability distributions of residual strength according to the various models for the data set of Ryder and Walker, at 289.58 MPa, 364000 cycles

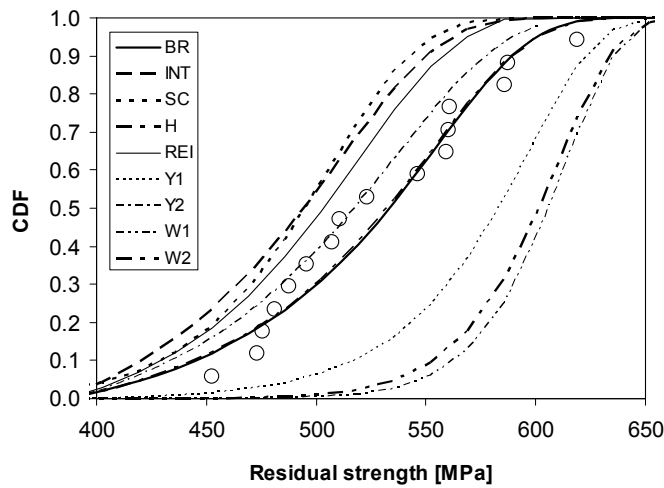


Fig. 40 Probability distributions of residual strength according to the various models for the data set of Yang et al., at 389.76 MPa, 56000 cycles

The third data set used for evaluation of the CDF predicted by each model is from the OPTIMAT material and more precisely the  $[\pm 45]_s$  ISO geometry

### 3. Modeling Residual Strength

coupons used to derive the shear properties of the UD laminate. Fatigue in this case is performed at a maximum cyclic stress of 55.62 MPa while the test is interrupted after 110000 cycles (approximately 50% of nominal fatigue life) for residual strength to be measured. Predictions are shown in Fig. 41. In this case also the OM model is applicable thanks to the availability of residual strength tests at various life fractions per stress level, and its statistical predictions are shown alongside with the rest of the models.

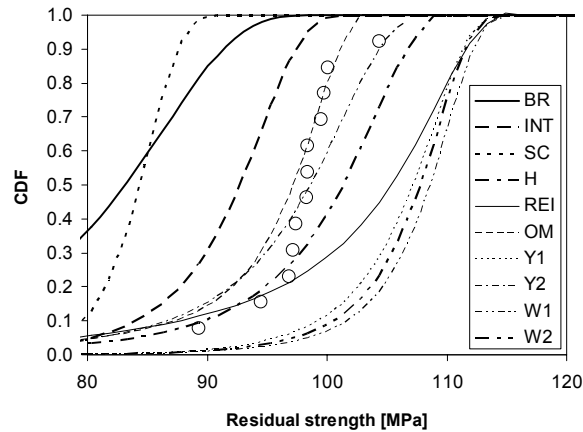


Fig. 41 Probability distributions of residual strength according to the various models for the data set of OPTIMAT  $[\pm 45]_s$  laminate at 55.62.76 MPa, 110000 cycles

From all the above figures it is obvious that some models succeed in predicting the statistical behavior of residual strength even though the majority of the models usually provide poor predictions. Leaving aside the predictions for Ryder & Walker at 289.58 MPa due to the slightly irregular probability distribution suggested by test results -which is followed practically by none of the models- in all other cases a number of models, e.g. Y2, H, REI, BR and OM, provide acceptable predictions both in terms of predicted scatter and mean value of the degraded strength distribution. It is also interesting that some of these models (Y2, H) give reasonable predictions in both the Carbon/Epoxy, fiber dominated laminates and the Glass/Epoxy, matrix dominated one, while others (REI, BR) appear to be less robust, producing in some cases good and in some cases less accurate predictions.

It must be pointed out that any conclusions regarding the quality of model predictions based only on Figs. 38 to 41 would be very risky, since the correct prediction of the CDF at a specific life fraction of a single stress level does not necessarily mean that the prediction would be equally good at other life fractions as well. In order to conclude on this, statistical predictions must be obtained at a wider range of life fractions or at least the average residual strength predicted by the model should corroborate satisfactorily with average experimental values at various life fractions. Consequently, the statistical predictions presented in this section are useful only in combination with the strength degradation curves -when available- discussed in the previous section. For instance, the good prediction of the CDF by model H and Y2 for most of the experimental data sets is not supported by equally good prediction of the experimental degradation curve and thus, it could yield inaccurate predictions at early life of the coupons. On the contrary, and even though it provides poor statistical modeling, the INT model simulates reasonably the degradation behavior of the specific material throughout its entire fatigue life.

In view of these remarks and in order to enhance performance comparison of the statistical predictions of the various models throughout the fatigue life, strength degradation curves corresponding to 90% and 10% reliability are drawn for the residual strength data set of Anderson (Fig. 42), for the unidirectional  $[0]_4$  laminate under  $R=0.1$  and  $R=-1$  stress ratios (Figs (43-48), as well as for the three stress levels of the  $[\pm 45]_S$  laminate (Figs. 49 to 51). Not all of the models, but some characteristic ones are implemented for this purpose, to preserve clarity: these are the BR, INT, REI, OM and Y2 models. The original procedure proposed by Yang (e.g. see [18]) is used for Y2 model, while for the other four, the respective equations, are used, i.e. Eq.(58), (61) and (65).

### 3. Modeling Residual Strength

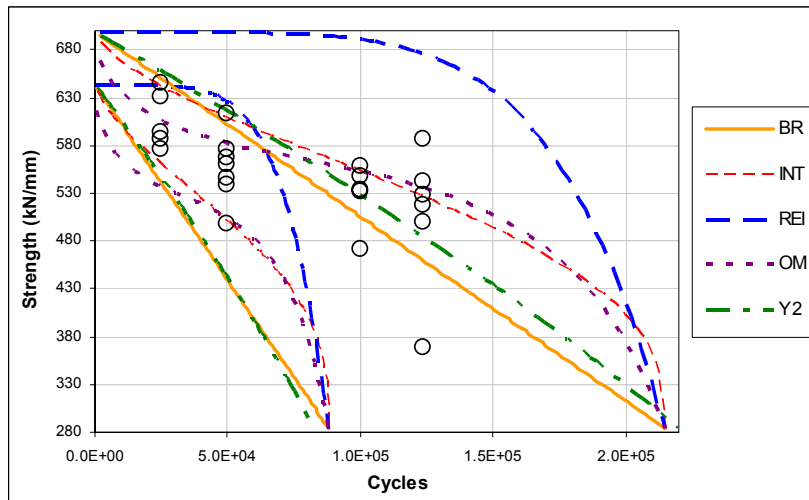


Fig. 42. Degradation curves of 10% (right curves) and 90% (left curves) reliability, predicted by different models for the data set of Anderson at the stress level of 284.2 MPa.

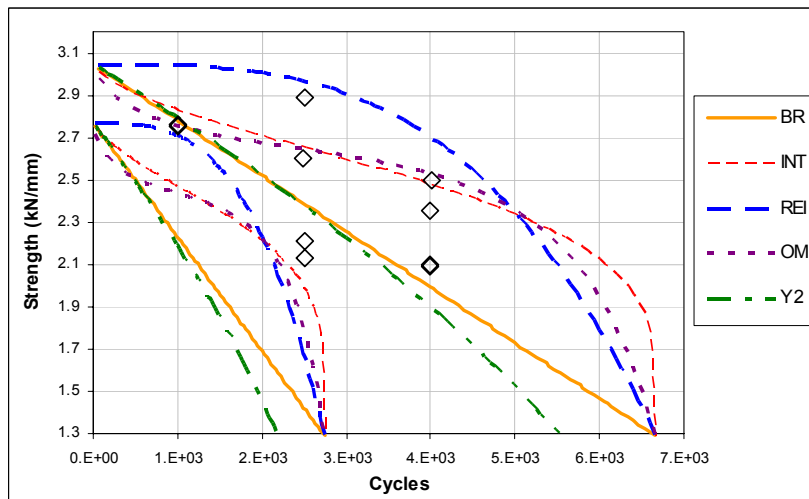


Fig. 43. Degradation curves of 10% (right curves) and 90% (left curves) reliability, predicted by different models for the 1.29 kN/mm stress level at  $R=-1$ .

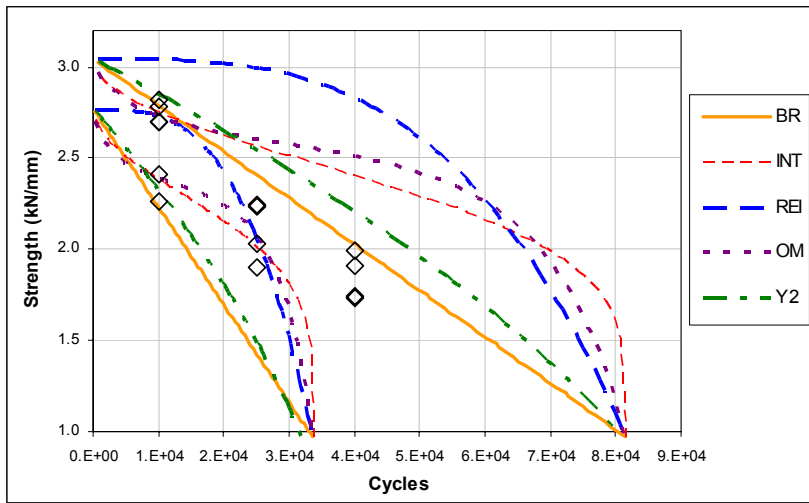


Fig. 44. Degradation curves of 10% (right curves) and 90% (left curves) reliability, predicted by different models for the 0.97 kN/mm stress level at  $R=-1$ .

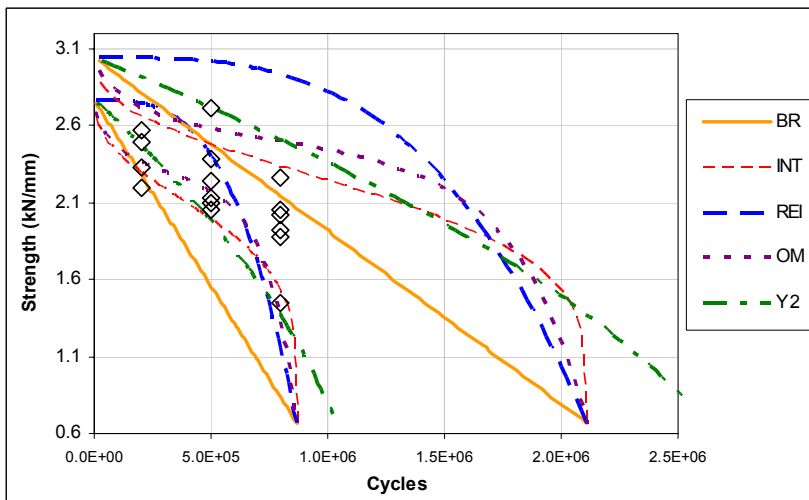


Fig. 45. Degradation curves of 10% (right curves) and 90% (left curves) reliability, predicted by different models for the 0.67 kN/mm stress level at  $R=-1$ .

### 3. Modeling Residual Strength

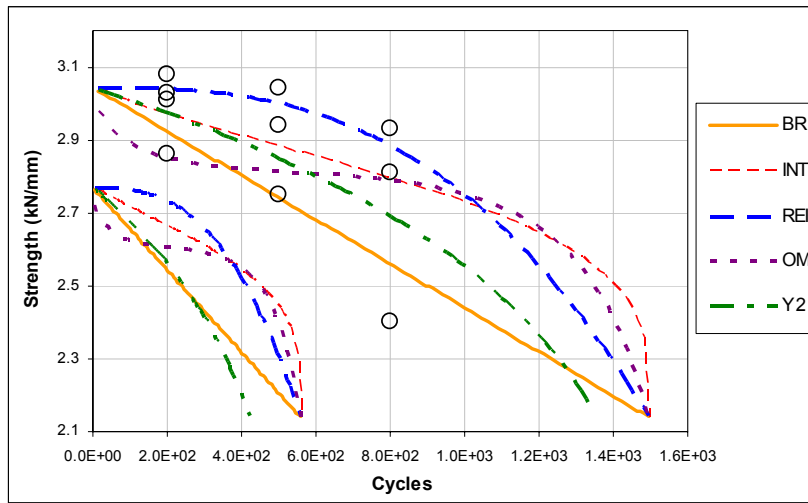


Fig. 46. Degradation curves of 10% (right curves) and 90% (left curves) reliability, predicted by different models for the 2.14 kN/mm stress level at  $R=0.1$ .

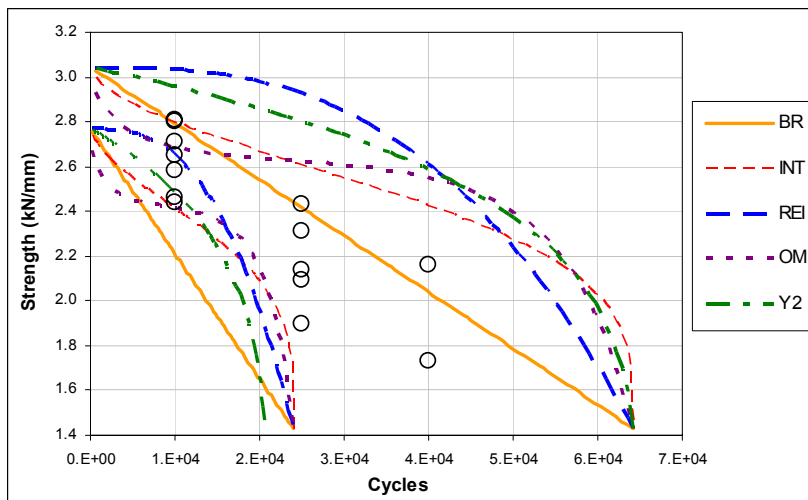


Fig. 47. Degradation curves of 10% (right curves) and 90% (left curves) reliability, predicted by different models for the 1.43 kN/mm stress level at  $R=0.1$ .

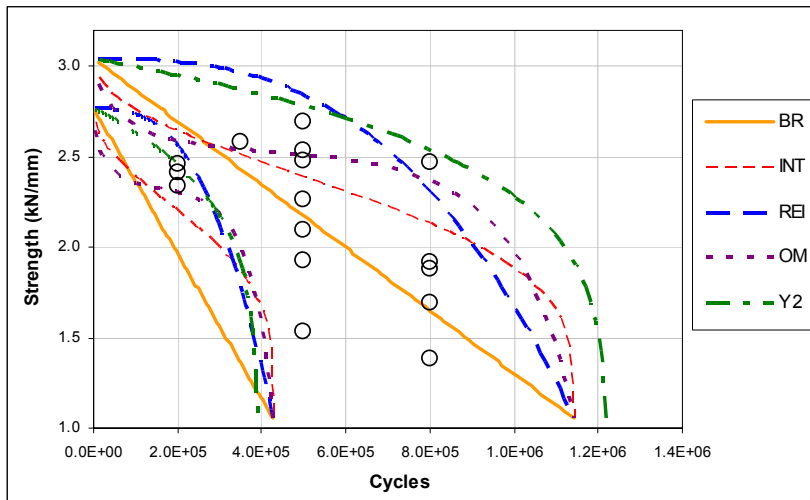


Fig. 48 Degradation curves of 10% (right curves) and 90% (left curves) reliability, predicted by different models for the 1.05 kN/mm stress level at  $R=0.1$ .

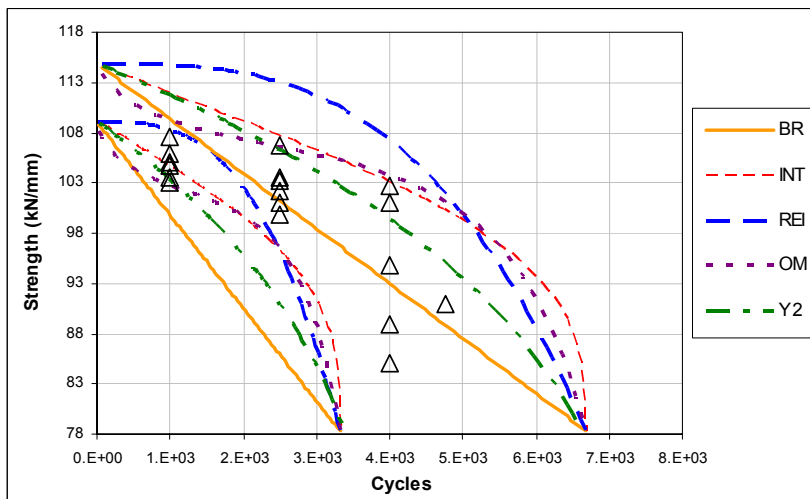


Fig. 49 Residual strength degradation curves of 90% and 10% reliability for the data set of OPTIMAT  $[\pm 45]_s$  at the stress level of 78.3 MPa.



### 3. Modeling Residual Strength

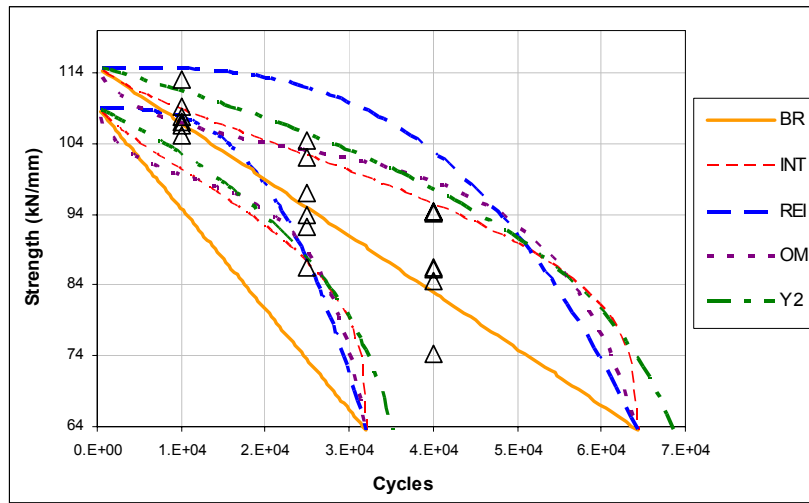


Fig. 50 Residual strength degradation curves of 90% and 10% reliability for the data set of OPTIMAT [±45]<sub>S</sub> at the stress level of 63.6 MPa.

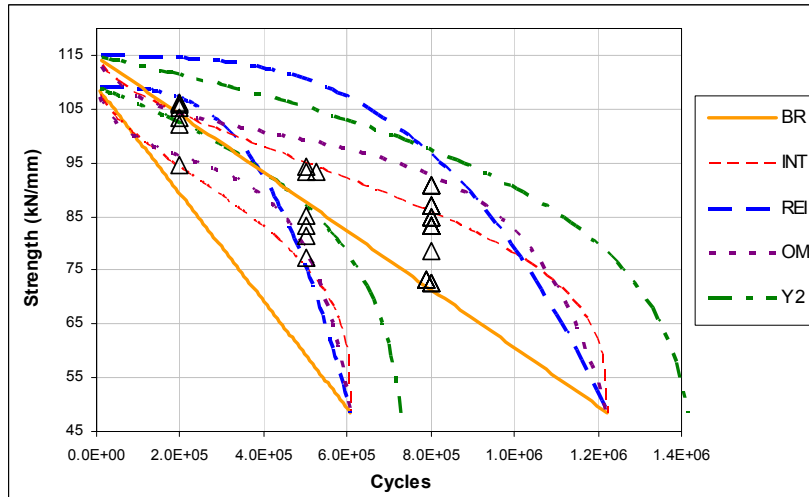


Fig. 51 Residual strength degradation curves of 90% and 10% reliability for the data set of OPTIMAT [±45]<sub>S</sub> at the stress level of 48.5 MPa.

Results indicates in most cases a good agreement between degradation curves and residual strength experimental data for the cases of OM and INT models: In all data sets only one or two test data lie outside the scatter bands drawn, being slightly above the theoretically expected 20%. An exception is the high fatigue stress levels of the [0]<sub>4</sub> laminate, where the already mentioned transition of the

fatigue damage mechanism, to which the presented modeling is blind, results in considerably conservative predictions as seen in Fig. 43 and Fig. 46. Of course, given the small size of each residual strength sample and the high variability of the phenomenon, any conclusions should be drawn on a qualitative rather than quantitative basis. To this must be added the increased variability of the residual strength tests referring to the OB unidirectional laminates since, in contrast to the other two datasets implemented, they have been performed at different testing facilities.

On the same basis, the other three models seem to deviate from the experimental trend: REI and Y2 predictions, even if they follow well the degradation in the 2<sup>nd</sup> half of fatigue life, fail to give accurate statistical predictions in the 1<sup>st</sup> half, where they overestimate considerably residual strength. Finally, BR model tends to be conservative, especially near the end of fatigue life, where almost all of test data lie above even the 10% reliability prediction.

Figs. 42-51 provide also a rough estimate of the expected premature failures at each stress level. If one considers for instance the group of 90%-reliability strength degradation curves, in the left lower corner of Fig. 49, it is seen that after  $N=3230$  cycles the strength has degraded down to 78.3 MPa, i.e. the value of  $\sigma_{max}$ . Consequently, 10% of the coupons planned for cyclic loading at this stress level and number of cycles will fail prematurely. Then with respect to the test results presented in the same figure it is concluded that for life fractions 0.2 and 0.5 less than 10% premature failures are expected while this is not the case for  $n/N=0.8$ .

### 3.5.3 Residual Compressive Strength

Compressive residual strength, in contrast to the tensile one, does not degrade significantly during cyclic loading, as already discussed during the presentation of the experimental data. As in the case of residual tensile strength under compression-compression fatigue, compressive residual strength is assumed to degrade steeply just before fatigue failure following the 'Sudden Death' or SD degradation model described by Eq.(62) with a value of  $k=50$ . Two typical examples of the degradation curves predicted by the SD model in the case of

### 3. Modeling Residual Strength

the UD laminate transversely to the fibers under  $R=10$  and in the fibre direction under  $R=0.1$ , are shown Fig. 52 and Fig. 53 respectively. Fig. 52 shows also the corresponding S-N curve of the material ( $R=10$ ) whose intersection with the compressive strength degradation curve indicates failure according to the fracture condition. In the case of Fig. 53 the S-N curve at  $R=0.1$  is not necessary since the residual compressive strength under tensile fatigue drops to zero at failure.

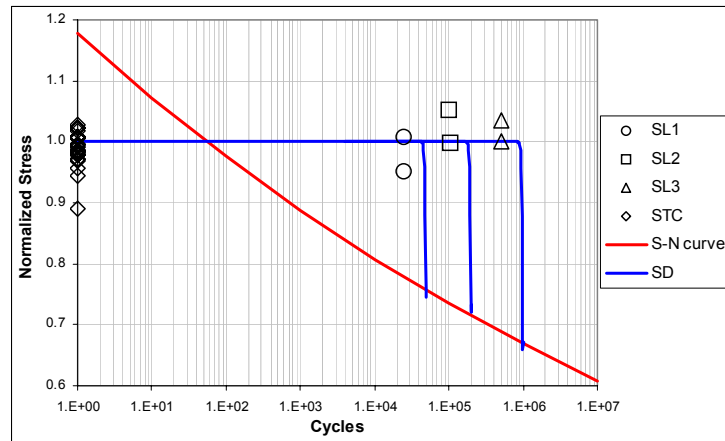


Fig. 52 Sudden death (SD) model predictions and experimental data for the residual compressive strength on the transverse direction of the OPTIMAT UD tested at  $R=10$  at three stress levels.

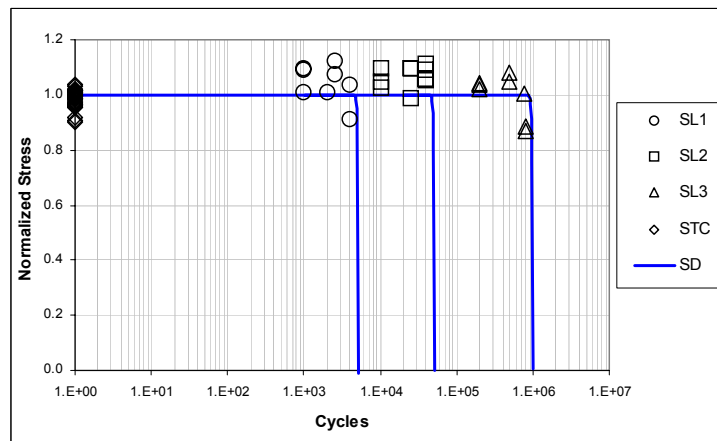


Fig. 53 Sudden death (SD) model predictions and experimental data for the residual compressive strength on the on-axis direction of the OPTIMAT UD tested at  $R=0.1$  at three stress levels.

### 3.5.4 Models Assessment

From the Different phenomenological, engineering models that have been fitted to experimental data three show satisfactory results. These are: The interaction model INT, the OM model and the 2<sup>nd</sup> model of Yang (Y2). The REI model, used from several authors, is also shown in the comparison, even though it tends to overestimate residual strength during a large initial part of the material's fatigue life, while the linear model is included in the discussion due to its simple form.

Both REI and Y2 model fail to predict the initial strength decrease observed on all laminates tested, both under tensile ( $R=0.1$ ) and alternating fatigue ( $R=-1$ ), while in addition to that, the majority of REI model predictions lie on the non-conservative side. On the other hand the Y2 model, apart from its inefficiency to describe the observed initial loss of strength, predicts satisfactorily the subsequent average strength degradation. Its complexity of course is a disadvantage e.g. for use in variable amplitude life predictions, but this can be considered of limited importance.

The OM model, developed in the course of this work, is flexible enough to follow well different degradation trends. Its implementation is simple and requires as limited an experimental data set as the INT model. Its degradation equation is not a monotonically decreasing one for any combination of the parameters  $k_1$  and  $k_2$ . This is the reason for which it can lead to false results when implementation is based on misleading residual strength tests. An equally flexible model, requiring a reasonable amount of experimental data, is the INT model which describes acceptably the degradation of average strength in all cases. Given its two parameters, its degradation equation as well as the fact that it is based on direct fitting, it is a competitive alternative for simply and effectively modeling various degradation trends, from slow wear out to sudden death.

Finally, the linear model (BR), as mentioned before, has been proved in all cases (especially in the more interesting lower stress levels) to lead to predictions which are either fair or lie on the conservative side and is definitely proposed as a safe alternative applicable in all cases where residual strength data are not available, or where cost related issues deter the completion of the -

### *3. Modeling Residual Strength*

usually large- experimental effort required for detailed residual strength characterization (See also [44]).

Regarding the statistical predictions of the models, it is difficult to draw definite conclusions based simply on CDF predictions at specific life fractions, while the limited number of tests and the experimental variations induced into the test program (different laboratories, differences in plate properties etc) slightly blur the picture for the OPTIMAT  $[0]_4$  laminate. Nevertheless, the tests available from Anderson et al. as well as the comprehensive data set from the OPTIMAT  $[\pm 45]_S$  laminate are used for evaluating the statistical modification proposed, in terms of reliability based degradation curves. The results suggest that the proposed methodology yields satisfactory statistical predictions both in the 10% and 90% reliability levels, in combination with the INT or OM deterministic degradation equations. BR model yields again predictions lying on the conservative side, which nonetheless can be considered quite acceptable, or even an advantage, for practical applications given the model's simplicity.



## 4 LIFE PREDICTION UNDER SPECTRUM LOADING

### 4.1 INTRODUCTION

In this section, the state of the art procedure for prediction of life of composite laminates under cyclic loads, either of constant (CA) or variable amplitude (VA), is discussed. A thorough investigation of the influence of the Counting Method, CLD choice and Damage Accumulation Rule is attempted, based on experimental data from three different spectrum patterns. Special focus is put on damage summation and especially on the alternative of implementing residual strength based models, such as the ones described in the previous chapter, into life prediction procedures under variable amplitude cyclic loading.

The investigated life prediction methodology considers the material macroscopically, in the laminate level without considering the characteristics of each individual ply. Consequently, it refers to a specific composite laminate for which all material properties are defined while any prediction of life refers to this particular laminate. This approach can be proved to be quite restrictive, especially during fatigue design of complex composite structures where life prediction must be performed for different lay-ups that vary considerably in terms of mechanical properties. In that case, full experimental characterization should be performed for each individual laminate, multiplying the experimental effort and cost.

In common practice a compromise is usually achieved by defining the properties of a small number of 'typical' laminates and assuming similar lay-ups to have a similar fatigue response (for instance approximating the fatigue

response of all fiber dominated laminates to by that of the UD material). In order to eliminate the errors induced by such assumptions, more detailed methods, e.g. the ply-to-laminate approach discussed in the following chapter, should be considered. An indispensable part of such approaches would be the standard life prediction methodology considered in the present section. In the following paragraphs it is implemented on the unidirectional (UD) reference material, presented in detail in the previous sections, in order to evaluate and assess various alternatives offered for the different modules it consists of. These are:

- (a) Cycle counting of the examined spectrum, in order to transform a random load time series to cycles or groups of cycles of specific mean value and amplitude, i.e. transform a loading spectrum to blocks of constant amplitude (CA) cycles.
- (b) Determination of fatigue life for each bin of constant amplitude (CA) cycles using an appropriate constant life diagram (CLD) definition.
- (c) Damage summation, which is the method for accumulating the damage induced by each individual CA fatigue cycle in order to predict when fatigue failure should occur.

While numerous publications concerning life prediction of composites under cyclic loading of variable amplitude are available in literature (see for instance, the works by Yang & Du [28], Hwang & Han [67], Adam et al. [32], Schaff and Davidson [68], Bond [69] and Philippidis & Vassilopoulos [70]), their large majority concerns specific life prediction methods, validated by comparing with experimental data on standardized loading spectra (e.g. WISPER, FALSTAF), realistic spectra or block loading sequences. Even though the basic concept remains unchanged, many alternatives regarding the above mentioned modules are proposed and validated. Nevertheless, limited effort is spent on assessing these alternatives based on a common experimental data set, studying their relative impact on the quality of the predictions or investigating the influence of the spectrum pattern itself (see [71], [72]).

Investigations of the efficiency of Palmgren-Miner rule in comparison with different damage accumulation metrics were presented by Schaff and Davidson [68], Bond [69], Philippidis & Vassilopoulos [70] and Hosoi et al. [73]. The role of S-N curve formulation was treated by Nijssen et al. [74] while cycle counting



#### *4. Life Prediction Under Spectrum Loading*

effects on the predictions were considered by Nijssen [75] and Vassilopoulos [76]. A comprehensive study of several life prediction parameters on standardized spectra was recently presented by Nijssen [77].

## 4.2 IMPLEMENTED SPECTRA

Three loading spectra representative of operating wind turbine rotor blades are considered in this study. The first is the WISPER stochastic loading spectrum the second is the NEW WISPER spectrum developed in the frame of OPTIMAT BLADES project while the third called MWIND is extracted from numerical aeroelastic simulations performed during the EU project MEGAWIND [78]

WISPER is a standardized loading spectrum introduced in 1988 by Tan Have [79], with the purpose of providing a reference variable amplitude test loading, applicable in the Wind Turbine Industry, which would enable the exchange and comparison between variable amplitude fatigue test results from various origins. The spectrum has been widely accepted as a means for comparing life prediction methodologies, ranking materials, structural details or fabrication techniques. The basis of the spectrum is measurements of the flap bending moment referring to the root area of nine Wind Turbine Rotor Blades of different diameters, materials and site characteristics. The diameters range from 11.7 to 80m while referring to a wide range of blade materials such as steel, Glass or Carbon reinforced plastics and wood epoxy. The spectrum, shown in Fig. 54, includes 265,423 load reversals between 64 discrete load levels that range from -24 to 39. The standard spectrum is multiplied by an appropriate factor to transform the non-dimensional reference levels to loads of desired magnitude, usually referring to by the spectrum's overall maximum load.

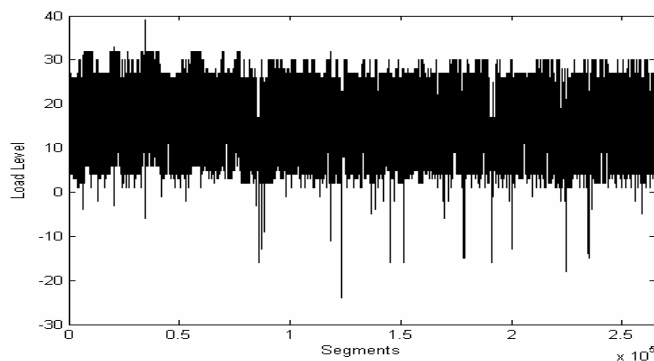


Fig. 54 WISPER spectrum

During the OPTIMAT project the development of an updated version of the WISPER spectrum, called NEW WISPER [80] has been decided for several

reasons, including the considerable increase in the size of Rotor Blades, the dominance of composites as their structural materials as well as changes in the control of the turbine reflected to the induced fatigue loads, such as the transition from stall control to full span pitch control and to variable operating speed. A visual comparison between the Wind Turbines used during the composition of the WISPER and NEW WISPER spectra is shown in Fig. 55.

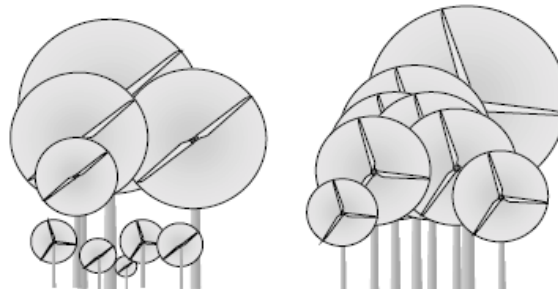


Fig. 55 Visual Comparison between Wind Turbines used in the composition of WISPER (left) and NEW WISPER (right) loading spectrum (picture taken from [80]).

The characteristics of the NEW WISPER sequence are:

8 turbines out of which 6 are of MW or MMW scale

Rotor diameters between 37m and > 100m

Rotor blades made of composites

6 turbines pitch controlled / 2 turbines stall controlled

5 turbines with variable speed / 3 with two fixed speeds

All turbines 3-bladed

The new spectrum is considerably shorter, including 95472 load reversals with the levels ranging from -17 to 37. The form of NEW WISPER is shown in Fig. 56. The sequence appears to be arrayed in an increasing ordered of similar variable amplitude blocks due to the fact that the randomization process has not yet been accomplished.

It is evident that both WISPER and NEW WISPER spectra do not represent design loads. They are merely reference load series developed for comparison purposes, composed from a variety of measured loads encountered at

characteristic parts of Wind Turbine blades and refer to a multitude of wind conditions that are likely to be encountered in a period of time.

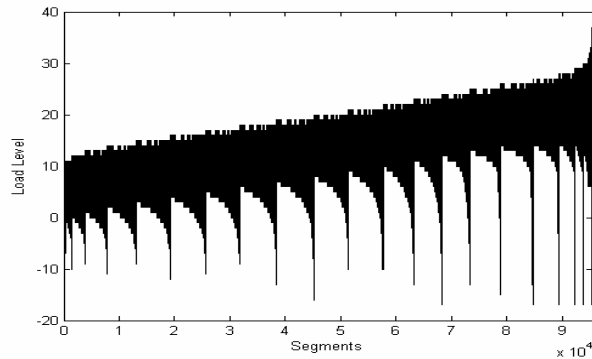


Fig. 56 NEW WISPER spectrum

A different loading spectrum investigated herein is the henceforth denoted MWIND or MW spectrum. It is a load series consisting of 5977 load reversals, obtained from numerical aero-elastic simulation of fatigue load cases in rotor blades. More specifically, the MWIND spectrum is representative of the axial normal stress at the pressure skin of a 30 m split rotor blade at a location 18.4 m distant from the root, on the main spar cap area. It is derived from simulation of a power production design load case, corresponding to  $21 \text{ ms}^{-1}$  wind speed and  $-10^\circ$  yaw error encoded as DLC 1.2 NTM (Normal Turbulence Model) according to IEC 61400-1 standard. Details on load cases considered, calculations and results from fatigue design considerations of the 30 m rotor blade are reported in [81]. Its shape is displayed in Fig. 57.

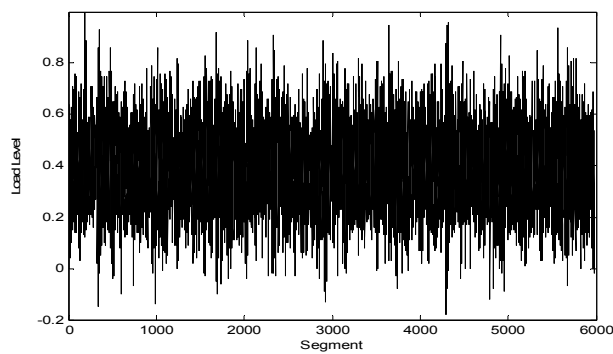


Fig. 57 MWIND spectrum

When comparing the composition of the three spectra in terms of the ranges of their fatigue cycles, the similarities between the first two artificial load series as well as the differences with the simulation's result become more apparent. As seen in Fig. 58, both W and NW have a similar composition with NW including about 10% higher loads throughout most of the cycles, while the small cycles of under about 20% of the maximum range are censored (see right end of the graph). On the contrary, the MW spectrum has about 70% of its cycles having a range lower than 20% of its maximum, while the medium ranges of its cycles (from 30% to 70% of the maximum value) are considerably more populated than in the other two cases.

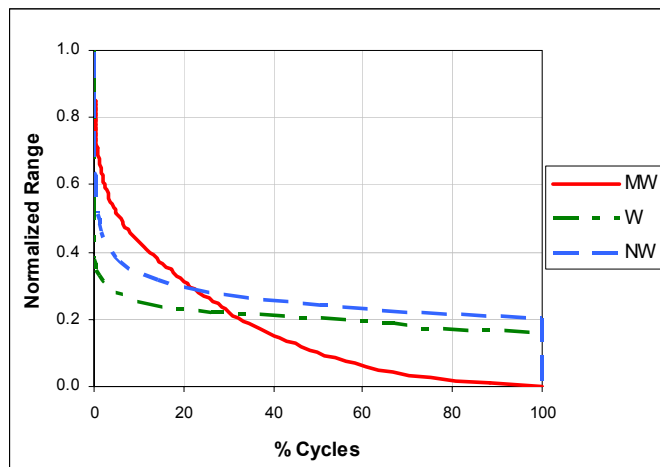


Fig. 58 Comparison of the cumulative composition of the three spectra in terms of stress ranges of their cycles.

Similar conclusions are drawn from the comparison of their spectral content, in terms of the load amplitudes ( $\sigma_a$ ) of their segments, normalized by their respective maximum values, which is shown in Fig. 59 with the percentile composition given in the vertical axis in logarithmic scale so that the differences in the rarer cycles become more apparent. The observed assemblage of the greatest part (up to 98%) of WISPER and NEW WISPER amplitudes between 30% and 50% of their maximum values is an expression of their artificiality up to a degree that would rarely be observed in structures undergoing stochastic loading. On the contrary, the shape of the density distribution of the MWIND spectrum resembles more to a white noise signal. Observing the composition in

terms of the mean stresses ( $\sigma_m$ ) of the segments (bottom graph of Fig. 59), there seems to be no qualitative difference between the three sequences, except from the smoother appearance of the MWIND and NEW WISPER spectra in terms of mean stresses in contrast to the composition of WISPER spectrum where the large majority of cycles come with high means (>60%).

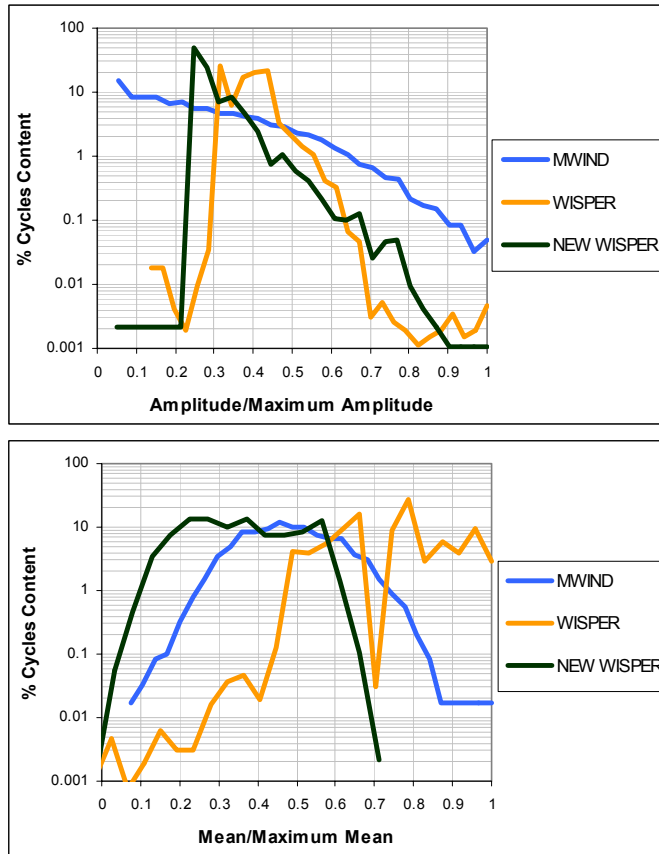


Fig. 59 Comparison of the three spectra in terms of amplitude (upper) and mean (lower) stress of their segments

The above comments regarding the composition of the three loading series are schematically resumed in Fig. 60, where the cycles are displayed as points in the mean stress-stress amplitude plane. From this figure it is evident that the average stress ratio of the three spectra differs, with NEW WISPER being shifted towards the tension-compression quadrant of the plane and MWIND

being confined in the tension-tension region. Furthermore, the large number of small amplitude cycles of MWIND is clearly seen along with the variety of their mean values ranging from very small to almost 75% of the UTS. Even though this range of small cycles have been excluded from the other two series, the NEW WISPER series retains the triangular form similar to MWIND which resembles to a more realistic spectrum composition in comparison to the more artificially distributed cycles of WISPER. Of course this representation by itself does not shown the whole picture, since each point in the graph could represent a single or several thousands of cycles.

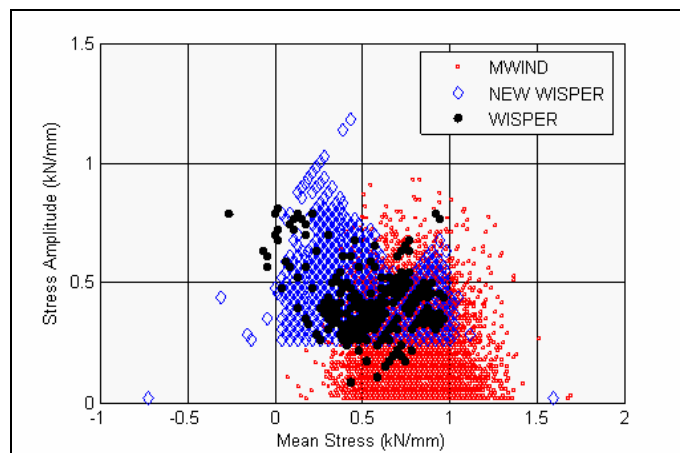


Fig. 60 Location of the cycles of the three spectra in the mean stress - stress amplitude space.

Apart from the differences and similarities in their composition, a closer investigation of the three spectra reveals another important difference, regarding the way the cycles are arrayed inside each of them. A rough idea can be obtained by a closer examination of a random spectrum's detail as seen in Fig. 61. Both WISPER and NEW WISPER have the artificial appearance of a composition of constant amplitude blocks. In addition to that, the majority of these blocks remains confined within a limited range of stress amplitudes as seen in Figs.58 and 59. Even if NEW WISPER seems smoother than WISPER in the small scale (due to the lack of randomization), it has a similar segment content and in a larger scale (several spectrum passes) it would be expected to

induce similar sequence effects as the latter one. The totally different picture seen in the MWIND spectrum's detail explains its noise-like density distributions discussed above. A multitude of small amplitude cycles interfere within larger load fluctuations and greatly increase the number of load reversals. As stated above, some of these small amplitude cycles can have a significant mean stress, almost up to 75% of the nominal strength as seen in Fig. 60, nevertheless, the mean stress of most of them remains below 30% and has limited impact on the material as far as fatigue damage is concerned.

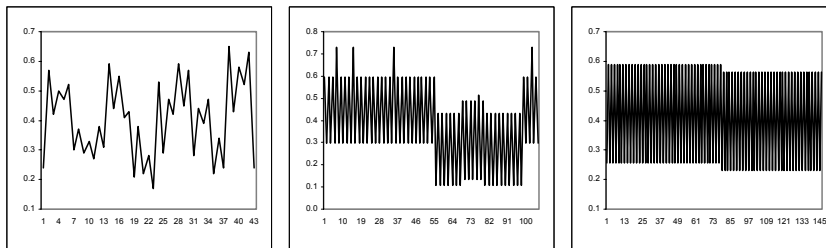


Fig. 61 Details of MWIND (left), WISPER (center) and NEW WISPER (right) spectra.

The actual load one would probably come up with through direct strain measurements on an operating blade, would be similar to the MW rather than to the W or NW sequences. In this view the MWIND spectrum becomes of special interest as far as life prediction is concerned.



## 4.3 LIFE PREDICTION METHODOLOGY

### 4.3.1 Cycle Counting Method

Cycle counting is the first procedure any loading spectrum must undergo in order to be analyzed and processed in terms of constant amplitude fatigue cycles, since all basic fatigue characterization of a material is performed through constant amplitude sinusoidal cycles. Several methods have been proposed for counting the cycles of a spectrum [82]. Some counting methods are briefly presented below:

*Level Crossing Counting.* According to this method the load axis is divided into a number of preset stress levels and one counting is recorded each time the load exceeds one. When all level crossings have been recorded, cycles can be formed by constructing first the largest possible cycle, then the second largest etc until all level crossings have been used. This way the spectral loading is transformed into a series of decreasing amplitude cycles. Of course, once this - most damaging- counting scenario has been obtained, the cycles can be rearranged in any desired order inducing secondary load-sequence effects.

*Peak Counting.* As in the above case, the procedure focuses on the identification of peaks and troughs of the considered spectrum. Once all these have been obtained, the first cycle is constructed by combining the highest peak with the lower trough etc, until all peaks have been used.

Both peak and level crossing counting methods yield most damaging cycle counting results, since they focus on the construction of the largest cycles possibly obtained from a specific spectrum. Further on, they totally neglect the order of occurrence of each loading event and thus load sequence effects, which depending on the shape of the spectrum could have a considerable effect, cannot be taken into account.

*Simple Range Counting.* This most simple method considers a range, i.e. the difference between two successive load reversals, to be one half cycle. Even though the order of occurrence of loading events is retained during counting, large cycles having a major impact on fatigue analysis may not be recorded by this counting procedure if they include smaller load fluctuations which will divide them into several smaller ranges.

*Rainflow Counting.* This name represents a family of methodologies developed from the early 1960s in an effort to analyze a spectrum into loading cycles as accurately as possible, i.e. based on stress-strain events (hysteresis loops) occurring inside the material during fatigue. The method has been introduced almost simultaneously by Matsuishi and Endo [83] (accessible in English in [84]) and de Jonge [85], while slightly different algorithms have been proposed up to date. For a comprehensive review of the rainflow counting method see [77].

A schematic interpretation of how a rainflow algorithm records cycles is shown in Fig. 62, in which a part of a loading spectrum (left) is interpreted in terms of stress-strain curves on the right hand side. The result counts three cycles (BC, EF and GH) while the segment AH that remains once closed cycles points are discarded is called residual.

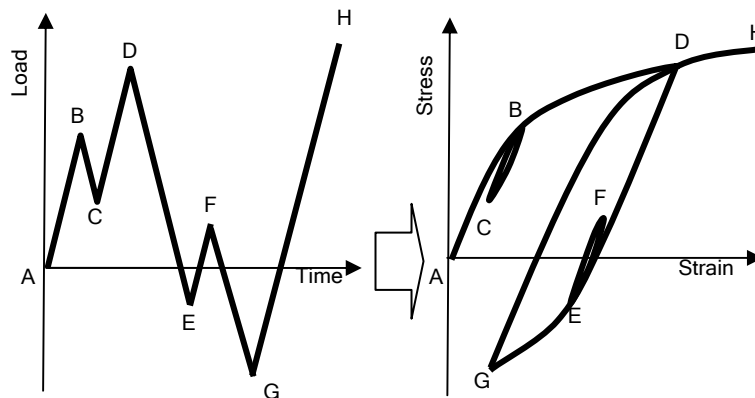


Fig. 62 Load time history and corresponding qualitative stress-strain graph, showing the hysteresis loops (BC, EF and DG) counted by Rainflow algorithm.

Despite the fact that Rainflow counting does yield accurately the fatigue cycles equivalent of a spectrum, it inevitably rearranges the load history and the spectrum needs to be preprocessed before being inserted into a life prediction algorithm. While the first is inevitable, it can be partly eliminated through the use of an adequate algorithm, such as the 'Algorithm II' proposed by Downing and Soccie [86], which counts a history of peaks and troughs, without rearranging them, in sequence as they occur. The closed loops are recorded immediately

after completion while the remaining peaks and troughs are processed again to leave in the end a number of half cycles as residual. A flowchart of the algorithm is shown in Fig. 63. The algorithm keeps track of the peaks and troughs that have not yet formed a closed loop through vector  $E$ , in which all read points are recorded and from which all points having formed a cycle are discarded.  $\Omega$  denotes the range under consideration while  $\Psi$  the previous one adjacent to  $\Omega$ .  $S$  is a tab placed initially at the beginning of the spectrum and progressing according to the simple rules demonstrated.

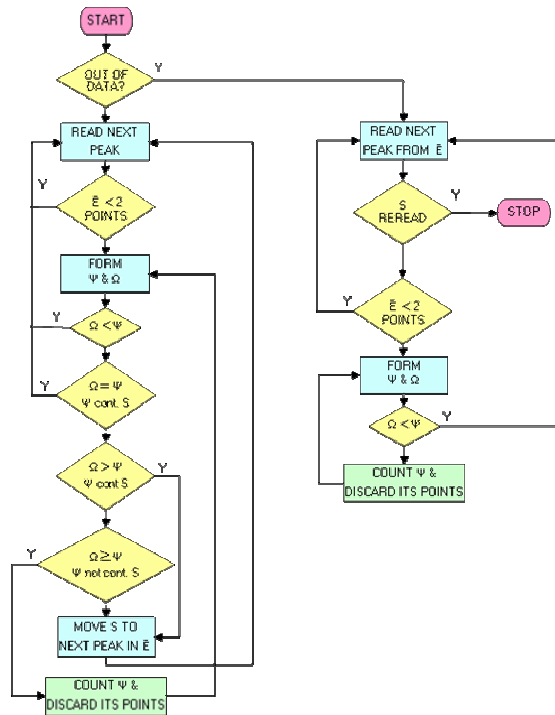


Fig. 63 Flowchart of the one pass Rainflow algorithm (Algorithm II) proposed by Downing & Soccie.

### 4.3.2 Constant Life Diagram

The problem of predicting life under constant amplitude fatigue of arbitrary mean stress and stress amplitude based on fatigue data coming from few specific stress ratios is dominant in any fatigue study involving variable amplitude or spectrum fatigue. The simplest formulation is the well established

Goodman Line displayed, in normalized values, in Fig. 64. Each line shown in the figure is constructed based on the static strength of the material (tensile and compressive) and one S-N curve (In this case at R=-1 stress ratio) and corresponds to a specific fatigue life: Constant amplitude fatigue performed under the mean stress and stress amplitude combinations lying along each line are assumed to result in a constant fatigue life. This type of diagram is subsequently called Constant Life Diagram or CLD.

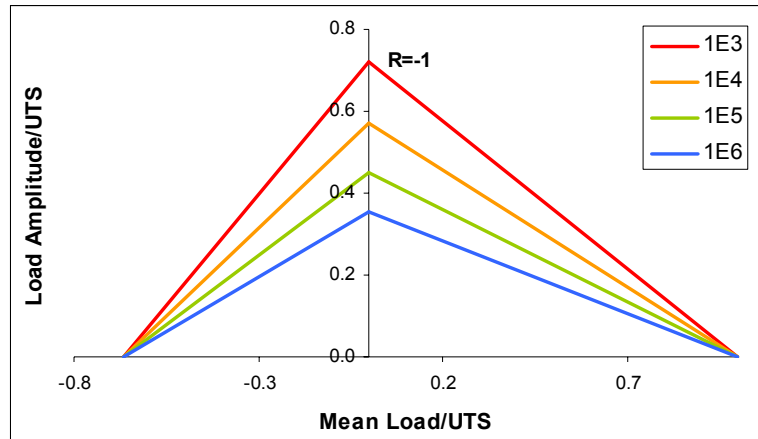


Fig. 64 Goodman Lines constructed for four different fatigue lives

Assuming as before the stress ratio R to be the ratio of the minimum versus the maximum cyclic load, the function relating the mean and amplitude load to the stress ratio R is given by:

$$\sigma_a = \sigma_m \frac{(1-R)}{(1+R)} \quad (68)$$

More than one S-N curves can be incorporated in a CLD, thus increasing, apart from the experimental cost, the accuracy of life prediction under different cyclic loads. The typical CLD requires three different S-N lines determination in order to have experimentally obtained input for the fatigue behavior of the material in the three main regions of the mean-amplitude space: Tension tension, tension-compression and compression-compression. The S-N most typically used are

at  $R=0.1$ ,  $R=-1$  and  $R=10$  correspondingly. Such a CLD is shown in Fig. 65 and will be called LCLD in the frame of this work.

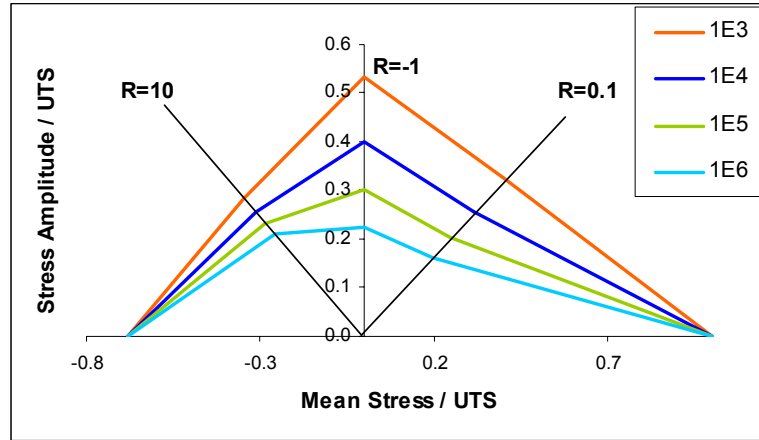


Fig. 65 Constant Life Diagram (CLD) constructed based on three S-N curves at  $R=0.1$ ,  $R=-1$  and  $R=10$ .

Assuming the above shown three experimentally derived S-N curves, at  $R_1=0.1$ ,  $R_2=-1$  and  $R_3=10$ , the S-N curve at an arbitrary stress ratio  $R'$  is derived from the following relationships [70]:

$$\sigma'_a = \frac{X}{\frac{X}{\sigma_{a_1}} + r' - r_1} \quad \text{for} \quad 0.1 < R' < 1 \quad (69)$$

$$\sigma'_a = \frac{\sigma_{a_1} (r_1 - r_2)}{(r_1 - r') \frac{\sigma_{a_1}}{\sigma_{a_2}} + (r' - r_1)} \quad \text{for} \quad -1 < R' < 0.1 \quad (70)$$

$$\sigma'_a = \frac{\sigma_{a_2} (r_2 - r_3)}{(r_2 - r') \frac{\sigma_{a_2}}{\sigma_{a_3}} + (r' - r_3)} \quad \text{for} \quad \begin{matrix} -\infty < R' < -1 \\ \& \quad 10 < R' < \infty \end{matrix} \quad (71)$$

$$\sigma'_a = \frac{X'}{\frac{X'}{\sigma_{a_3}} - r' + r_3} \quad \text{for} \quad 10 < R' < \infty \quad (72)$$

Where

$$r_i = \frac{1+R_i}{1-R_i} \quad \text{and} \quad r' = \frac{1+R'}{1-R'} \quad (73)$$

and  $\sigma_{a_i}$  stands for the S-N curve expressed in terms of stress amplitude:

$$\sigma_{a_i} = S_{o_i} N^{-\frac{1}{b_i}} \quad (74)$$

When Eqs.(73) and (74) are replaced into eqs.(69-72) the fatigue life can be numerically derived for any specified combination of  $\sigma_a'$  and  $R'$ . Alternatively, different values can be assigned to  $N$  in Eq.(74) and through substitution into Eqs (69-72) define a series of  $(N, \sigma_a')$  points along the S-N curve at  $R'$ . Once these points are known they can be fitted by an equation in the form of Eq.(74) to give the S-N at the stress ratio in question.

From Fig. 65 it is obvious that even if in certain cases the constant life lines are very close to the Googman assumption, in most cases the predicted behavior deviates considerably from it, especially in the compression-compression quadrant where the very flat S-N curve distorts the form of the CLD. Similar conclusions on the questionable verification of the linear Goodman interpolation between the fatigue and static experimental data are drawn from the fatigue tests on MD material performed during OPTIMAT project at 6 different  $R$  values ranging from  $R=0.5$  to  $R=10$ , see [77], as well as from the Glass/Polyester tests performed in [87] on on-axis and off-axis coupons from multidirectional composite plates. The detailed investigation performed by Mandell et al. [88] at 13 stress ratio indicates the relative importance of the region near  $R=-1$  where the failure modes change from tensile to compressive. Similar conclusions are also drawn in [89].

Alternatively non linear equations have been implemented to fit more efficiently the limited fatigue data that support the construction of the CLD. One such formulation implemented in this work is the one proposed by Gathercole at al. [34]. It is based on the following function:

$$\frac{\sigma_a}{X} = f \left( 1 - \frac{\sigma_m}{X} \right)^u \left( \frac{X'}{X} + \frac{\sigma_m}{X} \right)^v \quad (75)$$

$X, X'$  is the static tensile and compressive strength respectively, while  $f, u$  and  $v$  are considered herein to depend linearly on the logarithm of fatigue life  $N$ :

$$f = A_1 \log N + B_1$$

$$u = A_2 \log N + B_2 \quad (71)$$

$$v = A_3 \log N + B_3$$

To derive parameters  $A_i$  and  $B_i$  the following procedure is adopted: First, the mean stress and stress amplitude corresponding to known fatigue lives (e.g.  $10^3, 10^4$  and  $10^6$  cycles) are calculated for the three known S-N curves. Then  $f, u$  and  $v$  corresponding to each of those fatigue lives are calculated through LSQ fitting of Eq.(75) to the corresponding stresses in the mean-amplitude stress space. Finally, Eqs.(76) are fitted to the above calculated data. Fitting of  $f, u$  and  $v$  to the OPTIMAT UD data is shown in Fig. 66.

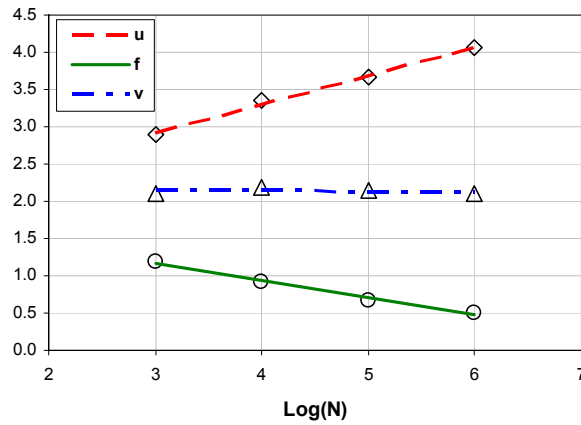


Fig. 66 Regression lines of the  $f, u$  and  $v$  parameters of BELL CLD, fitted on OPTIMAT UD at  $0^\circ$ .

The form of this type of CLD, called henceforth BELL, is displayed in Fig. 67.

All CLD formulations discussed above include the static strength data in tension and compression to which all constant life lines converge for  $R=1$ . Several issues arise from combining static strength with fatigue life test results, such as strain rate used and failure modes observed. The investigation of Mandell et al. [88] at stress ratios between  $R=0.5$  and  $R=0.9$  indicates that inclusion of the static data may lead to overestimation of fatigue lives at the specific stress ratios.

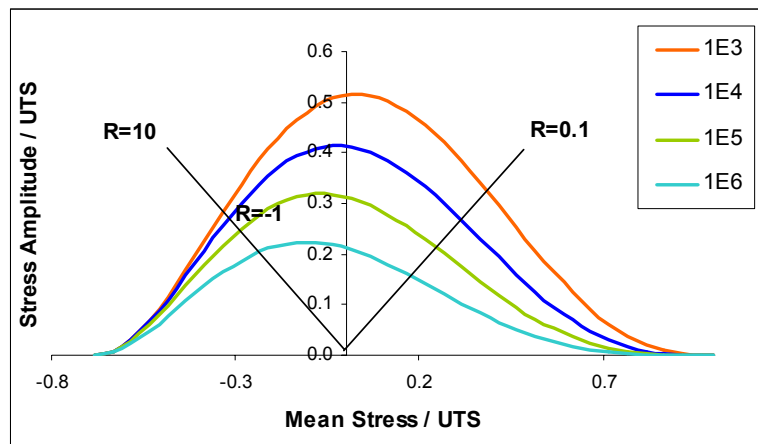


Fig. 67 BELL CLD constructed based on three S-N curves at  $R=0.1$ ,  $R=-1$  and  $R=10$ .

Apart from the above mentioned CLD types other assumption can be used to serve the same purpose. For instance performing fatigue tests at a single stress ratio and then assuming all the cycles of a spectrum to belong to this derived S-N curve is an alternative already proposed in literature. Undoubtedly, the latter assumption is an oversimplification, since it neglects the dominant dependence of fatigue life on the stress ratio amid other important parameters. Nevertheless, for certain spectra patterns, when all cycles remain relatively close to a single R-value it can lead to quite acceptable results. This CLD formulation is implemented in subsequent sections (based on the tension-tension  $R=0.1$  S-N curve) under the name R01.



In the  $(\sigma_m - \sigma_a)$  space, the above assumption implies that a constant life line forms an isosceles triangle, subtending  $n/4$  angles with the  $\sigma_m$ -axis (see Fig. 68), its equation being expressed by:

$$\sigma_a = \frac{\sigma_o}{N^k} - \sigma_m \quad (77)$$

Obviously, S-N curves at various R-values, having different  $\sigma_o, k$  parameters, lead to alternative CLD formulations. In addition, it can be shown that theoretical predictions derived by implementing the above CLD formulation, combined with the Palmgren-Miner rule, coincide with those of the WAR method, discussed in subsequent section.

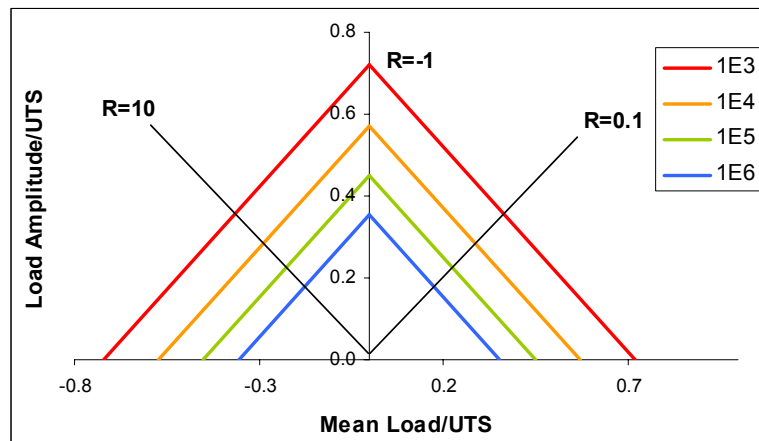


Fig. 68 CLD lines constructed based on the assumption that all cycles are described by a single S-N line ( $R=0.1$  in this case) independently of their stress ratio.

### 4.3.3 Damage Accumulation

The most commonly used damage metric is the well known Palmgren-Miner (PM) rule. It is a simple linear empirical rule and even though it cannot account for load sequence effects which are encountered in practice, e.g. Poursartip et al. [90], Gamstedt et al. [91], it is widely used in structural design applications. According to this rule it is assumed that each cycle or block of cycles under

specific fatigue loads contributes to the total damage an amount equal to the fraction of the life spent under these loads.

$$\sum_{i=1}^m \frac{n_i}{N_i} = D \quad (78)$$

The total damage  $D$  is most often taken as unity, even though its value has been proved in many cases to deviate considerably from this value as a consequence of the kind of applied fatigue load, load sequence etc, e.g. [8], [34]

As pointed out, the use of static strength degradation -or residual strength, as damage metric implemented in life prediction schemes appears to be potentially promising. Damage, in that case is expressed by the reduction of static strength of the material during cycling and is directly determined after each cycle of the loading spectrum. The degradation can depend on various loading parameters such as maximum cyclic load, stress ratio, loading rate etc. while sequence effects are theoretically taken into account, since the degradation after each cycle depends on the loading characteristics of the current cycle as well as on the loading history experienced by the material. Even in the case where linear strength degradation is assumed, the modified form of PM rule based on residual strength proposed by Broutman and Sahu [6] is proved to account for sequence effects in fatigue life under VA fatigue. Another benefit from the incorporation of residual strength as damage metric comes from the fact that fatigue damage is related to a basic mechanical property thus enhancing it with a clear physical interpretation rather than an empirical assumption.

According to the results discussed during the evaluation of the various residual strength models, few are the models that satisfactorily describe the phenomenon. Amongst them the INT and OM model appear to be more promising and consequently their implementation in life prediction under variable amplitude loading is attempted. The linear model being a competitive alternative is also implemented.

For predicting strength degradation under variable amplitude fatigue, especially for the case of non-linear residual strength models, the introduction of the

'equivalent number of cycles' quantity is necessary. The reasoning behind it is displayed in Fig. 69 for the simple case of two block loads.

The first loading block including  $n_1$  cycles at a maximum stress  $\sigma_{\max 1}$  causes the virgin material's static strength to degrade up to  $X_{r1}$ . When the second fatigue block of length  $n_2$  and maximum stress  $\sigma_{\max 2}$  is applied, the strength degradation follows a different path, which this time starts from the value  $X_{r1}$ . The equivalent number of cycles  $n_{eq}$  is the number of cycles at the new stress level  $\sigma_{\max 2}$  that would have caused static strength to degrade up to the value of  $X_{r1}$  at the beginning of the new fatigue block.

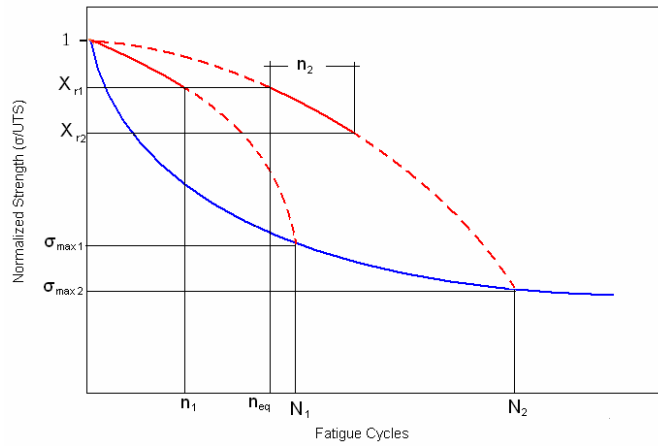


Fig. 69 Graphical demonstration of residuals strength prediction under two constant amplitude fatigue blocks.

Following the same reasoning the residual strength degradation equations after fatigue block loads each of length  $n_i$  at a maximum stress  $\sigma_{\max i}$  are formulated. For the case of the INT model the following expression is in order, through substitution of Eqs. 40 and 41 into Eq. 42 and solving of the occurring function for  $X_{r,i}$ , with  $n$  being replaced by the number of cycles  $n_i$  of the current block plus the equivalent number of cycles  $n_{eq,i}$ .

$$X_{r_i} = \left( 1 - \left( \frac{n_i + n_{eq_i}}{N_i} \right)^x \right)^{\frac{1}{y}} (X - \sigma_{\max_i}) + \sigma_{\max_i} \quad (79)$$

where

$$n_{eq_i} = \left( 1 - \left( \frac{X_{f_{i-1}} - \sigma_{max_i}}{X - \sigma_{max_i}} \right)^y \right)^{\frac{1}{x}} N_i$$

The respective expression for the OM model case is derived in a similar way through Eqs. 62 and 63:

$$X_{f_i} = X - (X - \sigma_{max_i}) \left( \frac{n_i + n_{eq_i}}{N_i} \right)^{k_1 \exp\left(k_2 \frac{n_i + n_{eq_i}}{N_i}\right)} \quad (80)$$

with the equivalent number of cycles  $n_{eq}$  being derived numerically before the application of each new block, through the following transcendental equation:

$$X_{f_{i-1}} = X - (X - \sigma_{max_i}) \left( \frac{n_{eq_i}}{N_i} \right)^{k_1 \exp\left(k_2 \frac{n_{eq_i}}{N_i}\right)} \quad (81)$$

Since the linear model of residual strength assumes constant degradation rate, its formulation for residual strength prediction after  $m$  blocks of constant amplitude cyclic loading proves to result in the following simple expression:

$$X_{f_m} = X - \sum_{i=1}^m \left( (X - \sigma_{max_i}) \frac{n_i}{N_i} \right) \quad (82)$$

All residual strength degradation formulations are subject to a stress ratio dependency. While in the linear model this effect is implied through the fatigue life (being itself dependent on the R-ratio), in most non-linear models, except perhaps the W3-W4A models of Sendeckyj, this can only be accounted for through a different set of each model's parameters. For the case of the OM and INT models discussed above, a functional form of the parameters could be derived through regression analysis based on the values of the parameters at the defined stress ratios ( $R=0.1$  and  $-1$  for the case of  $0^\circ$  UD). Nevertheless, as seen in Table 10, the parameters are not varying considerably and thus a simpler alternative is implemented: For the case of tension-tension fatigue the

R=0.1 residual strength parameters are implemented, while during reversed loading cycling are used those of R=-1.

In the present study, apart from the commonly used life prediction methodology discussed above, the weighted average range (WAR) method is presented. This method, introduced by Dover [92] for life prediction in the case of a propagating crack in metals, was later modified by Amijima et al. [93] and Brondsted et al. [94] for composite materials. The concept is based on the Palmgren-Miner rule and the definition of an equivalent stress level which can be calculated using fatigue life data. CA fatigue at this stress level would induce the same damage as the VA spectrum considered, for the same number of cycles. Considering a power law S-N equation of the form of Eq.(67) and the cycle counting results of a VA spectrum consisting of m CA blocks of  $n_i$  cycles each, at a maximum cyclic stress  $\sigma_{max_i}$  the equivalent stress is given by:

$$\sigma_{eq} = D^{-\frac{1}{b}} \left( \frac{\sum_{i=1}^m (n_i \sigma_{max_i}^b)}{\sum_{i=1}^m n_i} \right)^{\frac{1}{b}} \quad (83)$$

Concept implementation requires no CLD information and fatigue lives at all stress levels and stress ratios are calculated based on a reference S-N curve, as if all cycles belonged to that single stress ratio. It is obvious that the fundamental assumptions of the method, and consequently the obtained results, are the same as if R01 CLD is used along with the Palmgren Miner rule.

## 4.4 PREDICTIONS UNDER SPECTRAL LOADING

### 4.4.1 Algorithm

The computer program that simulates the residual strength degradation during variable amplitude loading, built in Matlab commercial code, is a straight forward implementation of the procedures presented in the previous section: For each cycle (or bin of cycles) except the first one, the equivalent number of cycles is calculated using the current residual strength at the beginning of the cycle along with its cyclic characteristics. Subsequently, the new residual strength at the end of the current cycle is calculated. At the end of each loop, the fracture condition is checked and if satisfied the material is assumed to break. The algorithm's input consists of the loading cycles in their order of occurrence while a preprocessor is used for calculation of the fatigue life that corresponds to each cycle according to the Constant life Diagram chosen. This especially useful for the case of repeated application of a spectrum, since it minimizes the effort for calculating fatigue lives at every spectrum pass. A flowchart of the algorithm is seen in Fig. 70.

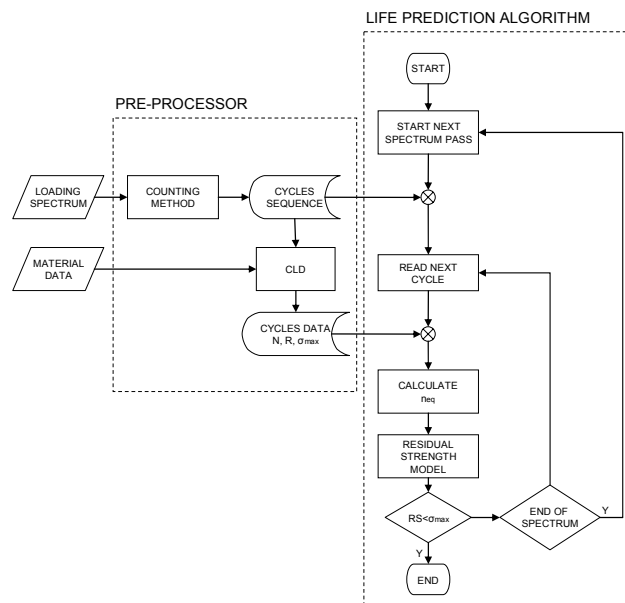


Fig. 70: Flow chart of the life prediction algorithm under variable amplitude fatigue.

Despite its extreme simplicity the algorithm in some cases proves to be rather slow, e.g. for the case of OM model, where the calculation of  $n_{eqj}$  in each loop through Eq.81 requires considerable computational time. Furthermore, the algorithm cannot advance when the residual strength degradation curve is at some point completely flat (tangent equal to zero for a life fraction relatively larger than the size of the current bin of cycles), since the equivalent number of cycles tends to zero for very small values of strength degradation

#### 4.4.2 Experimental Data

Tests for assessing the relative impact of each of the three modules of life prediction under variable amplitude fatigue are performed on two types of specimens: The  $[0_4]$  UD coupon of OB geometry which has been used for determination of all on-axis properties of the basic ply and the long  $[\pm 45]_S$  ISO coupon used for definition of the shear response [95]. All three spectra discussed in previous sections are implemented for the case of the UD laminate, while the  $[\pm 45]_S$  coupons are tested under a modified NEW WISPER load sequence, called herein NW\_mod, shifted so that the lowest level equal zero load. This modification has been necessary since the specific geometry is not capable of sustaining any compressive loads without the use of an anti-buckling device, while the use of such devices has been excluded from OPTIMAT project. Test results for UD are presented in Table 12. In all W, NW and MW spectral fatigue tests, three stress levels were considered to obtain a clear picture of the  $\sigma_{max}$ -N behavior in an  $\sigma_{max}$  range as wide as possible.

Regarding the  $[\pm 45]_S$  specimens, apart from the fatigue life tests performed under NW\_mod spectrum, a limited number of residual strength tests under spectrum loading has also been performed. Cycling is interrupted after an integer number of spectrum passes, approximately at 50% of the expected life, and then residual strength is measured using the standardized procedure as in all residual strength tests. Results from the NW\_mod tests, including residual strength measurements, are shown in Table 13.

Table 12 Spectrum fatigue test results from UD coupons.

	Coupon No	Stress Level kN/mm	Loading Rate kN/s	Max Load kN	N of passes
NW	GEV206-R0300-0802	1.619	294.94	40.84	11.00
	GEV206-R0300-0803	1.619	295.17	40.87	10.97
	GEV206-R0300-0113	1.619	290.54	40.23	11.00
	GEV206-R0300-0801	1.468	294.59	37.00	27.00
	GEV206-R0300-0038	1.377	334.10	33.24	60.86
	GEV206-R0300-0109	1.377	349.60	34.78	23.00
	GEV206-R0300-0805	1.377	348.12	34.63	31.98
	GEV206-R0300-0100	1.279	370.06	31.91	66.47
	GEV206-R0300-0101	1.279	366.80	31.62	42.84
	GEV206-R0300-0103	1.279	366.70	31.62	47.99
W	GEV206-R0300-0046	1.706	295.64	43.15	11.31
	GEV206-R0300-0045	1.706	294.94	43.05	11.02
	GEV206-R0300-0799	1.706	294.70	43.01	10.94
	GEV206-R0300-0097	1.451	344.06	36.08	46.63
	GEV206-R0300-0098	1.451	344.06	36.16	30.54
	GEV206-R0300-0099	1.451	344.06	36.15	60.13
	GEV206-R0300-0800	1.349	374.86	34.07	69.14
	GEV206-R0300-0807	1.349	373.67	33.96	83.13
		GEV206-R0300-0809	1.349	374.36	34.02
MW	GEV206-R0300-499	2.000	24.87	170.83	42.01
	GEV206-R0300-500	2.000	25.07	172.21	37.00
	GEV206-R0300-506	2.000	24.97	171.52	51.84
	GEV206-R0300-501	1.700	24.90	201.22	120.03
	GEV206-R0300-504	1.700	24.82	200.57	231.00
	GEV206-R0300-508	1.700	24.85	200.82	168.98
	GEV206-R0300-505	1.400	25.02	245.52	519.17
	GEV206-R0300-507	1.400	24.98	245.13	859.87
		GEV206-R0300-503	1.400	25.12	246.50



4. Life Prediction Under Spectrum Loading

Table 13 Spectrum fatigue and residual strength test results from UD and  $[\pm 45]_s$  coupons.

	Coupon No	Stress Level MPa	Loading Rate MPa/s	RS [MPa]	Passes
NW_mod	GEV208-I1000-0137	90.00	160.80		25.97
	GEV208-I1000-0138	96.00	150.74		10.98
	GEV208-I1000-0139	96.00	150.74		7.94
	GEV208-I1000-0140	96.00	150.74		9.85
	GEV208-I1000-0141	96.00	150.74		9.45
	GEV208-I1000-0142	102.00	141.86		3.99
	GEV208-I1000-0143	102.00	141.86		4.00
	GEV208-I1000-0144	102.00	141.86		6.25
	GEV208-I1000-0145	102.00	141.86		6.00
	GEV208-I1000-0146	102.00	141.86		5.00
NW_mod RS	GEV208-I1000-0147	96.00	150.74	108.57	5
	GEV208-I1000-0148	96.00	150.74	97.45	5
	GEV208-I1000-0149	96.00	150.74	103.60	5
	GEV208-I1000-0150	96.00	150.74	106.14	5
	GEV208-I1000-0151	96.00	150.74	106.70	5
	GEV208-I1000-0152	102.00	141.86	103.79	2
	GEV208-I1000-0153	102.00	141.86	104.90	2
	GEV208-I1000-0154	102.00	141.86	105.01	2
	GEV208-I1000-0155	102.00	141.86	102.63	2

All fatigue tests have been performed on two MTS hydraulic test rigs of 250 kN capacity, under load control, using hydraulic gripping. The loading curve between each peak and trough is of sinusoidal form and the mean loading rate is kept constant and similar to the rates of the fatigue tests previously performed, in order to avoid excessive heating during cycling and retain comparability between constant amplitude and variable amplitude tests, at least as far as frequency effects are concerned.

The loading rate is defined by assuming a cycle of sinusoidal form, having amplitude  $\sigma_a$  and frequency  $f_r$ . The average loading rate from peak to trough, equal to the tangent of the line that connects these two points, is equal to the

range of the cycle (twice its amplitude) versus half its wave length. Substituting the wavelength by the inverse frequency, the following equation is derived:

$$\dot{\sigma} = 4f_r\sigma_a \quad (84)$$

$\sigma_a$  is the maximum stress amplitude in the spectrum (in N), to set the upper limit for the stress rate, and  $f_r$  (in Hz) is the frequency applied to the CA fatigue test of equal stress [48]. All spectrum data are explicitly reported in [95]

## 4.4.3 Results and Discussion

### 4.4.3.1 Residual Strength vs Palmgren-Miner Rule

The effect of the choice of damage accumulation metric in a life prediction scheme is the first to be examined. In order to have a common base for the comparison of the Palmgren-Miner rule with residual strength based models a single counting method and CLD assumption is implemented. The rainflow algorithm of Downing and Soccie is applied, as described in the previous sections, while the LCLD assumption is used for deriving the fatigue life of each cycle. For the case of the  $[\pm 45]_S$  predictions where fatigue data are available at a single stress ratio, the linear (Goodman) constant life line is implemented, drawn based on the static tensile strength of the laminate and the S-N curve at  $R=0.1$ .

Test results for the  $[0_4]$  laminate, cycled with the W, NW and MW spectra, along with life predictions using the Palmgren-Miner rule as well as the residual strength models discussed above are presented in Fig. 71, 72 and 73 respectively.

4. Life Prediction Under Spectrum Loading

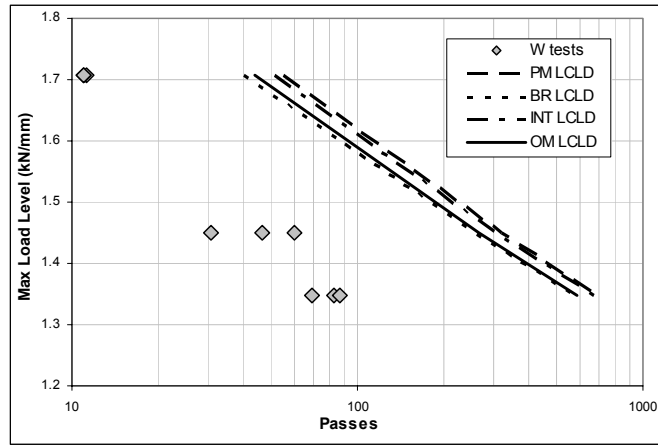


Fig. 71 Life predictions for the  $[0]_4$  laminate produced by various models for the WISPER spectrum.

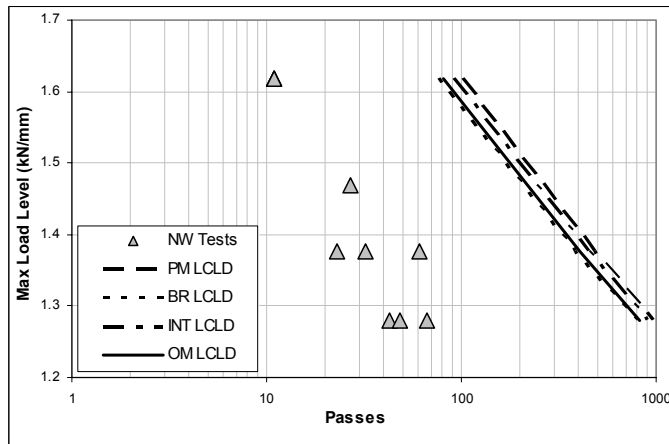


Fig. 72 Life predictions for the  $[0]_4$  laminate produced by various models for the NEW WISPER spectrum.

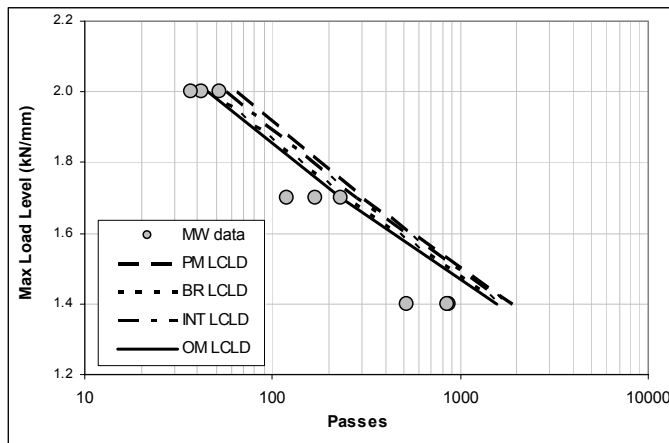


Fig. 73 Life predictions for the  $[0]_4$  laminate produced by various models for the MW spectrum.

The Palmgren-Miner (PM) as well as the residual strength based methodologies seem to overestimate considerably life under both W and NW spectra. On the contrary, predictions appear to be reasonable for the case of the MW time series. This difference should be attributed to the spectrum pattern; both W and NW are artificial spectra, composed of a variety of constant amplitude blocks, with NW being less uniform, starting with cycles of reversed loading and ending with higher loads in the purely tensile region. MW spectrum on the other hand is a more realistic loading series derived through numerical aeroelastic simulations and consisting of uniformly dispersed loading cycles of a comparatively wider variety of ranges, see Figs.58-61. When the loading spectrum consists of a composition of separate blocks of cycles the predictions are overoptimistic, more so when these blocks are sorted in increasing order of stress magnitude as in the NW spectrum (Fig. 56). When a more irregular loading series is applied the predictions are improved considerably.

It is interesting to note that load sequence effects, accounted for by residual strength based models but not by PM rule, do not seem to have a major effect on the results, and are not causing the above mentioned effect, since the predictions obtained in both cases, for all three loading spectra, show an average difference of 20% between the two cases, which tends to decrease for higher lives.

If sequence effects as accounted for by residual strength based models are not causing the very early (compared to the predictions) fracture of the material under W and NW loading, another more mechanistic explanation could be that the MW spectrum includes a large number of very low amplitude cycles dispersed between cycles of various amplitudes throughout the spectrum. These small cycles, met indeed during actual operation, are assisting in local stress relaxation, enabling the material to sustain more spectrum passes, as actually observed for the MW spectrum in Fig. 73.

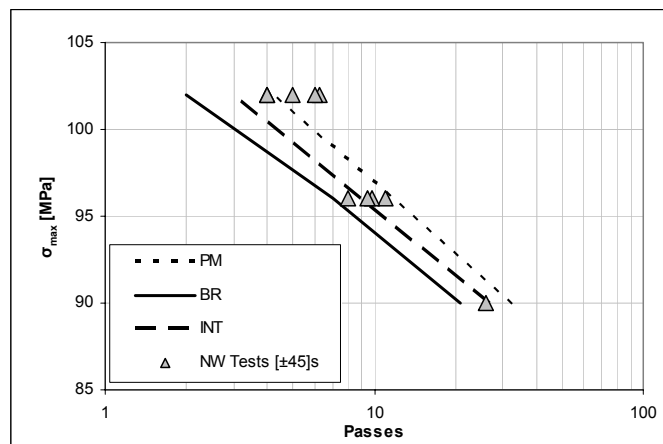


Fig. 74 Life predictions for the [±45]<sub>s</sub> laminate under the NW\_mod spectrum.

Regarding the predictions of the [±45]<sub>s</sub> specimens as seen in Fig. 74, there seems to be in all cases a satisfactory fit to the data. Palmgren-Miner rule in this case gives a good prediction, even though slightly on the non-conservative side for lower stress levels. INT model leads to a marginally better prediction than Miner, while linear strength degradation assumption results in predictions lying more on the conservative side. The result implies a different behavior in this case, since similar spectra (NW and NW\_mod) using similar assumptions, differ considerably in the quality of their predictions. This difference should be mainly attributed to the difference in the damage modes occurring during fatigue inside this purely matrix dominated laminate. In addition to that, the effect of the CLD may play a dominant role in such spectra as further discussed in subsequent sections. In the case of the [±45]<sub>s</sub> laminate the CLD is based on

a single S-N curve whose stress ratio lies close to the average ratio of the NW\_mod spectrum ( $R=0.5$ ).

The actual strength degradation predicted can be monitored throughout the fatigue life, enhancing life prediction methodologies with an easily understandable damage metric, useful in the assessment of the status of the material in applications other than fatigue life prediction. Such applications are e.g. extreme operational loads after fatigue or proof testing of the whole construction to ensure a safe life period.

Residual strength predictions for the case of the  $[\pm 45]_s$  laminate offer encouraging results when compared to the residual strength tests performed under NWmod spectrum, even though both the small data sample and the large scatter observed hinder the drawing of more definite conclusions. The strength degradation curves are shown in Fig. 75 for a higher maximum stress level on the left (90% of the UTS) and for a lower one on the right (85% of the UTS). While both models shown give an acceptable prediction of the residual strength, the non-linear OM model performs very satisfactorily, especially for the lower stress level. Nevertheless, the predicted fatigue life is considerably underestimated by both models for the higher stress level. The step-like behavior of the strength degradation curves is explained by the assemblage of most damaging fatigue cycles at the end of NW spectrum, which accelerates damage progression near the end of each spectrum pass.

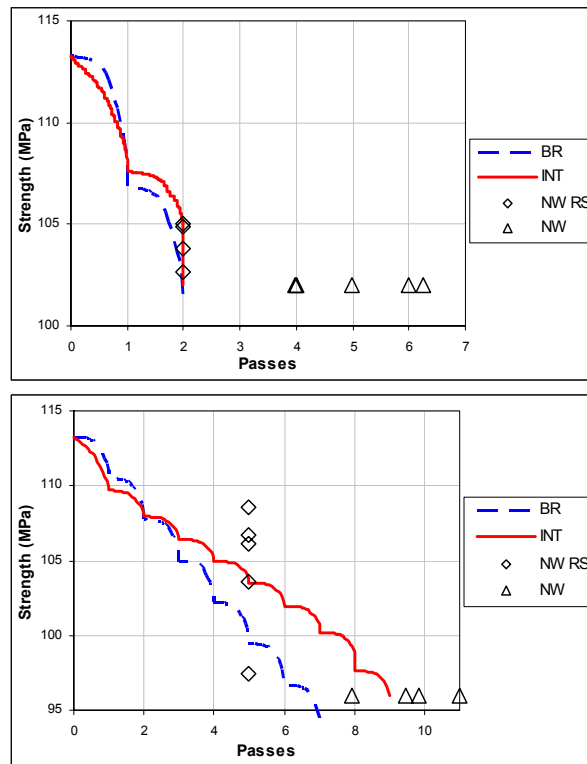


Fig. 75 Residual strength degradation of the  $[\pm 45]_s$  laminate, after application of the NWmod spectrum at a maximum stress level of  $S_{\max}=102$  MPa (upper) and  $S_{\max}=96$  MPa (lower).

In order to evaluate more accurately the residual static strength predictions after spectrum loading, a procedure similar to the CA characterization should be implemented, i.e. residual strength tests at least at three life fractions. In addition to that the statistical model could be implemented since scatter makes deterministic treatment questionable.

#### 4.4.3.2 Investigation of Different CLD Methods

All of the results presented in the previous section were based on a single CLD, the LCLD discussed above. Nevertheless, the predictions are expected to depend to some extent on the CLD choice. In order to investigate this, three different formulations have been implemented: the LCLD, the BELL and the

simple R01 assumption. All predictions presented are based on Rainflow Counting of the respective spectrum cycles, according to the previously discussed algorithm by Downing and Socie.

The form of the CLD curves referring to different numbers of fatigue lives is shown in a single graph in Fig. 76 in order to point out their differences in fatigue life estimates.

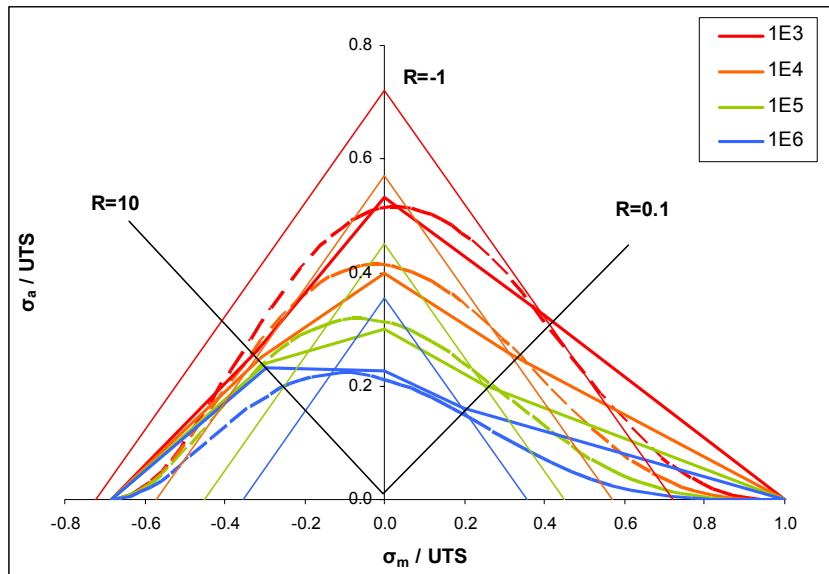


Fig. 76 Plot of the three CLD formulations implemented: LCLD in continuous, BELL in dashed and R01 in dotted lines, from tests on  $[0]_4$  laminate.

For the case of R01 CLD assumption, the residual strength based and PM based predictions are compared with the WAR model. In order to retain a clear picture in the graphs, and since all residual strength models have produced similar predictions in all cases, only the predictions of the BR model are shown. The results are presented in Fig. 77, 78 and 79.



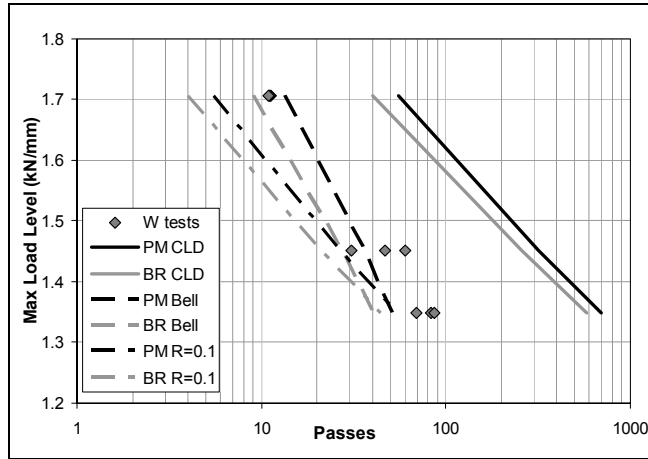


Fig. 77 Comparison of various models using different CLD assumptions on the [0]<sub>4</sub> laminate, under WISPER spectrum.

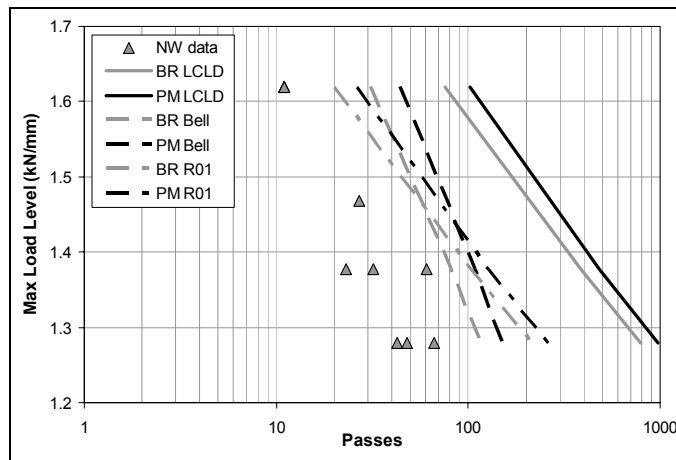


Fig. 78 Comparison of various models using different CLD assumptions on the [0]<sub>4</sub> laminate, under NEW WISPER spectrum.

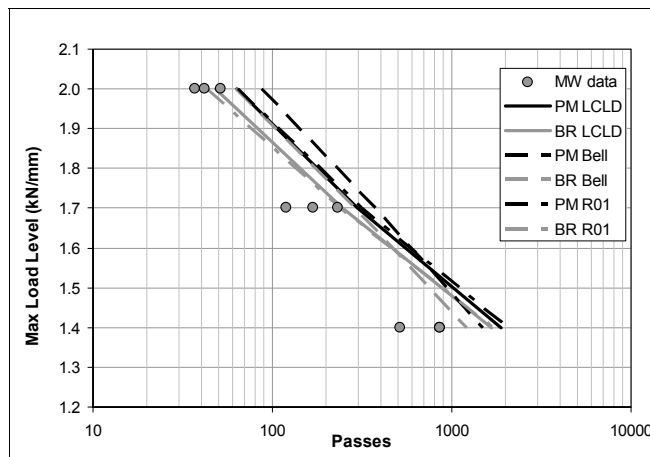


Fig. 79 Comparison of various models using different CLD assumptions on the  $[0]_4$  laminate, under MWIND spectrum.

Predictions regarding the  $[\pm 45]_s$  laminate under NW\_mod are shown in Fig. 80. The investigation in this case is focused on the comparison between the WAR, Palmgren-Miner rule and residual strength based models, since due to the single S-N curve available only the Goodman line, based on  $R=0.1$ , is applicable.

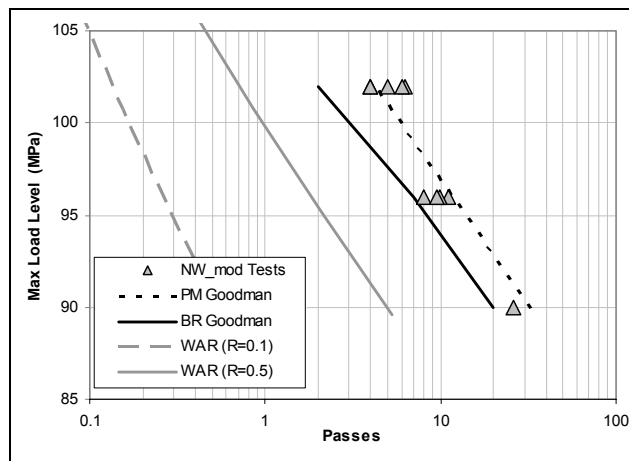


Fig. 80 Comparison of various models on the  $[\pm 45]_s$  laminate under NW\_mod spectrum.

The predictions do not indicate a common trend in all spectrum cases. Focusing on the [0<sub>4</sub>] laminate it is evident that for both W and NW spectra there seems to be a strong dependency on the CLD choice since it induces differences of up to almost an order of magnitude. Nevertheless the effort to describe the constant life lines as accurately as possible (e.g. LCLD) does not necessarily pay back in accuracy of the prediction, especially in comparison e.g. with the R01 assumption which produces in both cases better results.

On the contrary, the CLD choice for the case of the more realistic MW spectrum does not seem to be so critical: Similar results, showing differences of about one tenth of the one observed in the other two spectra cases. This is most interesting in combination with the fact that the difference in the predictions seems to decrease with increasing number of spectrum passes, since it implies that under operational loading conditions, usually causing low cyclic stresses, the CLD choice as well as the damage rule are not of uttermost importance.

Apart from this fact, use of BELL and R01 consistently leads to better results in comparison to LCLD. The first two differ from the latter in the area of stress ratios close to 1, in which the LCLD is determined under the assumption that for R-ratio values close to 1 all CLD lines converge to the UTS and UCS. While appearing reasonable, this assumption may not be accurate, as discussed e.g. in the work of Sutherland and Mandell [88] where fatigue tests are performed at 13 different stress ratios, especially in the tension-tension region, indicating that when the stress ratio comes close to unity the CLD lines do not converge to the UTS. This is of significant importance, since this assumption greatly affects the form of the CLD in the entire tensile (T-T) and compressive (C-C) regions and has a considerable impact on life estimates of the cycles of the specific spectra. Consequently, the difference in the CLD form in this particular region between BELL and R01 on one hand and LCLD on the other, clearly seen in Fig. 76, may be the key factor explaining the large differences observed in the results.

It must be noted here that the choice of the S-N curve in the R01 formulation is of paramount importance in the consistency of the theoretical predictions. This is shown in Fig. 81 where predictions by the BR model for other S-N curve expressions besides the R01 are compared with experimental data from WISPER spectrum. After cycle counting the WISPER spectrum, an average R value is calculated equal to 0.4 approximately. On the other hand, since there

are both tensile and compressive cycles in the load series one might think that  $R=-1$  could also be a representative S-N curve. Predictions with both the above mentioned R values are shown in Fig. 81 to be either optimistic or excessively conservative respectively. Theoretical predictions by the PM method with R01 CLD formulation are also included for comparison.

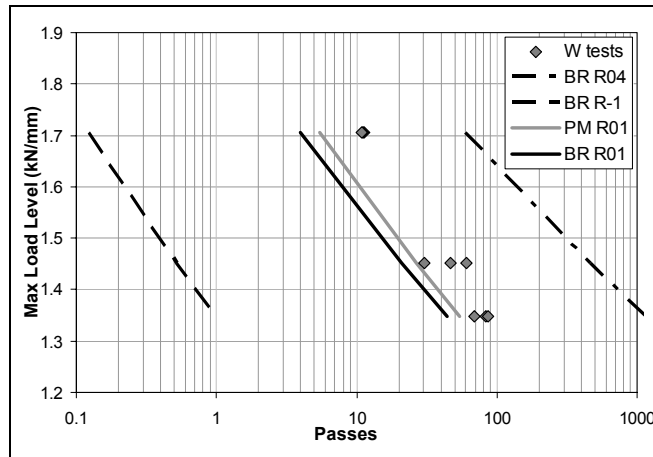


Fig. 81 Comparison of model predictions implementing alternative forms of the R01 formulation with experimental data of W spectrum on the  $[0]_4$  laminate.

Different conclusions are drawn for the case of the  $[\pm 45]_s$  coupons shown in Fig. 80, since PM based predictions are quite acceptable, in contrast to the non-conservative results obtained for the UD laminate. Of course the CLD formulation implemented may play a major part in this difference. Nevertheless, even the WAR method, which showed good results in the on-axis case, fails to predict accurately the behavior showing extremely conservative results. Undoubtedly, the absence of compressive cycles (due to the purely tensile form of the NW\_mod spectrum), the long coupon geometry adopted in this test series, along with the laminate itself (being matrix dominated results in completely different failure modes than its UD counterpart) are partly responsible for this.

Despite the important differences between the two laminates, similar conclusions can be drawn regarding the importance of the S-N curve choice in the WAR model and consequently in the R01 as well, the former yielding

identical results as R01 combined with PM rule. Altering the S-N curve from  $R=0.1$  to  $R=0.5$  (which is the average stress ratio of the NW\_mod spectrum) truncates the predictions almost by a decade. Nevertheless, the predictions remain considerably conservative, making again any rule of thumb for choosing a specific S-N curve in these formulations questionable.

#### 4.4.3.3 Investigation of Different Counting Methods

The investigation herein is confined to two different methods: The first one is the range-mean method [82], which considers each peak and trough pair to be a half cycle of a specific stress amplitude and mean value and the second one is the already described rainflow algorithm proposed by Downing and Socie [86], which has the advantage of partly retaining the sequence of loading events, since each cycle is saved immediately after it is completed inside the algorithm. Results produced using these counting methods are shown in Fig. 82, 83 and 84 for the three investigated spectra. In order to isolate the effect of the counting algorithm, the LCLD is implemented, even though a similar behavior is observed when other CLD assumptions (like R01 or BELL) are implemented. The predictions presented below refer to different damage accumulation assumptions such as linear and non-linear residual strength models and the Palmgren-Miner rule.

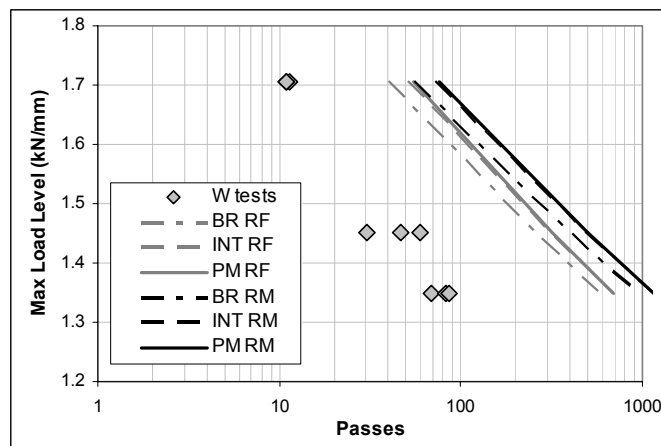


Fig. 82 Predictions of various models using range-mean and rainflow algorithm on Wisper spectrum for the  $[0]_4$  laminate.

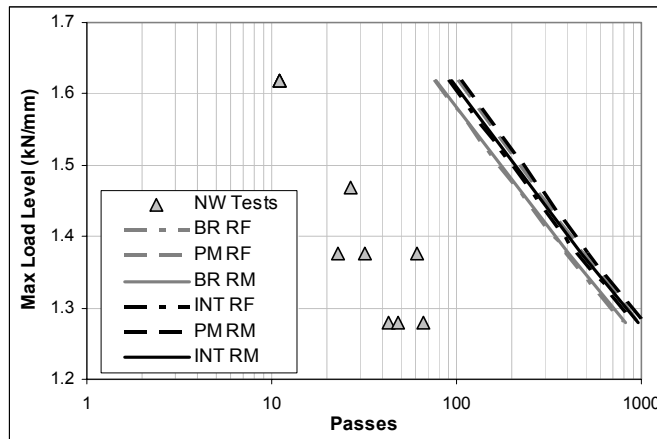


Fig. 83 Predictions of various models using range-mean and rainflow algorithm on New Wisper spectrum for the [0]<sub>4</sub> laminate.

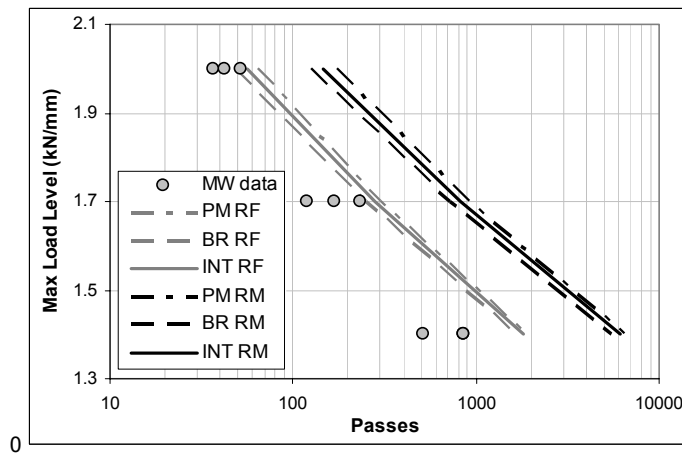


Fig. 84 Predictions of various models using range-mean and rainflow algorithm on MW spectrum for the [0]<sub>4</sub> laminate.

What predictions indicate, is that the more artificial the spectrum (e.g. NEW WISPER) the less important is the choice counting method applied, since a large part of the cycles are packed into CA blocks and consequently any counting routine would produce very similar results. This is especially true for the NW sequence where the lack of randomization leaves large constant

amplitude blocks unbroken resulting in very similar results between the two counting methods, as seen in Fig. 83.

On the contrary, for the realistic MW spectrum the results are quite different since the loading sequence does neither include cycles nor blocks of cycles and consequently the Range Mean method tends to break large segments into smaller ones due to continuous small fluctuations of the load. This becomes more evident if one looks into a random detail of each spectrum, as in Fig. 61. The large cycles, for the MW case, are broken into smaller segments and their impact is lessened by the Simple Range-Mean method. As a result the RM predictions are far more optimistic than the ones using RF counting (see Fig. 84). The limited irregularity observed in WISPER and even more in NEW WISPER supports this argument.

#### 4.4.4 Choosing a Methodology

The investigation of the three modules of life prediction methodologies performed above, scopes in the assessment of the possible alternatives and the proposal of a specific procedure for predicting life in a robust and efficient way. In several cases the state of the art methodology has lead to extremely optimistic predictions (an order of magnitude or more) while in some cases the high sensitivity of the results on parameters such as the choice of CLD demands a thorough study of the impact this might have on the safety factors imposed to composite structures during design.

Trying to analyze the results, two different cases arise and for each one different comments are in order: The first regards loading spectra such as the WISPER or NEW WISPER which consist mainly of smaller or larger constant amplitude fatigue blocks or in general variable amplitude loads that show a regular shape with limited noise. In this case the cycle counting algorithm seems to play a limited role, since almost all counting methods would come with results differing only in number of -usually large and damaging- cycles. Nevertheless the cases studied indicate that neglecting such cycles produces a limited effect to the predictions. On the contrary life predictions under such load sequences appeared to be very sensitive to the choice of CLD, even though the accuracy in the CLD formulation does not necessarily equally improve the

predictions, since very simple CLD assumptions, such as the R01, show in some cases better results. Anyhow, no definite conclusion can be drawn on the reasons of such behavior.

When focusing on the second case of spectra, which have a more random appearance, the predictions indicate that the counting algorithm is, very reasonably, of great influence. For this reason the Rainflow counting is suggested, but implemented in a way that would disturb the sequence of the loading events as little as possible, through recording of each hysteresis loop immediately after completion. On the contrary, the influence of the CLD on the predictions is limited, even though the investigated MWIND load sequence includes cycles at various stress ratios, and would be expected to be highly sensitive to CLD alterations. No clear explanation can be given to this effect. Nevertheless verifying this conclusion for the case of similar realistic spectra including more compressive or reversed fatigue cycles would be a great asset for life prediction schemes, since the time consuming and costly fatigue tests for CLD determination could be drastically decreased.

The effect of using residual strength as damage accumulation metric on the other hand does not depend on the shape and characteristics of the spectrum. In all cases a small but consistent improvement is achieved in comparison to the Palmgen-Miner rule, which nevertheless does not justify the excessive testing required for residual strength characterization. Of course, the benefits of implementing residual strength go beyond this small benefit of 10 to 20% in the predictions, since the correlation of damage accumulation with a mechanical property such as strength improves the macroscopic overview of the composite during fatigue. In this view, the BR linear model is a competitive candidate: No additional testing is required and it has been proved to yield acceptable or at least safe static strength predictions throughout the entire fatigue life.

Summarizing the above the following alternative for each module of the life prediction algorithm is proposed:

- 1- *Counting*. The use of Rainflow or other method that counts cycles as closed hysteresis loops is suggested.
- 2- *CLD assumption*. The region close to the R=1 line seems to have a significant effect on the results, indicating that CLD lines should not converge to



the UTS or UCS for  $R=1$ . A formulation like the R01 or BELL approximates in some cases such a behavior.

3- *Damage rule.* A net improvement can be achieved by adopting the linear residual strength model (BR) as damage metric, with the additional advantage that a clear physical meaning is attributed to the damage accumulation rule, while no additional experimental effort for residual strength characterization is required.



## 5 FATIGUE SIMULATION OF LAMINATES

### 5.1 INTRODUCTION

In the effort of developing applicable engineering models able to predict mechanical properties of composites, such as strength, stiffness or life after fatigue, while keeping low the experimental effort, several theories have been proposed up to date. Some of them try to link damage parameters in the micro or meso scale to useful engineering properties of a multidirectional laminate. For example, Talreja [96] characterizes the damage state of the composite through a vector set, each component representing a specific cracking mode, related theoretically to strength and stiffness properties. Daniel in [97] suggests that fatigue life can be expressed as a function of the number of cycles required for matrix crack saturation. Varna et al. [98] propose as characteristic property the crack opening displacement parameter, along with computational methodologies for its determination, related with stiffness degradation through their model. In a similar spirit, Charewitz et al. [99] link fatigue life or residual strength components with the density of various failure events in the laminate after fatigue. Observing macroscopically the constituents of the laminate, Reifsneider et al. developed the Critical Element Model [35, 100, 101] which distinguishes between critical (causing overall failure) and sub-critical (undergoing strength and stiffness degradation) elements inside the laminate. They propose strength and stiffness degradation (as several other researches do), as convenient quantities for the description of fatigue damage.

While models linking damage events in the micro-scale (e.g. crack density) to mechanical properties of composites may in the future become applicable for structural design, semi-phenomenological models as the latter ones, can offer a reasonable tool for design of composite structures, once the experimental effort

for complete mechanical characterization of the basic ply in terms of static strength, fatigue life and elastic behavior is spent. Despite this considerable experimental cost, they turn out to be more economical compared to the direct characterization of specific lay-ups, if one considers their general applicability once a basic ply has been fully characterized. More so, since in contemporary large scale composite structures, such as Wind Turbine Rotor Blades, made of multidirectional laminates composed of a basic prepreg or UD layer and undergoing dynamic loading, such methodologies have the advantage of modeling the direct consequences of damage and local failures in ply level (such as stiffness and strength loss). This 'progressive damage' approach makes possible the prediction and assessment of damage events, helping distinguishing between 'catastrophic' and 'non-catastrophic' failures and further on developing e.g. Last Ply Failure (LPF) instead of First Ply Failure (FPF) design tools, leading ultimately to full use of the composite material.

In this chapter, a plate theory model, under the name FADAS (Fatigue Damage Simulator) [102, 103] for residual strength, stiffness and life prediction of multidirectional laminates is presented. This work is the first part of a ambitious program, performed in the frame of the EU project 'UPWIND' [104], regarding the development of 2D and 3D finite elements simulating phenomenologically the fatigue process, including non-linear elastic behavior, strength and stiffness degradation, residual strains etc. In the present work a simplified version of the model, considering linear elasticity, is developed and tuned accordingly for the reference UD material. The model takes into account the outcomes of the residual strength models assessment, discussed in Chapter 3, as well as the investigation of the constitutive modules of life prediction schemes, performed in Chapter 4.

## 5.2 FADAS OVERVIEW

The input required for the implementation of FADAS includes the typical characterization of the material in terms of static strength and fatigue life as well as a number of elastic modulus measurements during cycling to determine the material's stiffness degradation behavior. These properties are required in the two principal directions of the basic lamina as well as in the in-plane shear direction. Once the necessary input is obtained, the methodology is able to predict life and residual strength of a multidirectional laminate under complex cyclic loads of constant or variable amplitude, provided that the loads on all direction are proportional to each other and that the laminate is a lay-up of a single material system. While the proportionality of the loads is adopted in order to have the same number of fatigue cycles in all material directions is by no means restrictive since the algorithm can be modified to consider independent load spectra for each direction of applied load, increasing of course its complexity and inducing time instead of number of cycles as basis for the progression of fatigue damage.

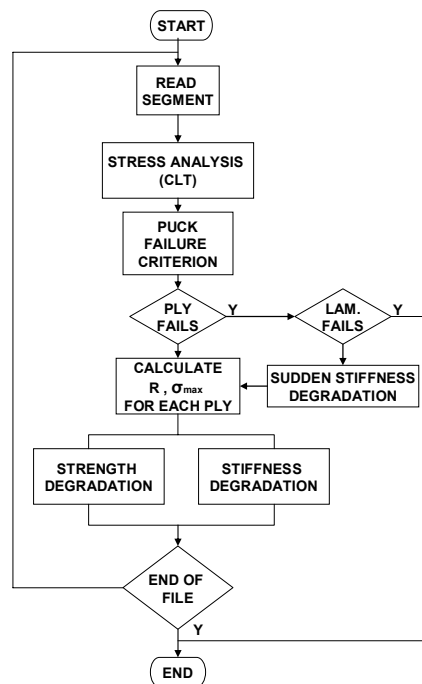


Fig. 85 Flowchart of the FADAS algorithm.

The algorithm proceeds with the calculation of stresses and strains that develop into each lamina due to the current load cycle, using Classical Lamination Theory (CLT). Stresses and strains are then rotated to the principal coordinate system of each ply. Subsequently, a Failure Criterion is applied and at the point when failure occurs, two separate cases are distinguished. The first one is the 'catastrophic case' leading to fracture of the entire laminate and the second is the non-catastrophic one, resulting in an updated strength and stiffness matrix of the failed layer. With any failure events having been accounted for, the algorithm progresses with the calculation of the gradual strength and stiffness degradation due to fatigue (residual strength and stiffness). The procedure then starts again for the following loading cycle.

During this procedure, possible non linear elastic behavior is not accounted for since the stress strain response of the composite is assumed linear for all in-plane properties. Even though this assumption can be considered reasonably valid regarding the fibre direction of the UD ply, this is usually not the case for the transverse direction or shear. These properties tend to have a non-linear elastic behavior, as stress-strain curves of static strength tests indicate. Nevertheless, the assumption of linearity greatly reduces the computational time while the benefit from incorporating such non-linearities into the models can be considered small especially when it comes to fibre dominated laminates.

Once these assumptions made, the algorithm progresses at reasonable speed either by single cycles, which is necessary for modeling spectrum fatigue, or by blocks of cycles, which accelerates the procedure during constant amplitude or block fatigue. A flowchart of the algorithm is shown in Fig. 85.

The simple reasoning of the algorithm refers directly to that proposed by Shokrieh et al. who developed their so called 'Generalized Material Property Degradation Model' [2, 3, 105, 106] or later on by Tserpes et al. [4] with the 'Fatigue Progressive Damage Model'. Both models consider the stress state developing into each ply during fatigue and use strength and stiffness degradation formulations to account for stress redistributions and modification of the failure tensor components. The FADAS algorithm advances this concept a bit further by adopting and validating the algorithm for Glass/Epoxy composites (instead of CFRP) as well as by tuning its modules in a way that

further simplifies the procedure, reduces experimental effort and thus enhances the applicability of the algorithm

## **5.3 MODULES OF FADAS**

The exact procedure constituting the FADAS algorithm has been optimized following the findings of the previous chapters. Design guidelines and regulations are also taken into account. The different modules are discussed in the following paragraphs.

### **5.3.1 Pre-Processing of Fatigue Loads**

Rainflow counting of the considered spectrum, which has been proved to be necessary in the case of relatively irregular variable amplitude cyclic loads, is not so imperatively required for more regular spectra. In the present work, fatigue loads used for validation of the algorithm are of constant amplitude. Nevertheless, when looking into the laminate, considering the stress redistributions caused by failures or gradual degradation, the cyclic stresses calculated for each ply/direction end up to be of variable amplitude. Despite that, and since such redistributions cause in most cases a gradual change of cyclic stresses, resulting to more or less regular spectrum patterns, the Simple Range-Mean algorithm can be applied. This choice, without being restrictive, has the benefit of skipping the cycle counting procedure while enabling the application of the external loads in blocks of cycles, which especially for the case of high cycle fatigue, reduces considerably the computational time.

### **5.3.2 Failure Criterion**

The failure criterion developed by Puck [107-109] is implemented, which accounts for different failure modes depending on the combination of stresses acting on each ply. An important asset of this criterion is that it distinguishes between the explosive mode C, having severe consequences on the laminate's integrity, and the less crucial mode B of matrix compressive failure, depending on the relative magnitude of the in-plane shear.

Briefly, the failure criterion of Puck considers 5 different failure modes. The first two refer to fibre failure (FF) under tension and compression, expressed respectively by:



$$f_{E(FF)}^T = \frac{1}{X_T} \left[ \sigma_1 + \left( \frac{E_1}{E_{f1}} v_{f12} m_{of} - v_{12} \right) \sigma_2 \right] \leq 1 \quad (85)$$

$$f_{E(FF)}^C = \frac{1}{X_C} \left| \sigma_1 + \left( \frac{E_1}{E_{f1}} v_{f12} m_{of} - v_{12} \right) \sigma_2 \right| + (10\varepsilon_6)^2 \leq 1 \quad (86)$$

The terms  $X_T$ ,  $X_C$ ,  $Y_T$ ,  $Y_C$  denote the on-axis and transverse tensile and compressive strength respectively.  $E_1$  and  $v_{12}$  are the on-axis Young modulus and Poisson ratio of the UD ply while  $E_{f1}$  and  $v_{f12}$  are the respective quantities for the fibre. The term  $m_{of}$  accounts for a stress magnification effect caused by the difference between the moduli of fibre and matrix.

The other three limit conditions concern different modes of matrix -or inter fibre-failure (IFF). The first one described by Eq.(87), called mode A, is caused by tensile stress in the transverse direction resulting to cracks that open transversely to the applied load, parallel to the fibres. The other two refer to compressive stresses in the transverse direction and the first one denoted as mode B (Eq.(88)) initiates for relatively high values of in-plane shear and results in matrix cracks transversely to the normal stress direction that tend to close. When transverse compressive stress increases with respect to the shear stress the failure mode changes to mode C, Eq.(89), causing cracks at a plane that is not perpendicular to the one defined by the in plane stresses.

$$f_{E(IFF)}^A = \sqrt{\left( \frac{\sigma_6}{S} \right)^2 + \left( 1 - p_{\perp\perp}^{(+)} \frac{Y_T}{S} \right)^2 \left( \frac{\sigma_2}{Y_T} \right)^2} + p_{\perp\perp}^{(+)} \frac{\sigma_2}{S} + \left| \frac{\sigma_1}{\sigma_{ID}} \right|^6 \leq 1 \quad (87)$$

$$f_{E(IFF)}^B = \frac{1}{S} \left( \sqrt{\left( \sigma_6^2 \right) + \left( p_{\perp\perp}^{(-)} \sigma_2 \right)^2} + p_{\perp\perp}^{(-)} \sigma_2 \right) + \left| \frac{\sigma_1}{\sigma_{ID}} \right|^6 \leq 1 \quad (88)$$

$$f_{E(IFF)}^C = \left[ \left( \frac{\sigma_6}{2(1+p_{\perp\perp}^{(-)})S} \right)^2 + \left( \frac{\sigma_2}{Y_C} \right)^2 \right] \left[ \left( \frac{Y_C}{(-\sigma_2)} \right) + \left| \frac{\sigma_1}{\sigma_{ID}} \right|^6 \right] \leq 1 \quad (89)$$

The shape of the failure locus according to Puck, in the transverse-shear stress space  $(\sigma_2, \sigma_6)$ , is graphically shown in Fig. 86 for the reference UD material (basic ply). The transition point from mode B to mode C, where the in-plane

shear has reached a value so that the transverse compression cannot impede failure at an inclined plane, is shown in the graph. Under mode C explosive failure occurs, which can cause to delaminations and/or local buckling, thus leading to a more catastrophic failure scenario than mode A or B.

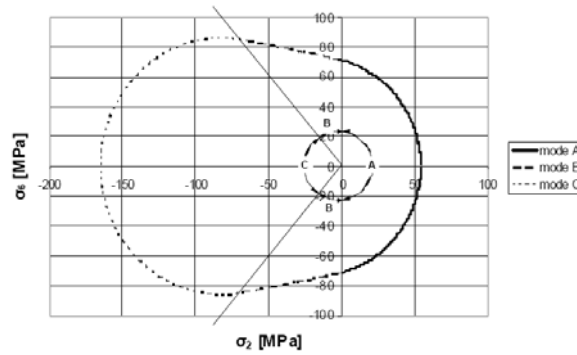


Fig. 86 Failure locus in the  $(\sigma_2, \sigma_6)$  stress plane, predicted with Puck failure criterion.

S in the Eqs.(87-89) is the in-plane shear strength of the ply. The term  $\sigma_1 / \sigma_{1D}$  accounts for matrix damage due to statistical fibre breakage before  $\sigma_1$  reaches its ultimate  $X_T$ , while factors  $p_{\perp\parallel}^{(+)}$  and  $p_{\perp\parallel}^{(-)}$  represent the slopes of the failure locus  $(\sigma_2, \sigma_6)$  at  $\sigma_2=0^+$  and  $\sigma_2=0^-$  respectively. Finally, parameter  $p_{\perp\perp}^{(-)}$  stands for the inclination of the failure locus  $(\sigma_2, \sigma_4)$ ,  $\sigma_4$  being the shear stress in the plane transversely to the fibre, at zero transverse stress.

Parameters included in the Failure Criterion of Puck, tuned accordingly for the reference UD material, are shown in Table 14 and Table 15. All stress quantities are in MPa and elastic moduli in GPa. The values shown in Table 14 are proposed by Puck [107] and are either assumed or experimentally derived, while the parameters in Table 15 refer to basic mechanical properties of the UD reference material which have been determined experimentally or indicated by the fibre manufacturer.

Table 14 Puck criterion parameters assumed in [107]

$p_{\perp\parallel}^{(+)}$	$p_{\perp\parallel}^{(-)}$	$p_{\perp\perp}^{(-)}$	$m_{\sigma}$	$\sigma_1 / \sigma_{1D}$
0.3	0.25	0.23	1.3	$0.9 f_{E(FF)}$

Table 15 Elastic properties of the reference UD used in the failure criterion of Puck.

	On-Axis {1}		Transverse {2}	Shear {6}
Elastic Properties	$E_{r1} = 72.45$	$\nu_{r12} = 0.22$	$E_2 = 15.15$	$G_{12} = 5.5$
	$E_1 = 39.04$	$\nu_{12} = 0.29$		

### 5.3.3 Sudden Stiffness Degradation

Failure at a specific ply of the laminate does not necessarily have the catastrophic consequences assumed in e.g. FPF design procedures. Depending on the failure mode described by Eq. (85-89) and the failure effort i.e. the value that the criterion reaches, different property discount strategies can be followed, varying from stiffness reduction to overall failure of the laminate. Fibre failure for instance, either in tension or in compression, due to the high energy release and the generalized damage it causes is always assumed to lead to overall failure of the laminate. When on the other hand matrix failure occurs on a lamina, its stiffness properties are degraded accordingly. Mode C, having more severe consequences, is assumed to cause a drastic drop of stiffness, while under mode A and B stiffness degrades by a factor which is a function of the failure effort calculated by the respective criterion. Its form is:

$$\eta = \frac{1 - \eta_r}{1 + c(f_{E(IFF)} - 1)^\xi} + \eta_r \quad (90)$$

Even though Puck [107] proposes specific values for the parameters  $c$  and  $\xi$  of Eq.(90), in this work they are derived through FEM simulation of static strength tests on the same material by trying to follow the experimentally observed behavior of a coupon loaded to failure under monotonic loading (see Antoniou et al. [110]). The FEM model used considers amongst others non linear elasticity in the transverse and shear direction which is mainly the cause for the large difference between the calculated and proposed values of  $c$  and  $\xi$ .

These parameters actually define the post-failure stiffness degradation behaviour while parameter  $\eta_r$  represents the remaining value of the considered

elastic property after damage has reached its saturation level. An example of how the degradation factor changes versus the failure effort for different values of  $\xi$ ,  $c$  and  $\eta_r$  is shown in Fig. 87.

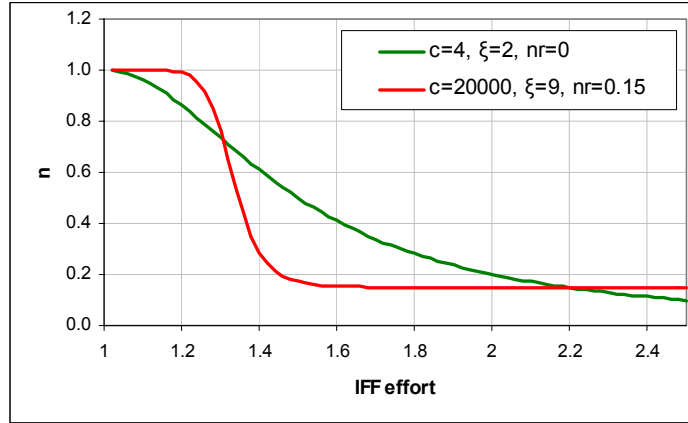


Fig. 87 Change of the degradation factor  $n$  versus the failure effort.

The degradation scenarios for each failure mode are summarized in Table 16. All Matrix failure modes leave the on-axis properties unaffected, while mode C causes a drastic reduction of both transverse and shear moduli. In Table 16 are also displayed the values of the parameters of Eq.(90).

Table 16 Degradation of Elastic Properties according to Failure Mode

Failure Mode	Degradation Imposed	Parameter Value
FF(T) $\hat{\eta}$ FF(C)	Failure of the Laminate	-
IFF(A)	$E_2 = \eta E_2$ $G_{12} = \eta G_{12}$	$c=20,000$ $\xi=9$ $\eta_r=0.05$
IFF(B)	$E_2 = \eta E_2$ $G_{12} = \eta G_{12}$	$c=20,000$ $\xi=9$ $\eta_r=0.15$
IFF(C)	$E_2 = 1E-06 E_2$ $G_{12} = 1E-06 G_{12}$	-

### 5.3.4 Residual Strength Degradation

Following the concluding discussion of the previous chapter, the linear BR model is chosen as damage accumulation metric. The static tensile strength degradation equations for the two principal directions and in-plane shear are respectively described by the following equations:

$$X_{Tr} = X_T - (X_T - \sigma_{1max}) \left( \frac{n}{N_1} \right) \quad (91)$$

$$Y_{Tr} = Y_T - (Y_T - \sigma_{2max}) \left( \frac{n}{N_2} \right) \quad (92)$$

$$S_r = S - (S - \sigma_{6max}) \left( \frac{n}{N_6} \right) \quad (93)$$

Considering only proportional fatigue loads the number of fatigue cycles  $n$  applied has a common value in all three equations and for all layers.  $N_i$  ( $i=1,2,6$ ) is the corresponding fatigue life calculated for the current maximum cyclic stress. Even though Eqs.(91-93) seem to be dependent only on the stress level, they also inherently include a stress ratio dependency through  $N_i$ , the latter referring to a specific stress ratio through use of an adequate CLD assumption. Naturally the above degradation equations can be implemented once the initial static strength and fatigue life response at arbitrary R-ratios are known.

Compressive strength on the other hand, in both the on-axis and transverse directions, has not shown signs of degrading significantly due to fatigue. Moreover, purely compressive cyclic stresses, as discussed in the case of residual strength after R=10 fatigue, do not seem to cause degradation of the tensile residual strength whatsoever. This observation simplifies the strength degradation conditions imposed: Fatigue is assumed to cause degradation only of the strength component of the respective sign leaving the strength of the opposite sign unaffected, while in the case of reversed loading, each strength component is assumed to degrade due to the extreme cyclic stress of the same sign. Consequently, when modeling compressive residual strength after compression-compression or tension-compression fatigue, a degradation

equation simulating constant strength throughout life with a sudden drop near failure is implemented:

$$X_{Cr} = X_C - (X_C - |\sigma_{1min}|) \left( \frac{n}{N_1} \right)^k \quad (94)$$

$$Y_{Cr} = Y_C - (Y_C - |\sigma_{2min}|) \left( \frac{n}{N_2} \right)^k \quad (95)$$

The exponent k is attributed a value of 20 to simulate the above mentioned behavior.

### 5.3.5 Gradual Stiffness Degradation

In-plane stiffness of the lamina, assumed in all cases linear, is degrading due to fatigue. In general this degradation is non linear and various formulations have been proposed in literature to describe it. Herein it is assumed to depend only on the fatigue life fraction, i.e. the fraction of the fatigue cycles versus the nominal fatigue life at the current stress level. Below, the degradation equation of the shear modulus is shown while the same formulation, fitted to the corresponding experimental data, is used for all in-plane elastic moduli.  $G_{12o}$  denotes the initial modulus while  $\kappa$  and  $\lambda$  are model parameters derived from stiffness data measurements.

$$\frac{G_{12}}{G_{12o}} = 1 - (1 - \kappa) \left( \frac{n}{N} \right)^\lambda \quad (96)$$

The case of the shear modulus degradation can be seen in Fig. 88. Parameters  $\kappa$  and  $\lambda$  for the case of the on-axis and transverse elastic moduli are presented in Table 17. It must be noted that the shear modulus is assumed to follow the same degradation behavior as the modulus degradation of the  $[\pm 45]_S$  laminate. In order to derive the actual shear modulus during fatigue, the degradation of Poisson ratio must be available, which is very difficult to obtain since strain gauge rosettes (necessary for this task) break after a few thousand of fatigue cycles

### 5. Fatigue Simulation Of Laminates

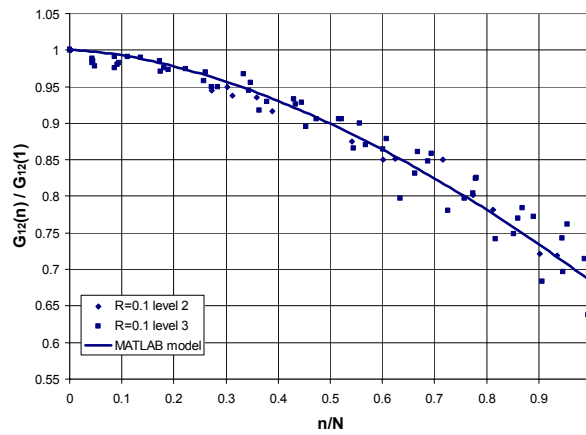


Fig. 88 Normalized residual shear modulus data after fatigue fitted by Eq.(96).

All stiffness degradation measurements are based on load-displacement measurements, available from the load cell and LVDT of the test rig, rather than from the more appropriate measurements of strain using e.g. clip gauges. This induces a series of errors mainly related to the compliance of the tabs and the tab-coupon interface as well as the stiffness of the test rig itself, resulting in exaggerated modulus degradation. In order to obtain more accurate measurements, strain measurement equipment should be mounted on the coupon during cycling.

Table 17 Stiffness degradation parameters for the principal directions and shear of the UD ply

	On-Axis {1}	Transverse {2}	Shear {6}
Stiffness Degradation Parameters	$\kappa=0.852$ $\lambda=0.419$	$\kappa=0.755$ $\lambda=3.167$	$\kappa=0.684$ $\lambda=1.654$

### 5.3.6 CLD Formulation

The determination of the fatigue life for each cycle, calculated on each lamina, is necessary in the definition of both strength and stiffness degradation models and consequently a CLD assumption must be defined. From the different alternatives investigated in chapter 4, the LCLD is chosen. Even though other formulations, like BELL or R01, have lead to improved predictions of life under VA fatigue, the LCLD, apart from being proposed by certification organizations (e.g. [111]) can be expected to yield good results since the FADAS validation tests are performed under stress ratio  $R=0.1$  or  $R=-1$ . Fatigue life determination in this case, with the cyclic stresses developing inside each ply being in the area of  $R=0.1$  or  $R=-1$ , is not greatly affected by the CLD choice, since experimental results for both stress ratios are directly available from fatigue tests. Moreover, cycles are not located in the  $R \rightarrow 1$  area where the form of the CLD is suspected to have a predominant role, greatly affecting life prediction.

The formulation is based on three S-N curves (at  $R=0.1$ ,  $-1$  and  $10$ ) regarding the on-axis and transverse directions, while prediction of the in-plane shear fatigue response of the material is obtained using Goodman Lines based on the S-N curve at  $R=0.1$ . In all cases, calculation of fatigue life at intermediate R-ratios is obtained using linear interpolation in the mean-amplitude stress space following the procedure discussed in [70] and [112]. The S-N curve data shown in Table 9 are used, while the shape of the LCLD for each principal direction and in shear are displayed in Fig. 89.

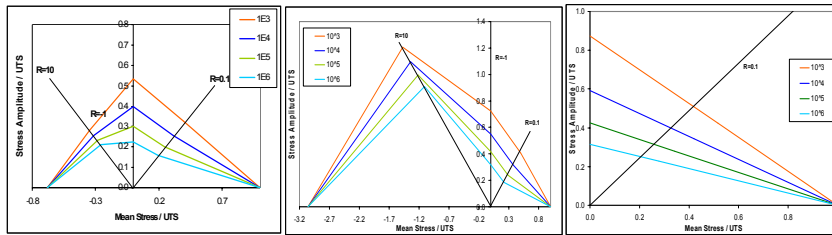


Fig. 89 Constant Life Diagrams of the reference UD ply: Parallel to the fibre (left), transversely to the fibre (centre) and in-plane shear (right).



### 5.3.7 Final Failure

The substitution of First Ply Failure (FPF) procedures by Last Ply Failure (LPF) in structural design comes with the inherent difficulty of strictly defining the fracture condition of the overall laminate. While in simple lay-ups, e.g. when the fibres are arrayed in the direction of the load, such a task is fairly simple, in more complicated ones, e.g. multi-directional lay-ups under plane stress conditions, a clear definition is not always obvious.

This problem in the present work is solved using two conditions: The first one regards fibre failure and according to it overall failure is assumed whenever a fibre failure takes place (in tension or compression). One of course could claim that this assumption does not necessarily hold since after fibre failure the load could be carried by other off-axis plies. Nevertheless, this is not usually the case in structural design of composites since a successful design implies the load transfer through the fibres. Additionally, as already mentioned, the high energy release occurring due to fibre failure usually causes extended damage in the adjacent plies.

The second condition regards matrix damage and considers overall failure to occur whenever a matrix failure mode takes place in each of the plies, at least one of them being of mode C (IFF(C)). In this case as well failure would not be necessary but it is certain that once this condition is reached the composite will be in bad shape, with extensive matrix damage, delaminations (caused especially by mode C failure) etc and subsequently its load carrying capacity will have been greatly reduced

## 5.4 FATIGUE SIMULATION OF MD LAMINATES

In this section, the FADAS algorithm is validated through comparison of its predictions with fatigue life experimental data performed on different lay-ups of the reference UD material and under different cyclic loads.

The algorithm is implemented in computer code using the MATLAB commercial software. The input is an array of peaks and troughs of the applied stress, and once all strength tensor components, fatigue response and degradation characteristics of the material are defined, the program predicts residual strength, stiffness and remaining life for the material throughout its entire fatigue life. The algorithm proceeds either by single cycles or by blocks of cycles (for the constant amplitude fatigue case), which greatly accelerates the procedure inducing minimal errors when the size of the blocks is carefully optimized through an iterative procedure.

### 5.4.1 Experimental data

The first set of verification tests is performed on a multidirectional laminate (MD), consisting of the reference UD lamina in a  $[(\pm 45/0)_4/\pm 45]_T$  lay-up. Even though the reinforcement material in all three directions is the same type of E Glass with the same roving type (see [54]), the area weight of each layer differs. Since in the CLT analysis performed only the total content of each orientation in the laminate is taken into account, the actual number of layers is replaced by a fictitious number of layers (of equal area weight this time) that results to the same percentile of each layer type inside the laminate (see Table 18).

Table 18 Equivalent number of layers, assuming equal area weight

Orientation [degrees]	Actual No of Layers	Nominal Area Weight [g/m <sup>2</sup> ]	Fictitious No of Layers	Content actual (fictitious) [%]
0°	4	1150	9	53.4 (53.0)
45°	5	400	4	23.3 (23.5)
-45°	5	400	4	23.3 (23.5)

5. Fatigue Simulation Of Laminates

Fatigue of the MD laminate is performed under CA fatigue of two stress ratios: In the tension-tension domain ( $R=0.1$ ) and under reversed loading ( $R=-1$ ). Coupons are of the standard OB geometry with a nominal thickness of 6.57mm. Test results at the  $R=-1$  stress ratio are shown in Table 19 while the ones at  $R=0.1$  are shown in Table 20. The tables also indicate the institute where the fatigue tests have been performed.

Table 19 Fatigue life test results on MD laminate under  $R=0.1$  (GEV207\_R0400\_XXX)

Coupon ID	Inst.	$\sigma_{max}$ MPa	N Cycles	Coupon ID	Inst.	$\sigma_{max}$ MPa	N Cycles
GEV207_R0400_0611	WMC	273.38	15617	GEV207_R0400_0294	DLR	194.98	1023212
GEV207_R0400_0768	WMC	278.06	14413	GEV207_R0400_0130	DLR	195.00	1550777
GEV207_R0400_0967	WMC	335.66	4504	GEV207_R0400_0119	DLR	195.27	1529500
GEV207_R0400_1037	WMC	194.03	1148206	GEV207_R0400_0126	DLR	249.98	72213
GEV207_R0400_0541	DLR	343.06	3058	GEV207_R0400_0296	DLR	259.97	42577
GEV207_R0400_0222	WMC	326.66	2514	GEV207_R0400_0121	DLR	259.99	57647
GEV207_R0400_0512	WMC	261.12	73313	GEV207_R0400_0133	DLR	260.02	71242
GEV207_R0400_0487	WMC	193.87	1495214	GEV207_R0400_0127	DLR	299.99	13591
GEV207_R0400_0273	WMC	199.36	346505	GEV207_R0400_0125	DLR	375.02	1548
GEV207_R0400_0583	WMC	273.80	10661	GEV207_R0400_0132	DLR	389.99	1177
GEV207_R0400_0597	WMC	274.60	10911	GEV207_R0400_0293	DLR	390.00	1028
GEV207_R0400_0861	WMC	274.21	14445	GEV207_R0400_0295	DLR	390.02	995
GEV207_R0400_0489	WMC	263.44	98460	GEV207_R0400_0128	DLR	400.00	771
GEV207_R0400_0592	WMC	346.35	2139				

The second set of tests is performed on off-axis coupons, cut from the same MD laminate as above, in order to alter the stress field and damage modes developing into each lamina, and especially that of the dominant  $0^\circ$  orientation [113]. The predicted interaction, in ply level, of all in-plane cyclic stresses is investigated in comparison to CA fatigue life data under reversed loading ( $R=-1$ ). Tested specimens are cut at  $10^\circ$  and  $60^\circ$  simulating a  $[(35/-55/-10)_4/35/-55]_T$  and a  $[(15/75/-60)_4/15/-75]_T$  laminate respectively. Test results are shown in Table 21.

Table 20 Fatigue life test results on MD laminate under R=-1 (GEV207\_R0400\_XXX)

Coupon ID	Inst.	$\sigma_{max}$ MPa	N Cycles	Coupon ID	Inst.	$\sigma_{max}$ MPa	N Cycles
GEV207_R0400_0063	VUB	117.83	2719725	GEV207_R0400_0112	DLR	134.99	655532
GEV207_R0400_0061	VUB	117.99	1623268	GEV207_R0400_0111	DLR	150.00	481189
GEV207_R0400_0058	VUB	146.43	477127	GEV207_R0400_0110	DLR	250.03	2074
GEV207_R0400_0055	VUB	148.49	360314	GEV207_R0400_0109	DLR	224.98	8234
GEV207_R0400_0054	VUB	177.49	78055	GEV207_R0400_0108	DLR	134.98	637851
GEV207_R0400_0053	VUB	177.75	83510	GEV207_R0400_0105	DLR	108.43	1590000
GEV207_R0400_0657	VUB	180.09	31694	GEV207_R0400_0106	DLR	124.97	1100000
GEV207_R0400_0658	VUB	179.53	17926	GEV207_R0400_0499	WMC	179.11	41120
GEV207_R0400_0659	VUB	132.13	231984	GEV207_R0400_0488	WMC	180.23	112810
GEV207_R0400_0660	VUB	133.20	193726	GEV207_R0400_0799	WMC	186.44	40297
GEV207_R0400_0052	VUB	265.39	269	GEV207_R0400_0472	WMC	132.01	1452093
GEV207_R0400_0051	VUB	263.88	241	GEV207_R0400_0829	WMC	240.20	2793
GEV207_R0400_0049	VUB	234.12	2091	GEV207_R0400_0486	WMC	268.83	410
GEV207_R0400_0035	VUB	98.99	7223777	GEV207_R0400_0507	WMC	132.88	817473
GEV207_R0400_0316	DLR	234.38	4265	GEV207_R0400_0599	WMC	283.57	362
GEV207_R0400_0708	DLR	103.77	596635	GEV207_R0400_0825	WMC	139.39	637298
GEV207_R0400_0107	DLR	249.83	959	GEV207_R0400_0783	WMC	137.76	1155325
GEV207_R0400_0131	DLR	276.42	727	GEV207_R0400_0477	WMC	226.21	941
GEV207_R0400_0129	DLR	184.98	48942	GEV207_R0400_0495	WMC	226.70	6764
GEV207_R0400_0124	DLR	250.01	1534	GEV207_R0400_0498	WMC	270.21	3910
GEV207_R0400_0120	DLR	185.03	59468	GEV207_R0400_0478	WMC	230.19	1256
GEV207_R0400_0118	DLR	200.00	16291	GEV207_R0400_0484	WMC	233.35	1510
GEV207_R0400_0117	DLR	250.01	2608	GEV207_R0400_0268	WMC	182.79	51545
GEV207_R0400_0115	DLR	124.39	2098460	GEV207_R0400_0023	WMC	81.20	8238763
GEV207_R0400_0116	DLR	184.98	57038	GEV207_R0400_0019	WMC	87.54	8463432
GEV207_R0400_0114	DLR	175.00	109901	GEV207_R0400_0272	WMC	103.82	6728478
GEV207_R0400_0113	DLR	134.99	735186				

Table 21 Fatigue life test results on 10° and 60° off-axis MD coupons under R=-1.

Coupon ID	$\sigma_{\max}$ MPa	N Cycles	Coupon ID	$\sigma_{\max}$ MPa	N Cycles
GEV207_R0410_0014	125.00	288857	GEV207_R0460_0011	58.38	246717
GEV207_R0410_0015	125.00	269976	GEV207_R0460_0012	58.38	186756
GEV207_R0410_0016	125.00	149301	GEV207_R0460_0013	58.38	241253
GEV207_R0410_0017	125.00	159209	GEV207_R0460_0014	58.38	353089
GEV207_R0410_0018	125.00	183573	GEV207_R0460_0015	58.37	283412
GEV207_R0410_0011	250.00	481	GEV207_R0460_0016	95.22	6177
GEV207_R0410_0012	250.00	854	GEV207_R0460_0017	113.43	1297
GEV207_R0410_0013	250.00	1131	GEV207_R0460_0018	113.43	1601
GEV207_R0410_0019	250.00	570	GEV207_R0460_0019	113.43	1587
GEV207_R0410_0020	250.00	559	GEV207_R0460_0020	113.44	1616

While the fatigue behavior of the MD laminate at 0° is expected to be driven by the 0° layers, which are dominating with more than 50% of the total reinforcement, in the case of the 10° off-axis a combination of shear and axial fatigue loads are expected to develop. On the 60° off-axis laminate on the contrary a combination of transverse and shear cyclic loads is most likely to occur on the former 0° layer, even though the 45° layer turned to -15° is expected to carry a substantial amount of load through its fibres. In general, both off-axis lay-ups are expected to develop a variety of combinations of on-axis, transverse and shear cyclic stresses and consequently help in the assessment of the failure criterion as well as of the matrix post failure degradation strategies assumed by the algorithm.

## 5.4.2 FADAS Results and Discussion

The life prediction methodology has been implemented in computer code using MATLAB commercial software, for the three kinds of coupons tested. Predictions of the MD laminate cut at 0°, under tension-tension fatigue (R=0.1) and reversed loading fatigue (R=-1) are shown in Fig. 90 and Fig. 91

respectively. In the abscissa is the maximum cyclic stress applied on the laminate and in the ordinate is the number of applied fatigue cycles.

In both cases the predictions are fair and lay slightly on the safe side of the experiments. The similar strength and stiffness results obtained for both cases from the FADAS simulation indicate as expected, that the behavior of the laminate under such loads is dominated by the  $0^\circ$  layer which finally fails under tension. The  $\pm 45^\circ$  layers undergo considerable damage in the transverse direction due to shear loading and are predicted to fail under mode A quite early in fatigue life, especially in higher load levels. This is a typical example of how first ply failure methodologies usually underestimate strength and life of composites. Degradation and failure of this matrix dominated ply, causes stress redistributions that result in a total increase of the  $0^\circ$  layer stress in the order of 10% according to the predictions of the algorithm. This extra loading of the UD layer shortens the fatigue life of the laminate by an estimated 20-30%. Nevertheless, the longer lives obtained by tests indicate that damage in the  $0^\circ$  layer inside the MD laminate is probably less than the that developing in a purely UD coupon (which has been used for parameter estimation). The reason for that is probably the fact that the UD layers do not act freely, being constrained by adjacent  $\pm 45^\circ$  layers that affect beneficially their performance. The FADAS model in its present form does not account for such effects.

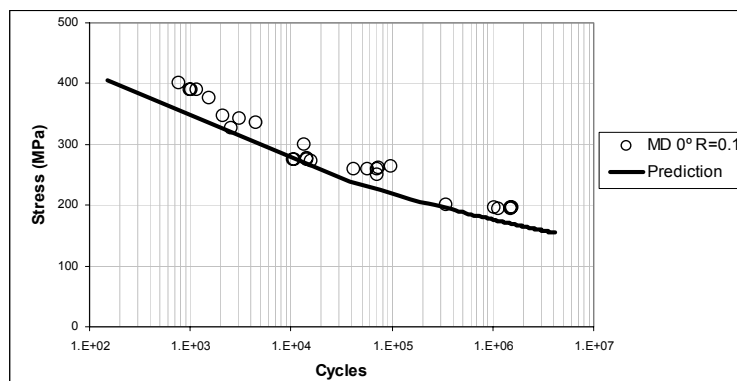


Fig. 90 S-N data and model predictions for the MD laminate at R=0.1.

### 5. Fatigue Simulation Of Laminates

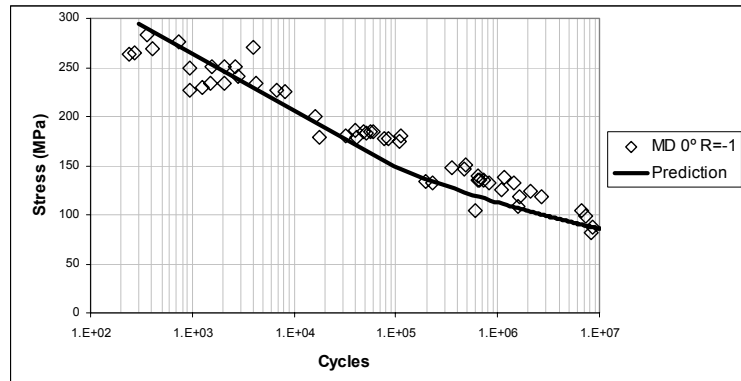


Fig. 91 S-N data and model predictions for the MD laminate at R=-1.

The predictions show the opposite trend in both off-axis data sets: Simulation results lay on the non-conservative side and even though the predictions are in general acceptable, there is again half a decade deviation from the test data, as seen in Fig. 92 and 93.

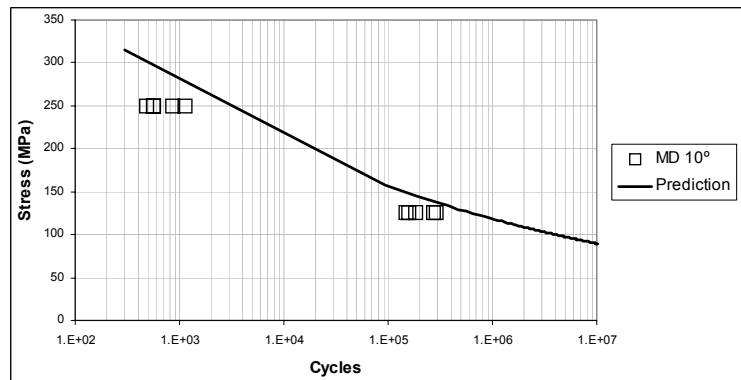


Fig. 92 S-N data and model predictions for the 10° off-axis MD laminate at R=-1.

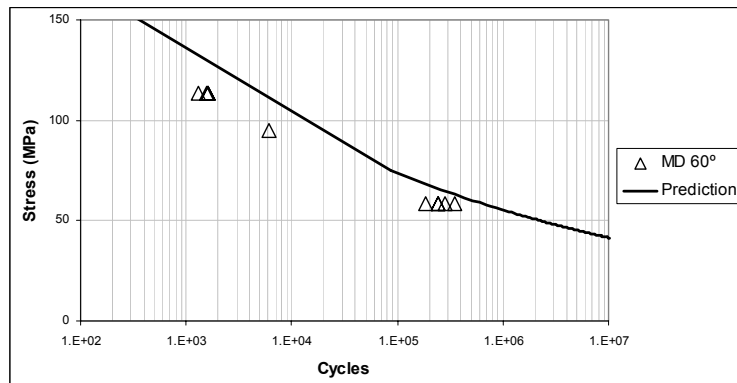


Fig. 93 S-N data and model predictions for the 60° off-axis MD laminate at R=-1.

Results indicate in both cases, that failure is dominated by the 10° or 15° ply of the 10° and 60° off-axis laminate respectively. The layer of each laminate that has the higher angle between load direction and reinforcing fibres, i.e. 55° and 75°, fails again rather early in fatigue life being the most vulnerable component of the laminate under the applied loads. Nevertheless, the overall failure of both laminates is hardly affected by such failures.

Stress redistributions caused either by sudden or gradual degradation mechanisms for each individual ply, become very complicated to follow in such MD lay-ups. In contrast to the on-axis MD laminate, where transverse cracking causes simply a stresses transfer towards the fibre direction of the on-axis ply, degradation in the 'most off-axis' plies either intensifies or reduces fibre, transverse and shear stresses of other oblique layers with an overall trend of steadily transferring loads towards the fibres of the best aligned (in respect to the external load) UD ply.

The complexity of damage evolution and redistribution of stresses is exemplified in Fig. 94, which shows residual strength and maximum cyclic stress for each ply orientation and in-plane property of an MD coupon at 60° off-axis, cycled at a maximum stress of 50 MPa (under R=-1), and predicted to survive 2,359,000 cycles. Fig. 94 as well as the output of the routine indicate, that final failure is due to fibre failure in the -15° ply. The other two plies undergo significant loss of strength in the transverse direction, while all three of them suffer shear strength degradation, which can be explained not only by the



5. Fatigue Simulation Of Laminates

shear stresses themselves, but also from damage induced through failure in the transverse direction which is inherently assumed to be affecting the shear load bearing capacity of the material.

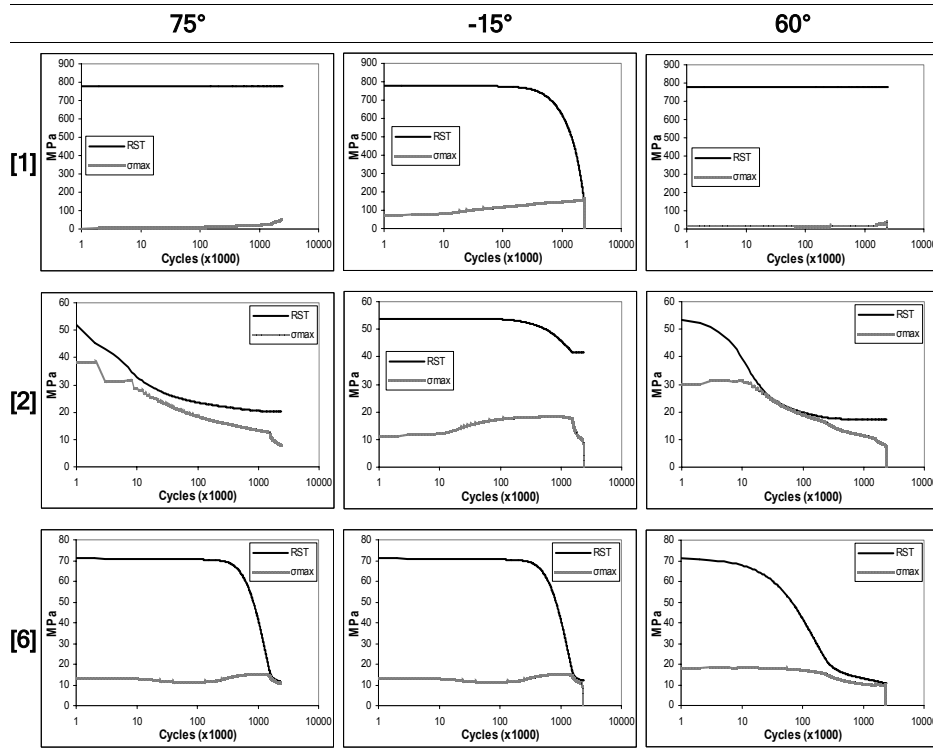


Fig. 94 Residual strength and maximum cyclic stresses predicted through FADAS for each in-plane property of each ply of the MD coupon at 60° off-axis, cycled at  $\sigma_{max}=50$  MPa, R=-1.

In Fig. 95 is shown a typical picture of failed MD coupons (GEV207\_R0460\_016 and GEV207\_R0460\_020) at 60° off-axis.



Fig. 95 MD coupons at 60° off-axis tested at R=-1.

Even though edge effects due to coupon geometry and post-failure damage makes the picture of the failed coupon hard to understand, ultimate failure of the laminate can be assumed to be driven by the failure of the  $-15^\circ$ . Of course test results as interpreted through visual observation of the failed coupons, as well as the results of the simulation itself, seen in Fig. 94, indicate the simultaneous propagation of a multitude of damage mechanisms on the laminate such as matrix cracks and matrix-fibre debonding which affects the inter-laminar layer causing extensive delaminations. Nevertheless this kind of damage propagation can be assumed to result in transferring loads from the damaged plies to the fibres of the  $15^\circ$  layer, causing ultimately this latter to fail as well, as clearly seen in Fig. 94. In this sense the predictions of FADAS algorithm seem to correlate satisfactorily with the fatigue test results.

## 6 CONCLUSIONS

The conclusions of this thesis can be drawn separately on each of the three main issues investigated: Modeling of the residual strength of a composite laminate, implementation of residual strength in standard life prediction schemes and development of a methodology for fatigue simulation of MD laminates based only on the characterization of their constitutive UD ply, using residual strength as damage accumulation metric. These three levels of looking into the residual strength phenomenon (basic modeling, evaluation of its implementation on modeling simple laminates and finally inclusion in a complete methodology for life prediction of arbitrary lay-up) constitute a thorough investigation of the residual strength phenomenon in Glass/Epoxy composites and more precisely of the potential of integrating phenomenological residual strength models into methodologies for predicting life and strength of these materials after cyclic loading.

This task has been attempted always bearing in mind that any finding should be assessed on its applicability on structural design reality and for that purpose the procedures considered refer to the ones currently used (or proposed by certification bodies), for design of large composite structures, such as Wind Turbine Rotor Blades. This is the reason for which the micromechanical aspects of residual strength have been not been taken into account: Models describing residual strength in terms of damage parameters in the micro scale have not yet reached their maturity so that they become applicable in design. Phenomenological models for the description of residual strength on the other hand are much more applicable, following the same modelling philosophy as for the majority of mechanical properties required in standard engineering practices (e.g. fatigue life or static strength).



## 6.1 RESIDUAL STRENGTH MODEL

A multitude of residual strength formulations of different degree of complexity has been implemented and validated on experimental data available in literature or produced in the frame of OPTIMAT BLADES project. All existing formulations have been implemented according to the respective procedure proposed, while those considering residual strength at a single stress level have been generalized to various stress levels using simple and efficient concepts (e.g. the equivalent static strength concept). Despite that, the majority of the models, fails to describe accurately the degradation of static strength, especially the drop of strength observed during the initial 20% of fatigue life in all laminates included in this study. Furthermore all of them fail to adapt to the change of fatigue damage mechanism taking place at higher stress levels. The most promising formulations, requiring nevertheless a number of tests for residual strength characterization of the material, are the interaction model (INT) and the OM model, the latter developed in the frame of the present thesis.

The above mentioned conclusions are rather qualitative, since the large scatter involved with fatigue and residual strength is partly impeding the quantitative assessment of the deterministic predictions of the models. Consequently, the use of statistical models for residual strength is highly advisable. The methodology developed for this purpose, i.e. for bringing even deterministic models up to the point of predicting residual strength at specific reliability levels, gives quite acceptable results both in fibre as well as in matrix dominated laminates. Best results are again obtained in combination with INT and OM models, while the linear model (BR) gives encouraging predictions (being slightly on the safe side) given the extreme simplicity of its formulation and the fact that it requires no residual strength characterization cost.



## 6.2 LIFE PREDICTION MODULES

With a number of acceptable candidates for modeling of residual strength, an investigation of the standard procedure for prediction of fatigue life under variable amplitude loading is performed. The main issues examined are the following

Replacement of Palmgren-Miner rule by a residual strength model.

Investigation of the relative importance of the CLD and Counting method.

Dependence of the above on the variable amplitude loading pattern.

Regarding the first objective, the incorporation of residual strength as damage metric seems to have a rather limited effect on the predicted life, independently of the spectrum pattern, the CLD choice or the Cycle Counting algorithm: In all cases an improvement of 10-20% is achieved depending on the residual strength degradation model assumed. In view of this and considering the benefits of attributing a physical meaning to damage accumulation (especially when used in more complicated models like FADAS), the most suitable residual strength formulation is the linear one (BR) due to its low cost of implementation (standard static strength and fatigue life characterization) and slightly conservative results.

Regarding the effect of using different CLD and Counting methods the conclusions seem to be highly dependent on the kind of spectrum loading considered. For the case of artificial spectra, like WISPER or NEW WISPER, the CLD choice plays a predominant role. In that case, the state-of-the-art constant life formulation based on three S-N curves leads to considerably optimistic predictions, at least for the case of fibre dominated laminates, while more acceptable results are obtained for matrix damage modes. On the other hand, other formulations, like e.g. the R01, give in some cases far better predictions, proving that experimental effort does not always pay back in quality of predictions. Nevertheless even such formulations have proved to be highly dependent on the S-N curve choice. Comparison of the results obtained with LCLD, BELL and R01 imply that better results are obtained when all constant life lines do not converge to the UTS and UCS.

On the contrary, the choice of counting method is of relatively small influence in the case of artificial spectrum patterns. This should be expected, since they mainly consist of constant amplitude blocks which are counted in similar ways by different algorithms. The complete opposite holds true for the case of more irregular spectra like the MWIND load series investigated in this work. Not only does counting play a significant role in life prediction, but the CLD choice does not seem to play such an important one. This means that for load series like the ones actually encountered by Wind Turbine Blade laminates the CLD choice is not utterly important and in this case simpler CLD assumptions, like WAR or R01, could be used, reducing this way the fatigue characterization cost of the material even by 60%.

Even if the above conclusions have been drawn mainly from tests on the reference UD material they are applicable for any fibre dominated laminate, once its static strength properties and fatigue response is experimentally defined. Nevertheless performing this characterization task for the variety of lay-ups included in a large composite structure is not always practical or efficient. For this reason algorithms like FADAS offer a viable alternative.



## 6.3 FATIGUE SIMULATION OF MD LAMINATES

The FADAS algorithm, developed and tuned accordingly for simulating the effect of fatigue damage on the strength and stiffness components of a multidirectional laminate consisting of the characterized reference UD, constitutes an effort for predicting more accurately the fatigue response of modern composite materials while keeping low the cost for material characterization. The results obtained from the algorithm prove that residual strength can be implemented in life prediction methodologies with limited experimental cost (since the linear BR model is applied) within reasonable computational time and with quite acceptable predictions.

During the development of the algorithm the focus has been put on the implementation of residual strength as damage accumulation, on strategies for modeling the failure event (failure criterion) as well as on the post-failure behavior of each ply. This is the reason why the CLD and Counting method are not thoroughly discussed in this part of the study, more so since the simulation of the laminate's response is performed under constant amplitude fatigue loading. Of course, as stated before, the cyclic stresses do not retain constant amplitude within each lamina but actually change due to the stress redistributions caused by stiffness loss and/or non-catastrophic failure. Nevertheless, in most cases these variations happen gradually and do not result in highly irregular loading series that would be counted differently by different Cycle Counting algorithms. For this reason, only the standard LCLD is implemented along with the Range-Mean counting algorithm (RM), since Rainflow Counting of each in-plane stress component of each individual ply would complicate the algorithm without any significant improvement of the predictions.

Following the above mentioned tuning of the procedure, the FADAS algorithm produces good predictions of fatigue life, both in the case of the on-axis MD laminate and in the case of off-axis laminates where more complicated combinations of damage modes are encountered. This is encouraging for the inclusion of such tools in fatigue life prediction of composite laminates, especially those that undergo complex cyclic stresses, since the implementation of uniaxial theories can lead to considerable errors in the calculation of the fatigue response

## 7 FUTURE RESEARCH

Despite the tedious experimental and theoretical effort performed in the frame of the present study, the complexity of the phenomena and methodologies investigated, inevitably resulted in several issues requiring further study.

Regarding residual strength modeling itself, the process for deriving the parameters of the best candidates (OM and INT), could be optimized on the basis of the ESS concept, in order to minimize the required experimental effort.

The statistical model proposed could be further developed to perform predictions at specific confidentiality levels and any such modeling should require experimental validation. This last task of course necessitates considerable effort and careful planning in order to eliminate any noise induced in the results.

The transition of the damage degradation behavior observed in the UD laminate also raises several questions on the mechanism of strength degradation. Especially, a closer look should be taken on the possibility of residual strength increase at higher stress levels which, partly due to experimental variations, has been considered as an artifact and has not been taken into account.

Regarding residual strength as damage accumulation metric, two main issues can be proposed for further study. The first one concerns the interpolation of the parameters of non-linear models between the stress ratios tested, or alternatively the development of more advanced theoretical models including the stress-ratio dependency (e.g. validation of the models proposed by Sendekyj). On the other hand, the problem of implementing the developed methodologies for the case of purely compressive loading spectra requires additional analytical effort as well as experimentation under e.g. Reversed WISPER spectrum.

Finally, the implementation of FADAS algorithm emphasized the importance of other issues indirectly related to residual strength-based applications, some of which are already being investigated, e.g. the development of more sophisticated algorithms including material non-linearity in the transverse and shear directions, residual strains etc, and their inclusion on Finite Elements, as well as the question on the form of the CLD (and especially in the area near

## *6. Conclusions*

R=1) which is of special interest and its deeper study, both experimental and analytical can be expected to weight on the quality of predictions.



## 8 REFERENCES

1. OPTIMAT BLADES, 'Reliable Optimal Use of Materials for Wind Turbine Rotor Blades', Contract no. ENK6-CT-2001-00552, <http://www.ecn.nl/optimat/>, (2001-2006) <http://www.ecn.nl/optimat/>.
2. Shokrieh M.M., Lessard L.B., 'Multiaxial Fatigue Behaviour of Unidirectional Plies Based on Uniaxial Fatigue Experiments- part I. Modeling', *Int J Fatigue* 1997, 19(3), pp. 201-207.
3. Shokrieh M.M., Lessard L.B., 'Fatigue Under Multiaxial Stress Systems', *Fatigue in Composites*, Ed. B. Harris, Woodhead Publishing 2003, pp.63-113.
4. Tserpes K.I., Papanikos P., Labeas G., Pantelakis Sp., 'Fatigue Damage Accumulation and Residual Strength Assessment of CFRP Laminates', *Composite Structures*, 2004, 63, pp. 219-230.
5. ASTM E 1150 E1150-87(1993) Definitions of Terms Relating to Fatigue (Withdrawn 1996) replaced by: ASTM E1823-07a Standard Terminology Relating to Fatigue and Fracture Testing, ASTM International, West Conshohocken, PA, [www.astm.org](http://www.astm.org).
6. Broutman L.J., Sahu S., 'A New Theory to Predict Cumulative Fatigue Damage in Fibreglass Reinforced Plastics', *Composite Materials: Testing and Design (2nd Conference) 1972*. Eds. Corten HT (American Society for Testing and Materials) STP 497, pp. 170-188.
7. Hahn H.T., Kim R.Y., 'Proof Testing of Composite Materials', *J Compos Mat* (1975), 9, pp. 297-311
8. Chou P.C., Croman R., 'Residual strength in fatigue based on the strength-life equal rank assumption', *Journal of. Composite Materials* (1978), 12, pp. 177-194.
9. Hahn H.T., Hwang D.G., 'Failure Characterization of Graphite/Epoxy Laminate Through Proof Testing', *ASTM STP 787* (1982), pp. 247-273.
10. Hahn H.T., 'Fatigue Behavior and Life Prediction of Composite Laminates', *ASTM STP 674* (1979), pp. 383-417.
11. Whitworth H.A., 'Evaluation of the Residual Strength Degradation on Composite Laminates Under Fatigue Loading', *Compos Structures*, 2000, 48, pp. 261-264.
12. Yang J.N., 'Fatigue and Residual Strength Degradation for Graphite/Epoxy Composites Under Tension-Compression Cyclic Loading', *Journal of. Composite Materials*, 1978, 12, pp. 19-39.
13. Yang J.N., Jones D.L., 'Statistical Fatigue of Unnotched Composite Laminates', in 'Advances in Composite Materials', ICCM-III, 1980, 1, pp. 472-483.
14. Yang J.N., Liu M.D., 'Residual strength degradation model and theory of periodic proof tests for Graphite/Epoxy laminates', *Journal of. Composite Materials*, 1977, 11, pp. 176-203.
15. Yang J.N., Sun C.T., 'Proof Test and Fatigue of Unnotched Composite Laminates', *Journal of. Composite Materials*, 1980, 14, pp. 168-176.
16. Yang J.N., Jones D.L., Yang S.H., Meskini A., 'A Stiffness Degradation Model for Graphite/Epoxy Laminates', *J. Compos Mater*, 1990; 24, pp. 753-769.
17. Lee L.J., Fu K.E., Yang J.N., 'Prediction of Fatigue Damage and Life for Composite Laminates Under Service Loading Spectra', *Compos Sci & Tech*, 1996, 56, pp. 635-648.
18. Yang J.N., 'Reliability Prediction for Composites Under Periodic Proof Tests in Service', *ASTM STP 617*, 1977, pp. 272-295
19. Yang J.N., Cole R.T., 'Fatigue of Composite Bolted Joints Under Dual Stress Levels' in 'Progress in Science and Engineering of Composites', ICCM-IV, 1982, Tokyo, pp. 333-340.

20. Yang J.N., Jones D.L., 'Statistical Fatigue of Graphite/Epoxy angle Ply Laminates in Shear', *Journal of Composite Materials*, 1978, 12, pp. 371-389.
21. Yang J.N., Miller R.K., Sun C.T., 'Effect of High Load on Statistical Fatigue of Unnotched Graphite/Epoxy Laminates', *J Compos Mat*, 1980, 14, pp. 82-94.
22. Ryder J.T., Walker E.K., 'Ascertainment of the Effect of Compressive Loading on the Fatigue Life Time of Graphite/Epoxy Laminates for Structural Application', AFML-TR-76-241, WPAFB, December 1976.
23. Yang J.N., Jones D.L., 'Effect of Load Sequence on the Statistical Fatigue of Composites', *AIAA Journal*, 1980, 18(12), pp. 1525-1531.
24. Radhakrishnan K., 'Fatigue and Reliability Evaluation of Unnotched Carbon Epoxy Laminates', *J Compos Mat*, 1984, 18, pp. 21-31.
25. Yang J.N., Jones D.L., 'Load Sequence Effects on the Fatigue of Unnotched Composite Laminates', *ASTM STP 723*, 1981, pp. 213-232.
26. Andersons J., Korsgaard J., 'Residual Strength of GRP at High Cycle Fatigue', *ICCM-11 (1997)*; II, pp. 135-144
27. Yang J.N., Jones D.L., 'Fatigue of Graphite/Epoxy [0/90/45/-45]S Laminates Under Dual Stress Levels', *Composites Technology Review*, 1982, 4(3), pp. 63-70.
28. Yang J.N., Du S., 'An Exploratory Study Into the Fatigue of Composites Under Spectrum Loading', *Journal of Composite Materials*, 1983, 17, pp. 511-526.
29. Chou P.C., Croman R., 'Degradation and Sudden Death Models of Fatigue of Graphite/Epoxy Composites', *Composite Materials: Testing and Design (5th conference)*, *ASTM STP 674 (1979)*, pp. 431-454
30. Adam T., Dickson R.F., Jones C.J., Reiter H., Harris B., 'A Power Law Fatigue Damage Model for Fiber-Reinforced Plastic Laminates', *Proc Instn Mech Engrs (1986)*; 200(C3), pp. 155-166
31. Adam T., Dickson R.F., Fernando G., Harris B., Reiter H., 'The Fatigue Behaviour of Kevlar/Carbon Hybrid Composites', *IMechE*, 1986, C275/86, pp. 329-335.
32. Adam T., Gathercole N., Reiter H., Harris B., 'Life Prediction for Fatigue of T800/5245 Carbon Fibre Composites: I. Variable-Amplitude Loading', *Fatigue (1994)*, 16, pp. 533-547
33. Harris B., 'A Parametric Constant-Life Model for Prediction of the Fatigue Lives of Fibre-Reinforced Plastics', *Fatigue in Composites*, Ed. Harris B., Woodhead Publishing Ltd (2003), pp. 546-568.
34. Gathercole N., Reiter H., Adam T., Harris B., 'Life prediction for fatigue of T800/5245 carbon-fibre composites: I. Constant amplitude loading', *Fatigue (1994)*, 16, pp. 523-532.
35. Reifsnider K.L., 'The Critical Element Model: A Modelling Philosophy', *Engng Fracture Mech*, 1986, 25, pp. 739-749.
36. Sendeckyj G.P., 1991, 'Life Prediction for Resin-Matrix Composite Materials', in *Composite Material Series*, Vol. 4, 10. Amsterdam: Elsevier, pp. 431-483.
37. Sendeckyj G.P., 'Fitting Models to Composite Materials Fatigue Data', *Test Methods and Design Allowables for Fibrous Composites*, *ASTM STP 734*, 1981, pp. 245-260.
38. Whitney J.M., 'Residual Strength Degradation Model for Competing Failure Modes', O' Brien T.K. (Ed.), *Long-Term Behavior of Composites*, *ASTM STP 813*, 1983, pp. 225-245.
39. Whitney J.M., 'Use of Lognormal Distribution for Characterizing Composite Materials', Daniel I.M. (Ed.), *Proc. 6th Conf. On Composite Materials: Testing and design*, *ASTM STP 787*, 1982, pp. 483-497.
40. Passipoularidis V.A., Philippidis T.P., 'Reliability Aspects of Strength Degradation after fatigue in Wind Turbine Rotor Blade Composites', *Proceedings of COMP07*:

## 8. References

- 6th International Symposium on Advanced Composites, Corfu - Greece, 16-18 May 2007, COMP07-85.
41. Passipoularidis V.A., Philippidis T.P., 'Strength Degradation due to Fatigue in Fiber Dominated Glass/Epoxy Composites: A Statistical Approach', (Accepted for publication in: Journal of Composite Materials)
  42. Whitney J.M., 'Fatigue Characterization of Composite Materials', Fatigue of Fibrous Composite Materials, ASTM STP 723, 1981, pp. 133-151.
  43. Schaff J.R., Davidson B.D., 'Life Prediction Methodology for Composite Structures. Part I- Constant Amplitude and Two Stress Level Fatigue', J Compos Mat, 1997, 31(2), pp. 128-157.
  44. Philippidis T.P., Passipoularidis V.A., 'Validated Engineering Models For Residual Strength Prediction', OB\_TG5\_R013, 2006, 39pp, ([http://www.kc-wmc.nl/optimat blades/ Publications](http://www.kc-wmc.nl/optimat/ blades/ Publications)).
  45. Shokrieh M.M., Lessard L.B., 'Progressive Fatigue Damage Modelling of Composite Materials- part II. Material Characterization and Model Verification', Journal of Composite Materials, 2000, 34, pp. 1081-1116.
  46. ISO 14129:1997(E), Fibre-reinforced plastic composites - Determination of the in-plane shear stress/shear strain response, including the in-plane shear modulus and strength, by the  $\pm 45^\circ$  tension test method
  47. Passipoularidis V.A., Philippidis T.P., 'Residual strength degradation in the principal directions of a UD Glass/Epoxy laminate', International Conference on Structures and Advanced Materials, Patras, Greece, 2-6 September 2007.
  48. Krause O., 'Testing Frequency for Dynamic Tests', OB\_TC\_N003\_DLR, December 2002 ([http://www.kc-wmc.nl/optimat blades/ Publications](http://www.kc-wmc.nl/optimat/ blades/ Publications))
  49. Krause O, 'General Test Specifications', OB\_TC\_R014.
  50. Philippidis T.P., Assimakopoulou T.T., Passipoularidis V.A., Antoniou A.V., 'Static & Fatigue Tests On ISO Standard  $\pm 45^\circ$  Coupons', OB\_TG2\_R020, 2004, 41pp, ([http://www.kc-wmc.nl/optimat blades/ Publications](http://www.kc-wmc.nl/optimat/ blades/ Publications)).
  51. ISO 527/5 (1997) Plastics - Determination of tensile properties - Part 5: Test conditions for unidirectional fibre-reinforced plastic composites
  52. ISO 14126:1999(E), Fibre-reinforced plastic composites. Determination of compressive properties in the in-plane direction
  53. ASTM D 3518M-94 American Society for Testing and Materials, 'Standard test method for in-plane shear response of polymer matrix composite materials by tensile test of a  $\pm 45^\circ$  laminate', ASTM, PO Box C700, West Conshohocken, PA, 19428-2959, USA, January 1995, 7 pp.
  54. Jacobsen T.K., 'Reference Material (OPTIMAT) Glass-epoxy', OB\_SC\_R001 (2002); 9p, ([http://www.kc-wmc.nl/optimat blades/ Publications](http://www.kc-wmc.nl/optimat/ blades/ Publications))
  55. ASTM 5379M98. American Society for Testing of Materials, 'Standard Test Method for Shear Properties of Composite Materials by the V Notched Beam Method', ASTM, PO Box C700, West Conshohocken, PA, 19428-2959, USA, 1999. 13 pages.
  56. ASTM D3479/D3479M-96(2007) Standard Test Method for Tension-Tension Fatigue of Polymer Matrix Composite Materials, ASTM International, West Conshohocken, PA, [www.astm.org](http://www.astm.org).
  57. ASTM D3039/D3039M-00(2006) Standard Test Method for Tensile Properties of Polymer Matrix Composite Materials, ASTM International, West Conshohocken, PA, [www.astm.org](http://www.astm.org).
  58. Philippidis T.P., Assimakopoulou T.T., Passipoularidis V.A., 'Preliminary Results on UD Reference Material (2nd Round)', OB\_TC\_R006-10049, 2002, ([http://www.kc-wmc.nl/optimat blades/ Publications](http://www.kc-wmc.nl/optimat/ blades/ Publications)).

59. Philippidis T.P., Antoniou A.V., Passipoularidis V.A., Assimakopoulou T.T., 'Static Tests On The Standard OB Unidirectional Coupon', OB\_TG2\_R018, 2004, 53pp, (<http://www.kc-wmc.nl/optimat blades/ Publications>)
60. Philippidis T.P., Passipoularidis V.A., Assimakopoulou T.T., Antoniou A.E., 'Fatigue Tests in the Fiber Direction Of UD OB Standard Specimen Main Test Phase I', OB\_TG1\_R013\_UP, 2006 (<http://www.kc-wmc.nl/optimat blades/ Publications>)
61. Philippidis T.P., Antoniou A.E., Assimakopoulou T.T., Passipoularidis V.A., 'Fatigue Tests on OB Standard Coupons at 90o Main Test Phase I', OB\_TG2\_R021\_UP, 2005 (<http://www.kc-wmc.nl/optimat blades/ Publications>)
62. OPTIDAT database: <http://www.kc-wmc.nl> (available upon request)
63. Philippidis T.P., Assimakopoulou T. T., Antoniou A. E., Passipoularidis V. A., 'Residual Strength Tests On ISO Standard  $\pm 45^\circ$  Coupons, Main test Phase I', OB\_TG5\_R008, 2005, 19pp, (<http://www.kc-wmc.nl/optimat blades/ Publications>).
64. Philippidis T.P., Assimakopoulou T.T., Antoniou A.E., Passipoularidis V.A., 'Residual Strength Tests on ISO Standard  $\pm 45^\circ$  Coupons, Main Test Phase II', OB\_TG2\_R037\_UP, 2006, (<http://www.kc-wmc.nl/optimat blades/ Publications>)
65. Philippidis T.P., Passipoularidis V.A., 'Residual Strength After Fatigue in Composites: Theory vs Experiment', Int J Fatigue, 2007, 29(12), pp. 2104-2116.
66. Van Paepegem W., Degrieck J., 'Coupled Residual Stiffness and Strength Model for Fatigue of Fibre-Reinforced Composite Materials', Compos Sci & Tech, 2002, 62(5), pp. 687-696.
67. Hwang W., Han K.S., 'Cumulative Damage Model and Multi-Stress Fatigue Prediction', J Compos Mater (1986), 20, pp.125-153.
68. Schaff J.R., Davidson B.D., 'Life Prediction Methodology for Composite Structures. Part II- Spectrum Fatigue', J Compos Mat, 1997, 31(2), pp. 157-181.
69. Bond I.P., 'Fatigue Life Prediction for GRP subjected to variable amplitude Fatigue', Composites: Part A, 1999, 30, pp. 961-970
70. Philippidis T.P., Vassilopoulos A.P., 'Life Prediction Methodology for GFRP Laminates under Spectrum Loading', Composites: Part A, 35(2004), pp. 657-666.
71. Passipoularidis V.A., Philippidis T.P., 'A Study of Factors Affecting Life Prediction of Composites under Spectrum loading', Article in press, Int J Fatigue, doi:10.1016/j.ifatigue.2008.070.010
72. Passipoularidis V.A., Philippidis T.P., 'Non Linear Damage Accumulation And Load Sequence Effects In Life Prediction Of GI/Ep Composites', Proceedings of the 27th RISO International Symposium On Material Science: Polymer Composite Materials for Wind Power Turbines, Editors: H. Lilholt, B. Madsen, T.L. Andersen, RISO National Laboratory, Roskilde, Denmark, 2006, pp 287-296.
73. Hosoi A., Kawada H., Yoshino H., 'Fatigue Characteristics of Quasi-Isotropic CFRP Laminates Subjected to Variable Amplitude Cyclic Two Stage Loading', Int J Fatigue (2006), 28, pp. 1284-1289.
74. Nijssen R.P.L., van Delft D.R.V., van Wingerde A.M., 'Alternative Fatigue Lifetime Prediction Formulations for Variable Amplitude Loading', AIAA paper 2002-0022, ASME Wind Energy Symposium, Reno, NV, 2002
75. Nijssen R.P.L., '(NEW) WISPER(X) load spectra; Test results and Analysis', OB\_TG1\_R024, (2005); 10p, (<http://www.kc-wmc.nl/optimat blades/ Publications>).
76. Vassilopoulos A.P., 'A New Software Framework for Fatigue Life Prediction of Composite Materials Under Irregular Loading', Advanced Composite Letters, 2006, 15, pp. 23-29.
77. Nijssen R.P.L., 'Fatigue Life Prediction and Strength Degradation of Wind Turbine Rotor Blade Composites'. PhD Thesis, Faculty of Aerospace Engineering, (2006), T.U. Delft.



## 8. References

78. MEGAWIND project, 'Development of a MW Scale Wind Turbine for High Wind Complex Terrain Sites', Contract no. ENK5-CT-2000-00328.
79. Ten Have A.A., 'Wisper: A Standardized Fatigue Load Sequence for HAWT-Blades', European Community Wind Energy Conference Proceedings, Herring, Denmark. 6-10 June, 1988. pp. 448-452.
80. Bulder B. et al., 'NEW WISPER Creating A New Standard Load Sequence From Modern Wind Turbine Data', OB\_TG1\_R020 (2005), 79 pages, (<http://www.kc-wmc.nl/optimat/ blades/ Publications>).
81. Philippidis T.P., 'Life Prediction Methodology and Results for 30 m Split Blade - Calculation of Equivalent Fatigue Loads for Full-Scale Dynamic Blade Test', Final Report; MEGAWIND project; 2005 30p. (available upon request)
82. ASTM E 1049-85 (reapproved 1997). Standard Practices for Cycle Counting in Fatigue Analysis, ASTM International, West Conshohocken, PA, [www.astm.org](http://www.astm.org).
83. Matsuishi M., Endo T., 'Fatigue of Metals subjected to varying stress', in Proceedings of the Kyushu Branch of Japan Society of Mechanics Engineering, Fukuoka, Japan (1968), pp37-40 (in Japanese).
84. Endo T., Matsuishi M., 'The Rainflow Method in Fatigue - the Tatsuo Endo Memorial Volume', Murakami Y. (Ed.), ISBN 0-7506-0504-9, July, 1991
85. De Jonge, J.B., 'The analysis of load-time histories by means of counting methods', in 'Helicopter Fatigue design guide', F. Liard (ed.), AGARD-AG-292, November, 1983
86. Downing S.D., Socie D.F., 'Simple Rainflow Counting Algorithms', Int J Fatigue (1982), 4, pp. 31-40.
87. Shaffer J., Philippidis T.P., Vassilopoulos A.P., 'The Handbook of Advanced Materials', Chapter 1: Polymer Composites, Wiley Interscience, 2004, ISBN 0471454753, pp 1-63,
88. Sutherland H.J., Mandel J.F., 'The Effect of Mean Stress on Damage Predictions for Spectral Loading of Fiberglass Composite Coupons', proc. Special Topic Conference 'Creating Torque from Wind', Delft, 19-21 April, 2004, pp. 546-555.
89. Delft D.R.V., Rink H.D., Joosse P.A., Bach P.W., 'Fatigue Behavior of Fiberglass Wind Turbine Blade Material at the Very High Cycle Range', Proceedings European Wind Energy Conference 1994, pp. 379-384
90. Poursartip A., Beaumont P.W.R., 'The Fatigue Damage Mechanics Of A Carbon Fibre Composite Laminate: II-Life prediction', Compos. Sci. Tech. 1986, 25, pp. 283-299.
91. Gamstedt E.K., Sjögren B.A., 'An Experimental Investigation of the Sequence Effect in Block Amplitude Loading of Cross-Ply Composite Laminates', Int. J. Fatigue (2002), 24, pp. 437-446.
92. Dover W.D., 'Variable Amplitude Fatigue Of Welded Structures', Fracture Mechanics: Current Status, Future Prospects. Ed. Smith R.A. (Pergamon Press, Cambridge 1979), pp. 125-147.
93. Amijima S., Tanimoto T., Matsuoka T., 'A Study on the Fatigue Life Estimation of FRP Under Random Loading', Progress in Science and Engineering of Composites. ICCM-IV, Tokyo 1982, Eds. Hayashi T., Kawata K., Umekawa S, pp. 701-708
94. Brondsted P., Andersen S.I., Lilholt H., 'Fatigue Damage Accumulation And Lifetime Prediction Of GFRP Materials Under Block Loading And Stochastic Loading', Proceedings of the 18th Risoe International Symposium on Material Science 1997. Eds. Andersen S.I., Brondsted P. et al., pp. 269-278.
95. Philippidis T.P., Passipoularidis V.A., Assimakopoulou T.T., Antoniou A.V., 'Variable Amplitude Fatigue Tests On Standard OB UD Coupon and ISO [ $\pm 45$ ]s Performed At UP', OB\_TG2\_R031, 2006, 18pp, (<http://www.kc-wmc.nl/optimat/ blades/ Publications>).

96. Talreja R., 'Fatigue of Composite Materials', Technomic, Lancaster, Pennsylvania, 1987.
97. Daniel I.M., 1998 William M. Murray lecture: 'Experimentation and Modelling of Composite Materials', *Experimental Mechanics* (1999), 39, pp.1-19.
98. Varna J., Joffe R., Talreja R., 'A Synergistic Damage-Mechanics Analysis of Transverse Cracking in  $[\pm\theta/90]_S$  Laminates', *Composite Science and Technology*, 2001, 61, pp. 657-665.
99. Charewicz A., Daniel I.M., 'Damage Mechanisms and Accumulation in Graphite/Epoxy Laminates', *Composite Materials: Fatigue and Fracture*, ASTM STP 907 (1986), pp. 274-297
100. Reifsnider K.L., Case S., Duthoit J., 'The Mechanics of Composite Strength Evolution', *Compos Sci Tech* 2000, 60, pp. 2539-2546.
101. Reifsnider K.L., Stinchcomb W.W., 'A Critical Element Model of the Residual Strength and Life of Fatigue-Loaded Composite Coupons', *Composite Materials: Fatigue and Fracture*, ASTM STP 907, 1986, pp. 298-313
102. Passipoularidis V.A., Philippidis T.P., 'A Life Prediction Methodology for Composites Based on Progressive Damage Mechanics', *Eccomas Thematic Conference on Mechanical Response of Composites*, Composites 2007, Porto-Portugal, 12-14 September 2007.
103. Philippidis T.P., Eliopoulos E.N., Antoniou A.V., Passipoularidis V.A., 'Material Model Incorporating Loss of Strength and Stiffness Due to Fatigue', *Upwind Project, Deliverable 3.3.1*, 2007, 117 pages.
104. UPWIND project, 'Integrated Wind Turbine Design', Contract no. 019945(SES6)
105. Shokrieh M.M., Lessard L.B., 'Multiaxial Fatigue Behaviour of Unidirectional Plies Based on Uniaxial Fatigue Experiments- part II. Experimental Evaluation', *Int J Fatigue* 1997, 19(3), pp. 209-217.
106. Shokrieh M.M., Lessard L.B., 'Progressive Fatigue Damage Modelling of Composite Materials- part I. Modelling', *Journal of Composite Materials*, 2000, 34, pp. 1056-1080.
107. Puck A. Schürmann H., 'Failure Analysis of FRP Laminates by Means of Physically Based Phenomenological Models', *Composite Science and Technology*, 2002, 62, pp. 1633-1662.
108. Puck A., Kopp J., Knops M., 'Failure Analysis of FRP Laminates by Means of Physically Based Phenomenological Models', *Composite Science and Technology*, 2002, 62, pp. 371-378.
109. Puck A., Schürmann H., 'Failure Analysis of FRP Laminates by Means of Physically Based Phenomenological Models', *Composite Science and Technology*, 1998, 58, pp. 1045-1067.
110. Antoniou A.E., Philippidis T.P., 'Optimizing Material Use in Blade Design by Improving Failure Prediction Methodology and Introducing Damage Tolerant Concepts in FRP Composites', *European Wind Energy Conference (EWEC) 2006 Proceedings* (<http://www.ewec2006proceedings.info/>)
111. DNV standard, 'Design and Manufacture of Wind Turbine Blades, Offshore and Onshore Wind Turbines', *Offshore Standard DNV-OS-J102*, October 2006
112. Nijssen R.P.L., Krause O., Philippidis T.P., 'Benchmark of Lifetime Prediction Methodologies', *OB\_TG1\_R012*, 2004, 33p, (<http://www.kc-wmc.nl/optimat/ blades/ Publications>)
113. Philippidis T.P., Antoniou A.E., Assimakopoulou T.T., Passipoularidis V.A., 'Fatigue Tests on OB Unidirectional & Multidirectional off-axis Coupons Main Test Phase I', *OB\_TG2\_R030\_UP*, 2006, (<http://www.kc-wmc.nl/optimat/ blades/ Publications>)

## 9 APPENDIX

Table A1: Static strength and elastic properties of the UD laminate on-axis.

Static Tension					Static Compression			
ID number	$X_T$ (MPa)	$\epsilon_{max}$ (%)	$E_1$ (GPa)	$\nu_{12}$	ID number	$X_C$ (MPa)	$\epsilon_{max}$ (%)	$E_1$ (GPa)
GEV206_R0300_0181	830.72	2.36	39.85	0.2910	GEV206_R0300_0585	-554.51	-1.41	38.90
GEV206_R0300_0182	777.26	2.04	39.25	0.2830	GEV206_R0300_0586	-563.22	-1.50	38.16
GEV206_R0300_0184	795.66	2.13	38.05	0.2630	GEV206_R0300_0587	-542.78	-1.38	39.07
GEV206_R0300_0185	776.33	2.22	36.75	0.2790	GEV206_R0300_0588	-532.05	-1.33	38.06
GEV206_R0300_0186	782.68	2.11	39.40	0.2430	GEV206_R0300_0590	-552.69	-1.43	38.58
GEV206_R0300_0187	800.30	2.04	39.75	0.2860	GEV206_R0300_0591	-564.06	-1.46	38.46
GEV206_R0300_0188	788.90	2.12	38.75	0.3140	GEV206_R0300_0592	-550.29	-1.41	38.03
GEV206_R0300_0189	778.13	2.07	39.20	0.3200	GEV206_R0300_0594	-537.45	-1.40	39.06
GEV206_R0300_0190	781.09	2.10	39.60	0.3020	GEV206_R0300_0595	-549.45	-1.44	39.80
GEV206_R0300_0191	774.23	2.11	39.50	0.3020	GEV206_R0300_0596	-526.59	-1.35	39.03
GEV206_R0300_0192	776.71	2.08	38.05	0.2730	GEV206_R0300_0597	-531.81	-1.47	38.51
GEV206_R0300_0193	777.75	2.05	40.20	0.2970	GEV206_R0300_0598	-488.35	-1.27	39.24
GEV206_R0300_0194	789.23	2.03	41.50	0.2790	GEV206_R0300_0599	-534.80	-1.40	38.88
GEV206_R0300_0195	801.17	2.16	39.31	0.3180	GEV206_R0300_0600	-541.21	-1.36	39.40
GEV206_R0300_0196	780.59	2.08	39.80	0.2798	GEV206_R0300_0602	-547.04	-1.42	38.63
GEV206_R0300_0197	768.23	2.05	39.03	0.2853	GEV206_R0300_0604	-521.73	-1.60	38.60
GEV206_R0300_0198	801.81	2.06	40.99	0.2820	GEV206_R0300_0605	-546.20	-1.36	39.30
GEV206_R0300_0199	739.42	2.04	37.85	0.3065	GEV206_R0300_0606	-555.34	-1.43	38.90
GEV206_R0300_0200	768.23	2.11	37.26	0.2400	GEV206_R0300_0607	-559.20	-1.47	40.10
GEV206_R0300_0201	793.22	2.12	38.90	0.2907	GEV206_R0300_0608	-537.78	-1.41	39.20
GEV206_R0300_0202	784.00	2.04	40.11	0.2438	GEV206_R0300_0609	-554.18	-1.44	39.20
GEV206_R0300_0203	829.44	2.26	39.70	0.3329	GEV206_R0300_0610	-562.55	-1.43	38.90
GEV206_R0300_0204	735.37	2.07	37.74	0.2673	GEV206_R0300_0601	-504.98	-1.32	38.34
GEV206_R0300_0205	802.78	2.09	39.28	0.2721	GEV206_R0300_0603	-501.75	-1.29	39.37
GEV206_R0300_0206	818.67	2.20	40.08	0.3290	GEV206_R0300_0589	-533.52	-1.45	37.44
GEV206_R0300_0207	713.87	1.90	38.94	0.3459	GEV206_R0300_0593	-523.25	-1.33	39.33
GEV206_R0300_0208	712.37	1.93	38.14	0.2793				
GEV206_R0300_0209	774.94	2.18	38.66	0.3086				
Average	780.47	2.098	39.04	0.2906		-539.11	-1.297	38.91

Table A2: Static strength and elastic properties of the UD laminate transversely to the fiber.

Static Tension					Static Compression			
ID number	$Y_T$ (MPa)	$\epsilon_{max}$ (%)	$E_2$ (GPa)	$\nu_{21}$	ID number	$Y_C$ (MPa)	$\epsilon_{max}$ (%)	$E_2$ (GPa)
GEV213_R0390_0001	53.9	0.44	14.02	0.0933	GEV213_R0390_0014	-170.8	-1.71	15.10
GEV213_R0390_0002	51.8	0.37	14.73	0.1019	GEV213_R0390_0017	-167.8	-1.78	14.70
GEV213_R0390_0003	54.1	0.42	14.35	0.0855	GEV213_R0390_0022	-163.4	-1.98	15.30
GEV213_R0390_0004	56.1	0.44	14.07	0.1066	GEV213_R0390_0028	-169.9	-2.18	15.03
GEV213_R0390_0005	53.7	0.41	13.84	0.0974	GEV213_R0390_0029	-165.4	-1.89	15.22
GEV213_R0390_0006	57.5	0.48	13.88	0.0897	GEV213_R0390_0030	-162.0	-1.88	14.95
GEV213_R0390_0007	59.9	0.49	14.01	0.0926	GEV213_R0390_0033	-170.7	-2.24	14.90
GEV213_R0390_0008	54.7	0.41	14.16	0.0992	GEV213_R0390_0034	-168.4	-2.04	15.10
GEV213_R0390_0009	56.8	0.44	14.69	0.0979	GEV213_R0390_0035	-164.8	-1.94	14.75
GEV213_R0390_0010	49.6	0.39	14.09	0.0958	GEV213_R0390_0036	-171.7	-1.89	15.03
GEV213_R0390_0011	52.5	0.38	14.42	0.0968	GEV213_R0390_0221	-168.2	-2.12	14.70
GEV213_R0390_0012	52.2	0.35	14.39	0.1021	GEV213_R0390_0222	-170.7	-2.26	15.00
GEV213_R0390_0013	56.7	0.44	13.90	0.0973	GEV213_R0390_0223	-164.7	-2.06	14.70
GEV213_R0390_0015	56.9	0.47	13.78	0.0934	GEV213_R0390_0224	-162.3	-1.97	15.01
GEV213_R0390_0016	51.7	0.43	7.74	0.0459	GEV213_R0390_0225	-166.1	-2.15	15.11
GEV213_R0390_0018	54.2	0.39	14.60	0.0956	GEV213_R0390_0226	-159.8	-1.83	15.10
GEV213_R0390_0019	51.1	0.38	14.29	0.1037	GEV213_R0390_0227	-163.9	-2.24	14.80
GEV213_R0390_0020	50.3	0.41	13.93	0.0847	GEV213_R0390_0228	-148.8	-1.64	14.65
GEV213_R0390_0021	52.2	0.42	14.17	0.0992	GEV213_R0390_0229	-164.4	-2.04	15.16
GEV213_R0390_0023	52.3	0.43	13.74	0.0891	GEV213_R0390_0230	-164.1	-1.99	14.39
GEV213_R0390_0024	51.1	0.38	13.66	0.0903	GEV213_R0390_0231	-161.6	-2.08	15.05
GEV213_R0390_0025	52.2	0.38	14.00	0.1075	GEV213_R0390_0232	-167.9	-2.03	15.10
GEV213_R0390_0026	52.9	0.43	13.60	0.0836	GEV213_R0390_0233	-163.4	-2.08	15.14
GEV213_R0390_0027	55.8	0.44	14.19	0.0925	GEV213_R0390_0234	-166.0	-2.03	15.66
GEV213_R0390_0031	57.1	0.48	13.88	0.0903	GEV213_R0390_0235	-166.2	-2.12	15.28
GEV213_R0390_0032	53.2	0.46	13.54	0.0899	GEV213_R0390_0236	-157.5	-1.76	15.00
Average	53.9	0.422	14.07	0.0950		-	-	
						165.02	1.997	15.00

9. Appendix

Table A3: Shear strength and elastic properties derived from the [ $\pm 45$ ] laminate.

Coupon ID number	UTS (MPa)	$\tau_{max}$ (MPa)	$\gamma_1$ at $\tau_{max}$ (%)	$G_{12}$ (GPa)	$E_x$ (GPa)	$\nu_{xy}$
GEV208_I1000_0001	111.00	55.50	3.14	4.337	14.42	0.5448
GEV208_I1000_0002	114.03	57.02	3.25	4.219	14.26	0.5105
GEV208_I1000_0003	109.97	54.99	3.12	4.348	14.15	0.5317
GEV208_I1000_0004	111.78	55.89	3.92	4.167	13.96	0.5293
GEV208_I1000_0005	111.11	55.55	3.45	4.151	13.79	0.5632
GEV208_I1000_0006	108.08	54.04	3.19	4.188	13.63	0.5988
GEV208_I1000_0007	110.11	55.06	3.54	4.250	14.21	0.5690
GEV208_I1000_0008	110.54	55.27	3.97	4.069	13.59	0.5624
GEV208_I1000_0009	111.65	55.82	3.32	4.072	13.24	0.5742
GEV208_I1000_0010	111.10	55.55	3.06	4.374	14.91	0.5223
GEV208_I1000_0011	114.81	57.40	3.60	4.243	14.18	0.5950
GEV208_I1000_0012	110.33	55.16	3.42	4.032	13.54	0.5097
GEV208_I1000_0013	115.26	57.63	3.13	4.396	14.12	0.4935
GEV208_I1000_0014	112.01	56.01	2.85	4.361	14.75	0.5713
GEV208_I1000_0015	115.62	57.81	3.63	4.281	14.36	0.4797
GEV208_I1000_0016	113.82	56.91	3.32	4.289	14.78	0.5896
GEV208_I1000_0017	112.03	56.01	3.37	4.196	14.14	0.5452
GEV208_I1000_0018	109.54	54.77	3.39	4.208	14.26	0.5587
GEV208_I1000_0019	115.43	57.71				
GEV208_I1000_0020	114.91	57.45	3.60	4.229	14.09	0.4826
GEV208_I1000_0021	114.47	57.23	3.23	4.266	14.23	0.5111
GEV208_I1000_0022	112.65	56.32	3.78	4.034	13.64	0.5233
GEV208_I1000_0023	108.70	54.35	2.91	4.271	14.33	0.4990
GEV208_I1000_0024	111.32	55.66	3.35	4.277	14.48	0.5389
GEV208_I1000_0025	114.50	57.25	3.48	4.320	14.40	0.5276
GEV208_I1000_0027	110.93	55.47	3.61	4.230	13.86	0.5263
Average	112.14	56.07	3.386	4.232	14.13	0.5383

Table A4: Fatigue life test results at 3 stress ratios. UD laminate parallel to fibers (GEV206\_R0300\_XXX).

R=0.1			R=-1			R=10		
No	Fmax/w [kN/mm]	N Cycles	No	Fmax/w [kN/mm]	N Cycles	No	Fmax/w [kN/mm]	N Cycles
0212	2.16	1189	0164	1.01	16435.5	910 <sup>3</sup>	-1.39	764708
0429	2.13	836	0165	0.686	897619	876 <sup>3</sup>	-1.40	99431
0430	2.15	1065	0167	1.015	45377	564 <sup>3</sup>	-1.73	8000
0431	1.41	51715	0169	0.811	314452	851 <sup>3</sup>	-1.80	617
0432	1.38	78760	0170	0.687	685783	883	-1.30	2602762
0434	1.01	1812119	0171	0.81	274849	879	-1.40	917908
0435	1.39	60922	0172	0.803	268157	930	-1.41	91658
0436	2.15	961	0173	0.801	204840.5	558	-1.59	120225
0441	1.39	50128	0174	1.003	46263	864	-1.61	434230
0443	1.01	1830946	0175	0.809	154582	347	-1.69	143229
0445	1.01	1278329	0178	0.696	661598	885	-1.72	493412
0446	1.39	72545	0179	1.008	44079	353	-1.77	26772
0496	2.14	976	0210	0.681	812946	421 <sup>3</sup>	-1.73	3284
0498	2.54	202	0211	1.006	36603	420 <sup>3</sup>	-1.77	398
0433	1.01	1528090	0426	0.995	93347	214 <sup>3</sup>	-1.81	469
0447	1.01	1081746	0162	1.29	3797	451 <sup>3</sup>	-1.62	845622
0428	2.14	440	0452	1.29	4300	449 <sup>3</sup>	-1.73	15990
0438	1.39	13010	0497	1.29	3228	427 <sup>3</sup>	-1.65	4605
0440	1.01	349482	0627	1.29	4810	612 <sup>3</sup>	-1.58	93273
			0628	1.29	5787	616 <sup>3</sup>	-1.59	4035
			0442	0.67	1734291	617 <sup>3</sup>	-1.68	6517
			0444 <sup>5</sup>	0.675	1420061	622 <sup>3</sup>	-1.67	952
			0625 <sup>5</sup>	0.67	1177955	611 <sup>2</sup>	-1.67	15820
			0177 <sup>1</sup>	0.606	1250000	626 <sup>2</sup>	-1.60	62784
			0213 <sup>1</sup>	4.413	380132	423	-1.74	2008
			0419 <sup>1</sup>	4.257	1598170	439	-1.71	5616
			0425 <sup>1</sup>	0.672	2000011	422	-1.76	197825
			0163 <sup>2</sup>	1.01	2229.5	454	-1.71	108808
			0168 <sup>2</sup>	0.711	407204	614	-1.67	358110
			0176 <sup>2</sup>	0.706	535131.5	96 <sup>4</sup>	-1.65	5868.5
						95 <sup>4</sup>	-1.58	120285
						94 <sup>4</sup>	-1.76	295
						91 <sup>4</sup>	-1.97	1.5

- 1 Runnout
- 2 Overheated
- 3 Buckled
- 4 Preliminary tests
- 5 Interrupted

9. Appendix

Table A5: Fatigue life test results at 3 stress ratios. UD laminate transversely to the fibers (GEV213\_R0390\_XXX)

R=0.1			R=-1			R=10		
No	$\sigma_{max}$ (MPa)	N Cycles	No	$\sigma_{max}$ (MPa)	N Cycles	No	$\sigma_{max}$ (MPa)	N Cycles
0238	24.00	393826	0244	25.00	111156	0246	-112.70	354604
0262	38.00	13235	0263	34.99	7530	0247	-144.20	3654
0264	36.00	20692	0270	32.00	15461	0252	-112.50	393994
0265	26.99	120382	0257	20.02	212743	0255	-156.50	572
0266	32.00	18918	0254	17.83	1380067	0256	-157.60	568
0101	48.00	836	0241	26.76	45598	0250	-119.70	78117
0102	48.00	756	0242	26.82	51941	0268	-133.10	23541
0041	30.74	145420	0248	26.63	54605	0239	-136.80	19268
0044	31.10	155609	0259	26.95	15561	0326	-136.80	5177
0082	31.12	54558	0267	46.93	511	0300	-136.80	10390
0061	31.10	35879	0107	17.69	470047	0301	-136.80	32399
0048	40.67	8846	0111	35.65	8185	0329	-136.80	24985
0045	31.50	90546	0112	35.65	3389	0325	-115.00	2414948
0050	40.67	8165	0113	35.65	5010	0271	-153.40	156
0051	40.67	9836	0280	46.93	370	0282	-149.60	171
0103 <sup>1</sup>	48.00	113	0291	46.92	545	0285	-153.40	486
0104 <sup>1</sup>	48.00	83	0295	46.92	374	0310	-114.00	1562675
0105 <sup>1</sup>	48.00	4	0274	26.95	9872.5	0316	-153.30	275
0294 <sup>2</sup>	30.00	7136	0305	26.95	10781	0321	-153.30	490
0237 <sup>2</sup>	20.00	1347843	0314	46.93	195	0323	-153.40	706
0253 <sup>2</sup>	21.00	1295067	0315	46.93	235	0330	-153.40	494
			0324	46.92	285	0296	-181.40	1
			0290	26.95	10150.5	0047	-113.90	150538
			0319	26.95	8216	0037	-113.90	107930
			0350	26.95	17716	0043 <sup>3</sup>	-31.50	538325
			0348	26.95	20684.5			
			0063	26.29	47141			
			0269	39.88	6			
			0302	46.92	6			
			0094	17.59	283034			
			0040	25.15	36008			
			0055	25.15	16841			
			0039 <sup>3</sup>	17.69	2505205			
			0038 <sup>3</sup>	17.69	1507006			
			0049 <sup>3</sup>	17.69	5038477			

- 1 Overloaded
- 2 Suspect plate
- 3 Runnout
- 4 Preliminary tests

Table A6: Fatigue life test results at R=0.1 of the  $[\pm 45]_S$  laminate.

Coupon ID number	$F_{max}$ (kN)	$\sigma_{max}$ (MPa)	$T_{max}$ (MPa)	N
GEV208_I1000_0028	8.511	89.749	44.874	693
GEV208_I1000_0029	8.572	89.756	44.878	1815
GEV208_I1000-0030	6.447	67.31	33.655	32140
GEV208-I1000_0031	4.918	51.533	25.767	449282
GEV208_I1000_0032	4.642	48.396	24.198	1163293
GEV208_I1000_0033	6.373	67.317	33.658	33338
GEV208_I1000_0034	4.591	48.404	24.202	681733
GEV208_I1000_0037	4.898	50.998	25.499	409880
GEV208_I1000_0038	8.604	89.755	44.877	1013
GEV208_I1000_0040	6.435	67.314	33.657	25897
GEV208_I1000_0041	6.47	67.313	33.657	37031
GEV208_I1000_0042	4.598	48.398	24.199	1151684
GEV208_I1000_0043	8.53	89.75	44.875	847
GEV208_I1000_0044	6.396	67.309	33.654	28048
GEV208_I1000_0045	4.585	48.389	24.195	1055861
GEV208_I1000_0046	8.547	89.751	44.876	942



9. Appendix

Table A7: Residual strength test results, transverse direction, R=0.1.

No	Lab		RS	Fmax	N	Freq.	Thick.	Width
			MPa	MPa	cycles	Hz	mm	mm
GEV213_R0390_0564	UP	RSTT20	51.21	41.59	1002	1.78	6.15	25.15
GEV213_R0390_0565	UP	RSTT20	50.50	41.59	1002	1.78	6.17	25.17
GEV213_R0390_0204	VUB	RSTT20	61.70	41.59	1000	1.78	6.24	25.05
GEV213_R0390_0133	VUB	RSTT20	46.99	41.59	1000	1.78	6.21	25.04
GEV213_R0390_0563	UP	RSTT50	51.08	41.6	2502	1.78	6.19	25.25
GEV213_R0390_0205	VUB	RSTT50	54.32	41.59	2500	1.78	6.22	25.08
GEV213_R0390_0140	VUB	RSTT50	57.80	41.59	2500	1.78	6.27	25.14
GEV213_R0390_0364	UP	RSTT50	46.34	41.98	2502	1.78	6.19	25.36
GEV213_R0390_0209	VUB	RSTT80	54.68	41.59	4000	1.78	6.21	25.05
GEV213_R0390_0566	UP	RSTT80	37.45	41.59	4002	1.78	6.04	25.27
GEV213_R0390_0177	VUB	RSTT20	48.84	31.85	10000	3.03	6.18	24.85
GEV213_R0390_0211	VUB	RSTT20	57.29	31.85	10000	3.03	6.21	24.86
GEV213_R0390_0360	UP	RSTT20	50.52	31.85	10002	3.03	6.32	25.4
GEV213_R0390_0561	UP	RSTT20	54.08	31.85	10002	3.03	6.22	25.31
GEV213_R0390_0562	UP	RSTT50	37.08	31.85	25002	3.03	6.15	25.23
GEV213_R0390_0182	VUB	RSTT50	55.71	31.85	25000	3.03	6.23	25.04
GEV213_R0390_0216	VUB	RSTT50	48.21	31.85	25000	3.03	6.26	24.86
GEV213_R0390_0357	UP	RSTT50	35.30	31.85	25002	3.03	6.25	25.42
GEV213_R0390_0358	UP	RSTT50	34.97	31.86	25002	3.03	6.28	25.4
GEV213_R0390_0359	UP	RSTT80	32.71	31.85	40002	3.03	6.33	25.35
GEV213_R0390_0219	VUB	RSTT20	54.10	22.51	200000	6.06	6.25	24.87
GEV213_R0390_0138	VUB	RSTT20	54.85	22.51	200000	6.06	6.26	25.26
GEV213_R0390_0353	UP	RSTT20	55.04	22.51	200002	6.06	6.24	25.35
GEV213_R0390_0356	UP	RSTT20	52.07	22.51	212502	6.06	6.24	25.39
GEV213_R0390_0136	VUB	RSTT50	46.37	22.51	500000	6.06	6.18	24.88
GEV213_R0390_0351	UP	RSTT50	39.65	22.51	500002	6.06	6.25	25.36
GEV213_R0390_0352	UP	RSTT50	50.02	22.51	500002	6.06	6.33	25.33
GEV213_R0390_0213	VUB	RSTT50	59.09	22.51	500000	6.06	6.19	24.91
GEV213_R0390_0354	UP	RSTT80	38.07	22.51	800002	6.06	6.36	25.39
GEV213_R0390_0355	UP	RSTT80	31.91	22.51	812520	6.06	6.29	25.33
GEV213_R0390_0207	VUB	RSTT80	42.87	22.51	800000	6.06	6.23	25.2
GEV213_R0390_0212	VUB	RSTT80	35.24	22.51	800000	6.06	6.27	25.15
GEV213_R0390_0139	VUB	RSTC20	-92.3	41.59	1000	1.78	6.27	25.09
GEV213_R0390_0143	VUB	RSTC50	-153.77	41.59	2500	1.78	6.25	25.25
GEV213_R0390_0149	VUB	RSTC50	-153.50	41.59	2500	1.78	6.3	25.26
GEV213_R0390_0181	VUB	RSTC20	-164.79	31.85	10000	3.03	6.16	24.94
GEV213_R0390_0197	VUB	RSTC50	-154.80	31.85	25000	3.03	6.22	25.86
GEV213_R0390_0184	VUB	RSTC20	-152.11	22.51	200000	6.06	6.33	24.94
GEV213_R0390_0201	VUB	RSTC20	-141.42	22.51	200000	6.06	6.16	24.84

Table A8: Residual strength test results, transverse direction, R=-1.

No	Lab	RS	Fmax	N	Freq.	Thick.	Width	
		MPa	MPa	cycles	Hz	mm	mm	
GEV213_R0390_0052	UP	RSTT20	57.48	40.63	202	1.15	6.32	24.96
GEV213_R0390_0083	UP	RSTT20	55.12	40.10	202	1.15	6.39	25.50
GEV213_R0390_0064	UP	RSTT35	53.12	40.10	352	1.15	6.32	25.08
GEV213_R0390_0056	UP	RSTT35	51.39	40.10	352	1.15	6.29	25.56
GEV213_R0390_0065	UP	RSTT50	51.06	40.10	502	1.15	6.35	25.24
GEV213_R0390_0066	UP	RSTT50	55.17	40.10	502	1.15	6.34	25.29
GEV213_R0390_0118	UP	RSTT80	53.20	40.10	800	1.15	6.29	25.21
GEV213_R0390_0363	UP	RSTT80	51.11	40.10	800	1.15	6.25	25.33
GEV213_R0390_0430	CRES	RSTT20	56.00	32.10	1000	1.81	6.17	25.16
GEV213_R0390_0431	CRES	RSTT20	51.31	28.67	1000	1.81	6.07	28.08
GEV213_R0390_0432	CRES	RSTT50	33.95	32.09	2500	1.81	6.00	25.10
GEV213_R0390_0429	CRES	RSTT50	51.52	32.15	2500	1.81	6.05	24.99
GEV213_R0390_0436	CRES	RSTT80	38.12	32.08	4000	1.81	6.14	25.08
GEV213_R0390_0437	CRES	RSTT80	38.71	32.08	4000	1.81	6.15	25.36
GEV213_R0390_0438	CRES	RSTT20	53.41	24.81	10000	3.13	6.07	25.30
GEV213_R0390_0059	UP	RSTT20	46.80	25.14	10002	2.91	6.30	25.55
GEV213_R0390_0060	UP	RSTT20	43.47	25.14	10002	2.91	6.32	25.57
GEV213_R0390_0439	CRES	RSTT20	47.19	24.64	10000	3.13	6.10	25.14
GEV213_R0390_0441	CRES	RSTT50	52.88	25.12	25000	3.13	6.16	25.28
GEV213_R0390_0054	UP	RSTT50	37.09	25.15	25002	2.91	6.27	25.46
GEV213_R0390_0058	UP	RSTT50	50.53	25.15	25002	2.91	6.29	25.54
GEV213_R0390_0116	UP	RSTT80	43.52	25.14	40002	2.91	6.40	25.04
GEV213_R0390_0117	UP	RSTT80	53.16	25.14	40002	2.91	6.38	25.10
GEV213_R0390_0068	UP	RSTT20	46.88	17.59	200002	5.96	6.37	25.24
GEV213_R0390_0084	UP	RSTT20	50.59	17.59	200002	5.96	6.27	25.60
GEV213_R0390_0444	CRES	RSTT20	43.88	17.68	200000	6.37	6.03	25.34
GEV213_R0390_0434	CRES	RSTT20	46.49	17.22	200000	6.37	6.13	25.10
GEV213_R0390_0115	UP	RSTT80	32.78	17.59	350011	5.96	6.38	25.17
GEV213_R0390_0089	UP	RSTT50	37.51	17.59	500002	5.96	6.23	25.40
GEV213_R0390_0067	UP	RSTT50	48.41	17.59	503632	5.96	6.39	25.21
GEV213_R0390_0445	CRES	RSTT50	37.96	17.30	500000	6.37	6.11	25.28
GEV213_R0390_0446	CRES	RSTT50	43.78	17.57	500000	6.37	6.07	25.34
GEV213_R0390_0114	UP	RSTT80	33.10	17.59	800002	5.96	6.34	25.13
GEV213_R0390_0097	UP	RSTC20	-157.27	35.66	1002	1.45	6.32	25.27
GEV213_R0390_0098	UP	RSTC20	-156.21	35.65	1002	1.45	6.32	25.32
GEV213_R0390_0099	UP	RSTC50	-157.06	35.66	2501	1.45	6.32	25.25
GEV213_R0390_0100	UP	RSTC50	-157.13	35.65	2502	1.45	6.43	25.10
GEV213_R0390_0091	UP	RSTC20	-151.47	25.15	10002	2.91	6.36	25.16
GEV213_R0390_0092	UP	RSTC20	-153.21	25.15	10002	2.91	6.34	25.13
GEV213_R0390_0090	UP	RSTC50	-154.16	25.15	25002	2.91	6.37	24.99
GEV213_R0390_0096	UP	RSTC50	-155.24	25.15	25002	2.91	6.41	25.16
GEV213_R0390_0088	UP	RSTC20	-163.30	17.59	200002	5.96	6.23	25.37

9. Appendix

Table A9 (Continued) : Residual strength test results, transverse direction, R=-1.

No	Lab		RS	Fmax	N	Freq.	Thick.	Width
			MPa	MPa	cycles	Hz	mm	mm
GEV213_R0390_0093	UP	RSTC20	-158.87	17.92	200002	5.96	6.21	25.33
GEV213_R0390_0095	UP	RSTC50	-161.16	17.59	488243	5.96	6.31	25.19

Table A10: Residual strength test results, transverse direction, R=10.

No	Lab		RS MPa	Fmax MPa	N cycles	Freq. Hz	Thick. mm	Width mm
GEV213_R0390_0411	CRES	RSTT20	54.44	-138.39	1000	1.67	5.95	25.14
GEV213_R0390_0412	CRES	RSTT20	55.96	138.33	1000	1.67	6.10	24.98
GEV213_R0390_0413	CRES	RSTT50	54.88	-136.44	2500	1.67	6.15	25.13
GEV213_R0390_0332	UP	RSTT50	44.54	-138.63	2499	1.66	6.18	24.88
GEV213_R0390_0373	UP	RSTT50	42.96	-132.34	25000	2.00	6.26	25.39
GEV213_R0390_0389	UP	RSTT20	52.74	-126.11	10005	2.73	6.26	25.39
GEV213_R0390_0341	UP	RSTT20	56.48	-126.11	10000	2.73	6.14	25.14
GEV213_R0390_0417	CRES	RSTT20	58.53	-124.38	10000	2.73	6.19	25.15
GEV213_R0390_0418	CRES	RSTT20	52.33	-125.59	10000	2.73	5.98	25.13
GEV213_R0390_0374	UP	RSTT50	44.90	-126.11	25092	2.73	6.35	25.37
GEV213_R0390_0375	UP	RSTT50	45.22	-126.11	25119	3.20	6.22	25.37
GEV213_R0390_0383	UP	RSTT80	49.11	-126.11	40000	2.73	6.30	25.39
GEV213_R0390_0345	UP	RSTT80	49.02	-126.11	40000	2.73	6.10	24.98
GEV213_R0390_0277	UP	RSTT20	49.70	-119.12	40391	2.80	6.11	25.11
GEV213_R0390_0338	UP	RSTT20	57.09	-119.12	40003	2.80	6.25	24.97
GEV213_R0390_0334	UP	RSTT50	38.55	-119.12	102000	2.80	6.05	24.92
GEV213_R0390_0569	UP	RSTT50	49.34	-119.12	100001	2.80	6.07	25.10
GEV213_R0390_0339	UP	RSTT80	52.45	-119.12	160000	2.80	6.10	25.07
GEV213_R0390_0346	UP	RSTT80	50.24	-119.12	160001	2.80	6.13	25.02
GEV213_R0390_0384	UP	RSTT20	47.49	-111.49	206532	3.20	6.27	25.38
GEV213_R0390_0385	UP	RSTT20	46.26	-111.49	204393	3.20	6.33	25.29
GEV213_R0390_0423	CRES	RSTT20	57.01	-106.53	200000	3.20	6.10	25.13
GEV213_R0390_0424	CRES	RSTT20	52.02	-108.64	200000	3.20	6.15	25.13
GEV213_R0390_0382	UP	RSTT50	50.15	-111.50	513634	3.20	6.36	25.36
GEV213_R0390_0568	UP	RSTT50	51.18	-111.49	513005	3.20	6.04	25.12
GEV213_R0390_0288	UP	RSTT80	49.65	-111.50	800000	3.20	5.99	25.30
GEV213_R0390_0391	UP	RSTT80	49.80	-111.49	820285	3.20	6.20	25.40
GEV213_R0390_0386	UP	RSTC50	-159.03	-126.11	25001	2.73	6.24	25.37
GEV213_R0390_0390	UP	RSTC50	-168.39	-126.11	25127	2.73	6.37	25.41
GEV213_R0390_0342	UP	RSTC50	-166.51	-119.12	103219	2.80	6.07	25.01
GEV213_R0390_0308	UP	RSTC50	-175.86	-119.12	101111	2.80	6.20	25.07
GEV213_R0390_0309	UP	RSTC50	-167.18	-111.49	500425	3.20	6.00	25.20
GEV213_R0390_0344	UP	RSTC50	-172.99	-111.50	500000	3.20	6.04	25.14

9. Appendix

Table A11: Residual strength test results, on-axis direction, R=0.1.

No	Lab		RS	Fmax	N	Freq.	Thick.	Width
			kN/mm	kN/mm	cycles	Hz	mm	mm
GEV206_R0300_0407	RAL	RSTT20	3.03	2.14	200	1.50	3.77	25.22
GEV206_R0300_0041	UP	RSTT20	2.86	2.14	201	1.50	3.75	25.17
GEV206_R0300_0042	UP	RSTT20	3.01	2.14	201	1.50	3.76	25.19
GEV206_R0300_0634	RAL	RSTT20	3.08	2.14	200	1.50	3.79	25.43
GEV206_R0300_0755	VUB	RSTT20	3.42	2.14	200	1.50	3.77	25.21
GEV206_R0300_0408	RAL	RSTT50	2.75	2.14	500	1.50	3.81	25.16
GEV206_R0300_0753	VUB	RSTT50	3.40	2.14	500	1.50	3.76	25.19
GEV206_R0300_0636	RAL	RSTT50	2.94	2.14	500	1.50	3.71	25.54
GEV206_R0300_0221	VUB	RSTT50	3.04	2.14	500	1.50	3.88	24.83
GEV206_R0300_0283	VUB	RSTT20	3.35	2.14	500	1.50	3.76	25.54
GEV206_R0300_0395	RAL	RSTT80	2.81	2.14	800	1.50	3.83	25.22
GEV206_R0300_0409	RAL	RSTT80	2.40	2.14	800	1.50	3.79	25.28
GEV206_R0300_0304	VUB	RSTT80	2.93	2.14	800	1.50	3.71	25.42
GEV206_R0300_0751	VUB	RSTT80	3.14	2.14	800	1.50	3.79	25.17
GEV206_R0300_0659	RAL	RSTT20	2.44	1.43	10001	3.35	3.71	25.46
GEV206_R0300_0639	RAL	RSTT20	2.46	1.43	10000	3.35	3.76	25.69
GEV206_R0300_0485	VUB	RSTT20	2.65	1.43	10000	3.35	3.90	25.24
GEV206_R0300_0770	VUB	RSTT20	2.80	1.43	10000	3.35	3.67	25.26
GEV206_R0300_1113	WMC	RSTT20	2.81	1.43	10002	3.35	3.73	25.30
GEV206_R0300_0839	WMC	RSTT20	2.58	1.43	10003	3.35	3.65	25.54
GEV206_R0300_0570	WMC	RSTT20	2.71	1.43	9996	3.35	3.60	25.37
GEV206_R0300_0223	VUB	RSTT50	2.43	1.43	25000	3.35	3.76	25.12
GEV206_R0300_0630	RAL	RSTT50	1.90	1.44	25000	3.36	3.76	24.74
GEV206_R0300_0775	VUB	RSTT50	2.31	1.43	25000	3.35	3.59	25.20
GEV206_R0300_0680	RAL	RSTT50	2.14	1.43	25000	3.35	3.70	25.51
GEV206_R0300_1107	WMC	RSTT50	2.09	1.43	24990	3.35	3.69	25.32
GEV206_R0300_0220	VUB	RSTT80	2.16	1.43	40000	3.35	3.82	24.92
GEV206_R0300_0684	RAL	RSTT20	2.41	1.05	200000	5.00	3.76	25.53
GEV206_R0300_0892	WMC	RSTT20	2.46	1.05	199980	6.19	3.55	24.92
GEV206_R0300_0393	RAL	RSTT20	2.34	1.05	200000	4.81	3.84	25.19
GEV206_R0300_1109	WMC	RSTT35	2.58	1.05	349953	6.19	3.65	25.31
GEV206_R0300_0683	RAL	RSTT50	2.10	1.05	500001	5.00	3.72	25.49
GEV206_R0300_0913	WMC	RSTT50	2.54	1.05	499998	6.19	3.57	24.97
GEV206_R0300_0686	RAL	RSTT50	1.53	1.05	500000	5.00	3.73	25.55
GEV206_R0300_1105	WMC	RSTT50	1.93	1.05	499887	6.19	3.66	25.26
GEV206_R0300_1111	WMC	RSTT50	2.26	1.05	499916	6.19	3.68	25.24
GEV206_R0300_0288	VUB	RSTT50	2.69	1.05	500000	6.19	3.75	25.39
GEV206_R0300_0297	VUB	RSTT50	2.48	1.05	500000	6.19	3.74	25.41
GEV206_R0300_0404	RAL	RSTT80	1.92	1.05	800000	5.00	3.80	25.21

Table A12 (Continued) : Residual strength test results, on-axis direction, R=0.1.

No	Lab		RS kN/mm	Fmax kN/mm	N cycles	Freq. Hz	Thick. mm	Width mm
GEV206_R0300_0873	WMC	RSTT80	1.38	1.07	799837	6.19	3.60	24.94
GEV206_R0300_0677	RAL	RSTT80	1.69	1.05	800000	5.00	3.72	25.61
GEV206_R0300_0301	VUB	RSTT80	2.47	1.05	800000	6.19	3.75	25.37
GEV206_R0300_0291	VUB	RSTT80	1.88	1.05	800000	6.19	3.73	25.51
GEV206_R0300_0901	WMC	RSTT20	2.08	0.83	1999784	9.93	3.65	25.01
GEV206_R0300_0862	WMC	RSTT20	2.08	0.83	2432081	9.93	3.63	25.03
GEV206_R0300_0912	WMC	RSTT50	2.25	0.83	4999918	9.93	3.63	24.90
GEV206_R0300_1110	WMC	RSTT50	1.91	0.83	4999459	9.93	3.67	25.26
GEV206_R0300_0635	RAL	RSTC20	-2.20	2.14	200	1.50	3.75	25.55
GEV206_R0300_0756	VUB	RSTC20	-1.61	2.14	200	1.50	3.72	25.24
GEV206_R0300_0284	VUB	RSTC20	-1.66	2.14	200	1.50	3.85	25.36
GEV206_R0300_0754	VUB	RSTC50	-1.60	2.14	500	1.50	3.75	25.25
GEV206_R0300_0637	RAL	RSTC50	-1.99	2.14	500	1.50	3.72	25.58

9. Appendix

Table A13: Residual strength test results, on-axis direction, R=-1.

No	Lab	RS	Fmax	N	Freq.	Thick.	Width	
		kN/mm	kN/mm	cycles	Hz	mm	mm	
GEV206_R0300_0678	RAL	RSTT80	2.10	1.29	4000	1.23	3.71	25.58
GEV206_R0300_0819	WMC	RSTT80	2.35	1.29	4000	1.23	3.70	25.49
GEV206_R0300_0685	RAL	RSTT80	2.09	1.29	4000	1.23	3.75	25.48
GEV206_R0300_0576	WMC	RSTT80	2.50	1.29	4002	1.23	3.72	25.42
GEV206_R0300_0849	WMC	RSTT20	2.70	0.97	9982	2.17	3.78	25.41
GEV206_R0300_0416	RAL	RSTT20	2.41	0.97	10000	2.17	3.80	25.30
GEV206_R0300_0571	WMC	RSTT20	2.78	0.97	9997	2.17	3.72	25.34
GEV206_R0300_0355	WMC	RSTT20	2.82	0.97	9999	2.17	3.70	25.43
GEV206_R0300_0644	RAL	RSTT20	2.26	0.97	10000	2.17	3.81	25.50
GEV206_R0300_0641	RAL	RSTT50	1.90	0.97	25000	2.17	3.74	25.65
GEV206_R0300_0581	WMC	RSTT50	2.24	0.97	25008	2.17	3.77	25.35
GEV206_R0300_0417	RAL	RSTT50	2.03	0.97	25000	2.17	3.79	25.16
GEV206_R0300_0572	WMC	RSTT50	2.23	0.97	25008	2.17	3.64	25.25
GEV206_R0300_0400	RAL	RSTT80	1.99	0.97	40000	2.17	3.76	25.29
GEV206_R0300_0682	RAL	RSTT80	1.73	0.97	40000	2.17	3.72	25.53
GEV206_R0300_0381	WMC	RSTT80	1.74	0.97	39984	2.17	3.72	25.40
GEV206_R0300_0845	WMC	RSTT80	1.91	0.97	39996	2.17	3.71	25.59
GEV206_R0300_0418	RAL	RSTT20	2.33	0.67	200000	4.56	3.80	25.23
GEV206_R0300_0543	WMC	RSTT20	2.50	0.67	199985	4.56	3.63	25.23
GEV206_R0300_0557	WMC	RSTT20	2.57	0.67	199981	4.56	3.67	25.19
GEV206_R0300_0386	RAL	RSTT20	2.20	0.67	200000	4.56	3.77	25.23
GEV206_R0300_0357	WMC	RSTT50	2.13	0.67	500003	4.56	3.66	25.38
GEV206_R0300_0922	WMC	RSTT50	2.71	0.67	499994	4.56	3.56	25.02
GEV206_R0300_0567	WMC	RSTT50	2.39	0.67	499939	4.56	3.66	25.23
GEV206_R0300_0857	WMC	RSTT50	2.24	0.67	499951	4.56	3.78	25.52
GEV206_R0300_0398	RAL	RSTT50	2.10	0.67	500000	4.56	3.79	25.18
GEV206_R0300_0389	RAL	RSTT50	2.05	0.67	500000	4.56	3.76	25.29
GEV206_R0300_0541	WMC	RSTT80	1.88	0.67	799957	4.56	3.68	25.34
GEV206_R0300_0535	WMC	RSTT80	2.26	0.67	799903	4.56	3.73	25.32
GEV206_R0300_0643	RAL	RSTT80	2.02	0.67	800000	4.56	3.76	25.57
GEV206_R0300_0560	WMC	RSTT80	1.92	0.67	799871	4.56	3.67	25.27
GEV206_R0300_1112	WMC	RSTT80	2.05	0.67	799818	4.56	3.70	25.23
GEV206_R0300_0388	RAL	RSTT80	1.45	0.67	800000	4.56	3.78	25.22
GEV206_R0300_0863	WMC	RSTT20	2.34	0.50	2127140	8.09	3.61	24.98
GEV206_R0300_0896	WMC	RSTT20	2.76	0.50	2008924	8.09	3.68	24.94
GEV206_R0300_0578	WMC	RSTC20	-2.22	1.28	1000	1.23	3.72	25.34
GEV206_R0300_0818	WMC	RSTC20	-2.05	1.29	999	1.23	3.69	25.59
GEV206_R0300_0650	RAL	RSTC20	-2.23	1.29	1000	1.23	3.77	25.47

Table A14 (Continued) : Residual strength test results, on-axis direction, R=-1.

No	Lab		RS kN/mm	Fmax kN/mm	N cycles	Freq. Hz	Thick. mm	Width mm
GEV206_R0300_0812	WMC	RSTC50	-2.18	1.29	2505	1.23	3.57	25.60
GEV206_R0300_0647	RAL	RSTC50	-2.28	1.29	2500	1.23	3.76	25.65
GEV206_R0300_0833	WMC	RSTC50	-2.05	1.29	2042	1.23	3.70	25.52
GEV206_R0300_0889	WMC	RSTC80	-1.85	1.29	4003	1.23	3.59	24.82
GEV206_R0300_0898	WMC	RSTC80	-2.10	1.29	4001	1.23	3.61	25.17
GEV206_R0300_0908	WMC	RSTT50	1.83	0.50	5285884	8.09	3.60	25.00



9. Appendix

Table A15: Residual strength test results, [ $\pm 45$ ]s specimens (GEV208-I1000-XX), R=0.1.

No	$\sigma_{\max}$ (MPa)	RTS (MPa)	n	No	$\sigma_{\max}$ (MPa)	RTS (MPa)	n
0035	48.5	83.25	500002	0101	48.5	72.46	800002
0036	48.5	81.26	500002	0102	48.5	78.73	800002
0047	48.5	106.13	200002	0103	48.5	73.18	787818
0048	48.5	103.29	200002	0104	48.5	90.70	800002
0049	48.5	87.67	500002	0105	48.5	92.15	500002
0050	48.5	109.20	200001	0106	48.5	94.15	500329
0051	48.5	77.43	500002	0107	48.5	85.13	500002
0052	63.6	104.94	25002	0108	48.5	93.31	500002
0053	63.6	97.01	25002	0109	48.5	102.21	200002
0054	63.6	102.20	25002	0110	48.5	106.51	200002
0056	63.6	104.47	25002	0111	48.5	94.71	200002
0057	48.5	106.01	199554	0112	48.5	105.37	200002
0058	63.6	109.51	10002	0113	63.6	106.52	10002
0059	63.6	107.24	10002	0114	63.6	109.26	10002
0060	63.6	107.78	10002	0115	63.6	106.57	10002
0063	48.5	84.76	800002	0116	63.6	105.12	10002
0064	48.5	86.73	800002	0117	63.6	90.83	25002
0065	78.3	103.20	2502	0118	63.6	92.15	25002
0066	78.3	106.81	2502	0119	63.6	86.38	25002
0067	78.3	101.10	2502	0120	63.6	93.86	25002
0068	78.3	106.18	2502	0121	63.6	86.23	40002
0069	63.6	113.18	10002	0122	63.6	84.06	40002
0070	63.6	83.89	40002	0123	63.6	86.56	40002
0072	63.6	84.62	40002	0124	63.6	74.35	40002
0074	78.3	106.25	1002	0125	78.3	90.93	4767
0075	78.3	107.59	1002	0126	78.3	88.91	4002
0076	78.3	104.74	1002	0127	78.3	96.04	4002
0077	78.3	105.88	1002	0128	78.3	94.82	4002
0078	78.3	87.53	4002	0129	78.3	102.30	2502
0079	78.3	84.95	4002	0130	78.3	102.19	2502
0080	78.3	102.79	4002	0131	78.3	99.89	2502
0081	78.3	100.96	4002	0132	78.3	103.60	2502
0082	63.6	94.48	40002	0133	78.3	104.98	1002
0083	63.6	94.18	40002	0134	78.3	103.09	1002
0084	63.6	94.36	40002	0135	78.3	105.08	1002
0085	48.5	83.27	800002	0136	78.3	103.62	1002
0086	48.5	93.44	525330				

Table A16 (Continued) : Residual strength test results, [ $\pm 45$ ]s specimens (GEV208-I1000-XX), R=0.1.

No	$\sigma_{max}$	RTS	n	No	$\sigma_{max}$	RTS	n
	(MPa)	(MPa)			(MPa)	(MPa)	
0087	48.5	87.15	800002				
0088	55.6	94.52	110002				
0089	55.6	89.34	110001				
0090	55.6	97.17	110002				
0091	55.6	98.41	110002				
0092	55.6	97.40	110002				
0093	55.6	96.89	110002				
0094	55.6	104.36	110002				
0095	55.6	99.77	110002				